Electrochemical Studies of Transition Metal Complexes

Peter I. Usher

Ph.D. Thesis

University of Edinburgh

1995

For Gillian and my family

ACKNOWLEDGEMENTS

I would like to thank Dr. L.J. Yellowlees for her advice, guidance and continual encouragement and enthusiasm throughout this work.

I would also like to thank Marcus Manning, who synthesised the complexes studied in chapter 3, and who performed the initial electrochemical investigations of the products.

Thanks are due to Mr. A. Taylor for running various mass spectra, Mrs. L. Eades for carrying out the CHN analyses, and Mr. S. Mains for the manufacture and repair of electrodes for the OTE cell.

I would like to express my gratitude to the SERC/ESPRC for funding, and the University of Edinburgh for use of facilities.

Finally, I would like to thank everyone else who has helped me, and worked alongside me in Lab 291. Special thanks must go to Lockhart, Ken, Steve and Paul for their help and support.

Abstract

This thesis is concerned with the spectroscopic, electrochemical and spectroelectrochemical investigation of a range of transition metal species, all containing the ligand 2,2'-bipyridine (bpy). All the complexes studied exhibit rich electrochemistry and electronic absorption spectra.

Chapter one details the electrochemical and spectroelectrochemical techniques used in this work, and presents a brief overview of the reasons why we study transition metal complexes in this manner.

Chapter two is concerned with the solvent dependent behaviour of complexes of the form $[M(bpy)_2(CN)_2]$ (M = Fe, Ru or Os). The electrochemistry, UV/visible spectroscopy and spectroelectrochemistry of these complexes in a range of solvents is described, and both reduced and oxidised forms of the complex are investigated. The solvent dependent characteristics of the complexes are compared with a range of solvent parameters, and show best agreement with Acceptor Numbers. Analysis of epr data for the oxidised complexes, and spectroelectrochemical experiments suggest that the solvent interaction responsible for this behaviour is minimised on removal of an electron.

Chapter three details a range of mono- and bi-metallic complexes containing $Ru(bpy)_2$ or $Fe(bpy)_2$ units and poly-aromatic bridging ligands. The electrochemistry, UV/visible spectroscopy and spectroelectrochemistry of these complexes is described.

Chapter four details the attempted synthesis of three complexes utilising cyanide ligands as a bridge between two metal centres. These complexes are based

around either a $[Ru(bpy)_2(CN)_2]$ or $[Pt(bpy)(CN)_2]$ centre. The electrochemistry, UV/visible spectroscopy and spectroelectrochemistry of the products is reported, and the likely nature of the products is discussed.

List of Abbreviations

A	Absorbance
ac	Alternating current
A.N.	Acceptor Number
bpy	2,2'-bipryridine
c.e.	Counter electrode
CT	Charge transfer
cyt	Cytochrome
DMA	Dimethyl acetamide
DMF	N,N-dimethyl formamide
DMSO	Dimethylsulphoxide
D.N.	Donor Number
dpp	2,3-dipyridylpyrazine
dpq	2,3-dipyridylquinoxaline
dpb	2,3-dipyridylbenzoquinoxaline
E_{appl}	Applied potential

EtOH	Ethanol
epr	Electron paramagnetic resonance
Fc	Ferrocene
Fc^+	Ferrocinium
IVCT	Intervalence charge transfer
LMCT	Ligand to metal charge transfer
MeCN	Acetonitrile
MeOH	Methanol
$MeNO_2$	Nitromethane
MLCT	Metal to ligand charge transfer
NIR	Near infra-red
nmr	Nuclear magnetic resonance
OTE	Optically transparent electrode
Ox	Oxidised species
r.e.	Reference electrode
Red	Reduced species

R_s	Solution resistance
R_u	Uncompensated solution resistance
SHE	Standard hydrogen electrode
TBA	Tetrabutylammonium
terpy	2,2':6',2"-terpyridine
UV	Ultraviolet
VIS	Visible
w.e.	Working electrode
ε	Extinction co-efficient
Δ	Axial splitting parameter
V	Rhombic splitting parameter
λ	Spin-orbit coupling constant
ν_{max}	Wavelength of maximum absorption
ν	Scan speed
ω	Frequency

Table of Contents

Chapter 3 : Complexes with Polypyridyl Bridging Ligands

List of Figures

List of Tables

Structures of ligands

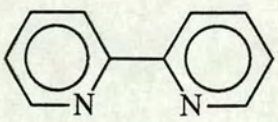

2,2'-bipyridine

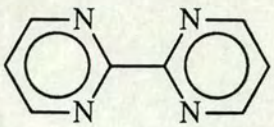

2,2'-bipyrimidine

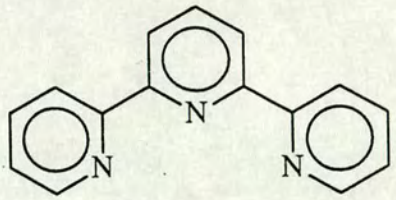

2,2';6,2"-terpyridine

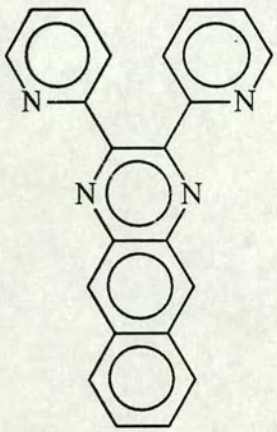

2,3-di-2-pyridylbenzoquinoxaline

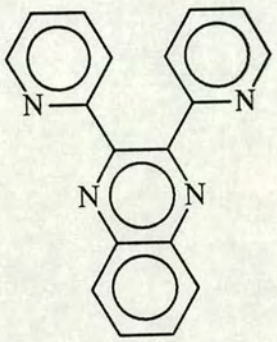

2,3-di-2-pyridylquinoxaline

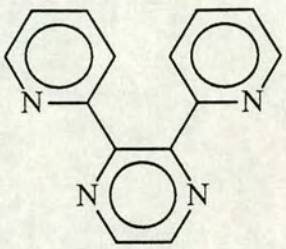

2,3-di-2-pyridylpyrazine

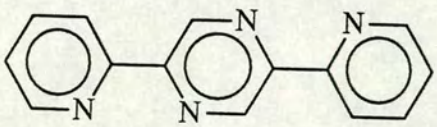

2,5-di-2-pryridylpyrazine

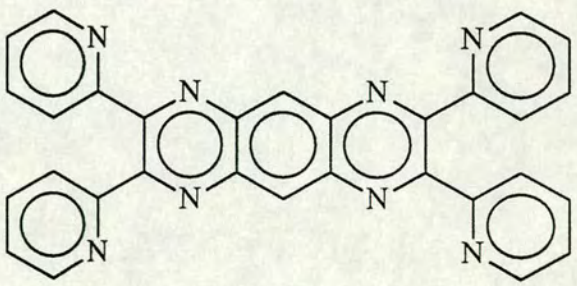

2,3,7,8-tetra-2-pyridyl-pyrazino[2,3-g]quinoxaline

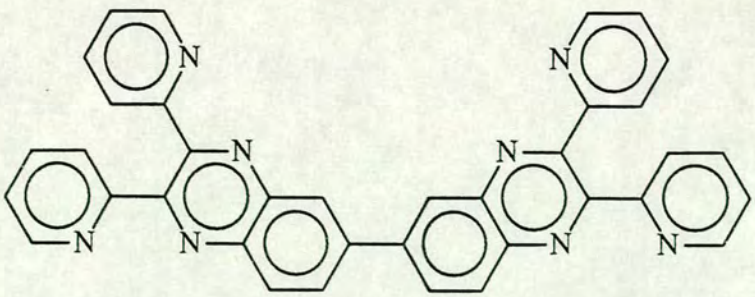

2,2',3,3'-tetra-2-pyridyl-6,6'-biqunoxaline

Chapter 1 : Electrochemical and Spectroelectrochemical Techniques

1.1 : Introduction

This thesis is concerned with the synthesis, characterisation and behaviour of a range of transition metal complexes containing the M(bpy) unit (bpy = 2,2'-bipyridine). Some of these complexes are simple mono-metallic species, whilst others use a range of bridging ligands to form bi- and tri-metallic species. All the species studied contain redox active metal sites, and, in addition, most of the ligands used also display redox processes. As a result, an important part of this work is the assignment and interpretation of the observed redox processes and the charge transfer processes seen in the electronic absorption spectra of the complexes.

The study of electron transfer processes is important in widely diverse areas of chemistry, from corrosion and its prevention, through solar energy to the chemistry driving natural processes such as photosynthesis. Thus the study of the electrochemical properties of the species involved in these processes becomes of vital importance.

Corrosion processes involve the oxidation of metals, and are often initiated by environmental factors. Corrosion can lead to many structural problems, and the costs arising from these can be considerable. As a result, numerous methods of corrosion prevention have been devised, some of which are based upon the redox properties of the metals involved.

The most common metal involved in corrosion processes is iron, often in the form of steel. Metallic iron is readily oxidised by the action of oxygen or water ($Fe^{2+} + 2e^- \rightarrow Fe$, $E^0 = -0.41$ V vs. SHE)[1]. One method of prevention is to coat the

iron or steel with a less readily oxidised metal. Commonly, metals such as tin ($Sn^{2+} + 2e^- \rightarrow Sn$, $E^0 = -0.14$ V)[1] or nickel ($Ni^{2+} + 2e^- \rightarrow Ni$, $E^0 = -0.23$ V)[1] are used for the coating. As long as the coating remains intact, oxidation of the iron is prevented. However, should the coating be broken, the iron will actually be oxidised more rapidly, as electrons flow from the iron to the less readily oxidised plating metal.

An alternative approach uses this sacrificial corrosion by plating the steel with a more readily oxidised metal, typically zinc ($Zn^{2+} + 2e^- \rightarrow Zn$, $E^0 = -0.76$ V)[1] in the case of galvanised steel. Even if the coating is damaged the flow of electrons is from the zinc to the iron, thus inhibiting corrosion of the steel.

Aluminium, which is very readily oxidised ($Al^{3+} + 3e^- \rightarrow Al$, $E^0 = -1.71$ V)[1], is corrosion inhibited by formation of a thin film of aluminium oxide on the surface of the aluminium. Aluminium oxide is extremely stable, impervious to water and strong enough that it cannot be easily removed. Thus, to protect aluminium structures, a protective layer of oxide is created by making aluminium the anode in an electrolytic cell, in the process called anodising. This technique can also be used for other metals, such as magnesium[2].

In recent years there has been a large increase in interest in renewable energy sources. One of the most commonly discussed source of energy is solar power. Hence there has been a great deal of research into solar energy dyes. Perhaps the most well known compound studied as a potential dye is tris(bipyridyl)ruthenium(II), $[Ru(bpy)_3]^{2+}$. This species fulfils many of the requirements of an effective solar dye. It absorbs strongly in the visible ($\nu_{max} = 22100$ cm^{-1}, $\varepsilon = 13700$ $mol^{-1}dm^3cm^{-1}$)[3]. It has a long lived excited state (0.7 μs in aqueous solution at room temperature)[4], resulting

from excitation of an electron from the ruthenium to the ligand π^* orbitals. Studies have shown that the promoted electron is localised on one of the ligands, and thus the excited state is most accurately described as $[Ru^{III}(bpy)^0{}_2(bpy)^-]^{*\,2+}$ [3,5].

This excited state can undergo a range of 'quenching' reactions, including disproportionation to $[Ru(bpy)_3]^{3+}$ and $[Ru(bpy)_3]^{+}$ [6,7]. Much of the interest in the complex stems from the fact that these disproportionation products are thermodynamically capable of splitting water to yield hydrogen and oxygen, whilst regenerating the starting complex[8] (see figure 1.1).

Redox processes are very significant in biological systems. Among the processes that rely on the redox properties of the metalloenzymes involved are photosynthesis, respiration and numerous metabolic pathways[9].

Figure 1.1 : Splitting water by $[Ru(bpy)_3]^{2+}$

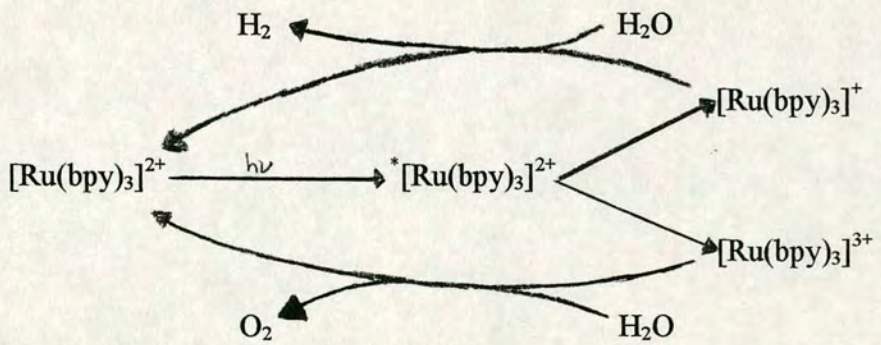

Figure 1.2 : Mitochondrial Electron Transport Chain (part)

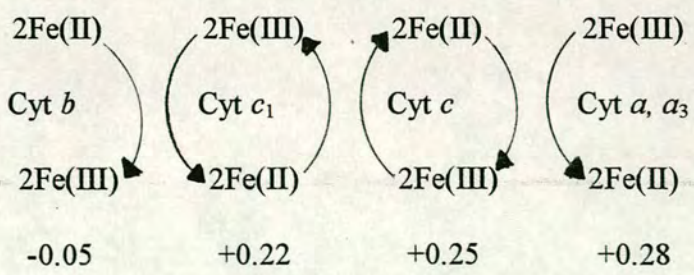

The activity of many of these enzymes is controlled by the redox behaviour of the metal centre(s) involved. In naturally occurring enzymes the metal at the active site has a suitable range of accessible oxidation states and a variable co-ordination geometry which gives the desired behaviour.

A good example of this can be seen in the mitochondrial electron transfer chain which facilitates the reaction of $NADH^+$ with O_2, specifically in the section of the chain involving cytochromes, a group of proteins containing iron in a porphyrin (heme) environment. Four cytochromes are involved in the electron transfer process. These are cytochrome a, b, c and c_1, and all have different redox properties. A simplified diagram of the relevant part of the electron transfer chain is shown in figure 1.2.

The co-ordination of the iron in each cytochrome moiety is broadly similar, consisting of an equatorial tetradentate porphyrin ring, and two axial donors, often part of the protein structure of the metalloenzyme. The exact nature of the substituents, however, allows a chain to be formed, where each iron in turn passes an electron to a more easily reduced iron centre, and in turn is ready to accept another electron. At the left hand end as written, the iron centre receives an electron from a more easily oxidised coenzyme, whilst at the right hand end of the scheme, the final metalloprotein passes its electrons to oxygen, reducing it to water.

Many transition metal complexes have been studied to better understand electron transfer processes. In the case of solar dyes, complexes have been designed to lengthen the excited state lifetime, thereby permitting more efficient energy/electron transfer. One profitable method has been to separate the donor and

acceptor sites within a species which may overcome the unwanted back reaction, or passes the energy absorbed on[10,11].

In the case of biological systems, many complexes have been proposed as 'model' systems, allowing investigation into the effects of co-ordination geometry and donor atoms on redox behaviour[12-14]. Because of this research, electrochemical and spectroscopic studies of transition metal complexes, and other inorganic species, is an important area of study. A brief introduction to the techniques used in this work is given in the next section.

1.2 : The Electrochemical experiment

Electrochemical experiments have been used for a wide range of preparative, analytical and investigative purposes. Although the various methods used can be widely different, the basic principles and factors to be considered remain constant throughout.

The first, and perhaps most important, consideration is the aim of the experiment. This has obvious ramifications for cell and electrode design, and may well effect the choice of solvent and bulk electrolyte. A brief outline of each of these factors is given below.

1.2.1 : Cell Design

There are a number of factors to be considered in the design of a good electrochemical cell. All the techniques used in this work utilise some form of the three electrode cell (for reasons see the discussion on electrodes) and thus this section will only be concerned with such cells.

The requirements of a good electrochemical cell are:

1. The resistance of the cell should be minimised. This is of particular importance when performing experiments with organic solvents or high currents. The lower the resistance, the smaller the potential drop associated with the cell. Thus, ideally, the electrodes should be close to one another. In addition, for voltammetric studies, the working electrode should be kept small so that all points on the surface are effectively equidistant from the normally much larger counter electrode.

2. The geometry and placement of both the working and counter electrodes should be optimised to achieve a uniform current density.

3. It should be possible to regulate the temperature of the cell and its contents.

4. The cell must protect its contents from the surrounding environment (e.g. water, atmospheric oxygen).

5. The cell should be easily dismantled and assembled.

6. For electrosynthetic and coulometric studies, the working and counter electrodes should be well separated, thus preventing mixing of the species generated. This is commonly achieved by placing the electrodes in compartments separated by a glass frit.

A schematic of the cell used for voltammetric experiments is shown in figure 1.3, while that used for coulometric experiments is shown in figure 1.4. The basic design of the cells is similar, with the coulometry cell separating the w.e and c.e compartments by two glass frits. The frits allow good electrical contact, whilst preventing easy transport of chemical species between the compartments.

Figure 1.3 : Typical cell design for voltammetric experiments

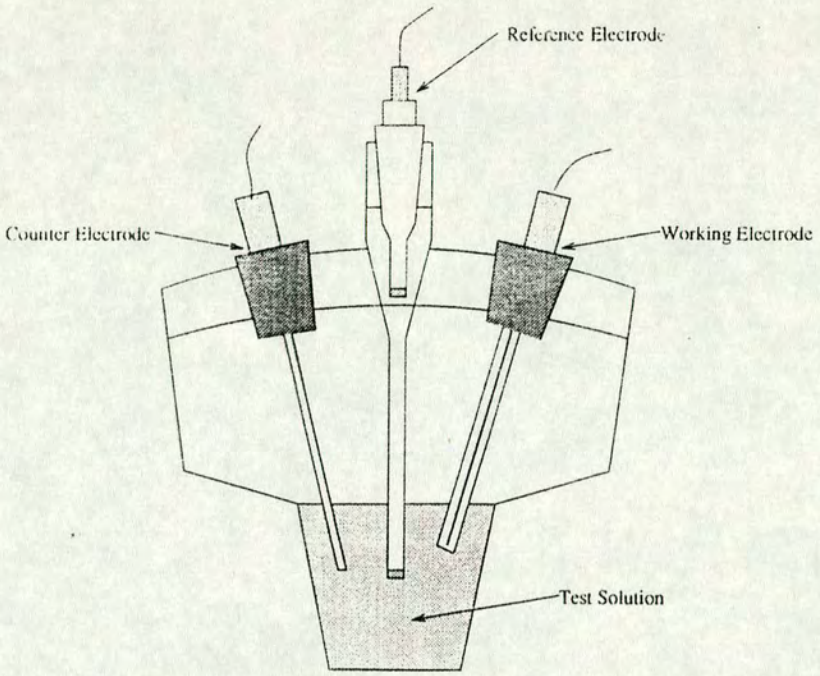

Figure 1.4 : Three compartment cell for electrosynthesis

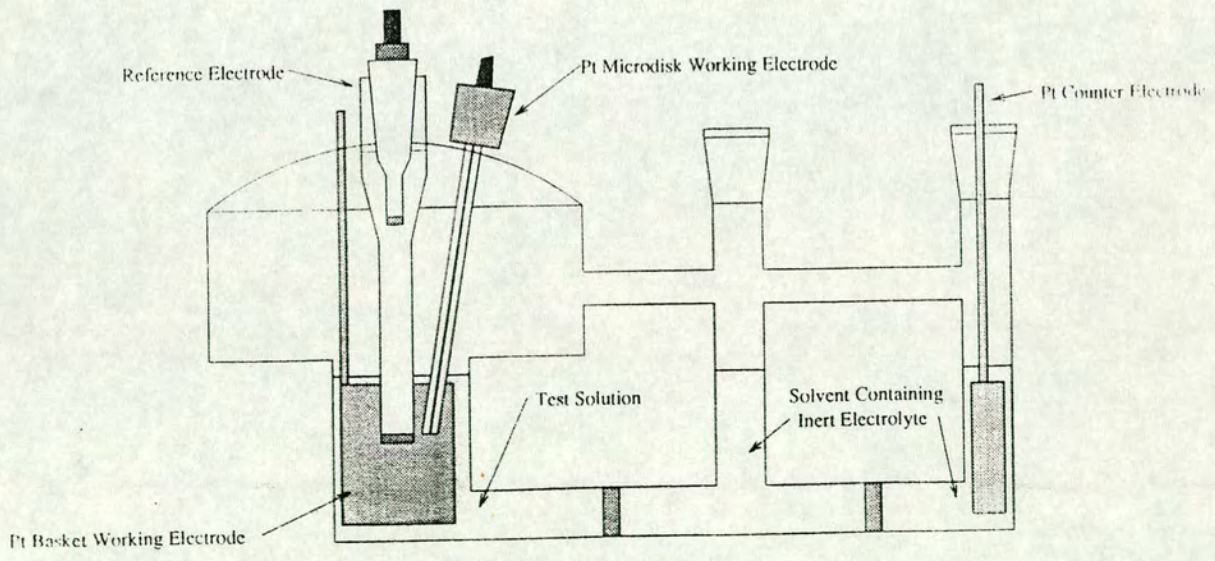

1.2.2 : Electrode design

When considering the design of electrodes in electrochemistry experiments, a primary concern is the minimisation of any potential drop. Firstly consider a two electrode cell, consisting of a working electrode and a non-polarisable reference electrode (see Figure 1.5). This set-up has an inherent resistance associated with the solution under examination, R_S. If the applied potential is E_{appl}, it can be seen that the potential at the working electrode, E, will be given by

$$E_{appl} = E + iR_S$$

Under conditions where either the current flow, i, or R_S is small, a two electrode cell may be used, as the potential drop is minimised. However, when electrochemical experiments are conducted in organic solvents, the high solution impedance results in a significant voltage drop.

To minimise this potential drop, we typically use a three electrode cell, as detailed in figure 1.3. In this configuration, the current is passed between the working electrode and the counter electrode, while the potential is measured relative to a reference electrode. The circuitry used to measure the potential has a very high resistance, and thus the current flow between working and reference is minimal. Therefore, the term iR_S is minimised. As essentially no current passes through the reference electrode, its potential will remain constant and equal to its open circuit value. The three electrode cell is therefore used in the majority of electrochemical experiments.

However, even in this system, the iR_S term is not completely negated. There is still a significant potential drop between the working and counter electrodes. The

Figure 1.5 : Simple 2 electrode cell

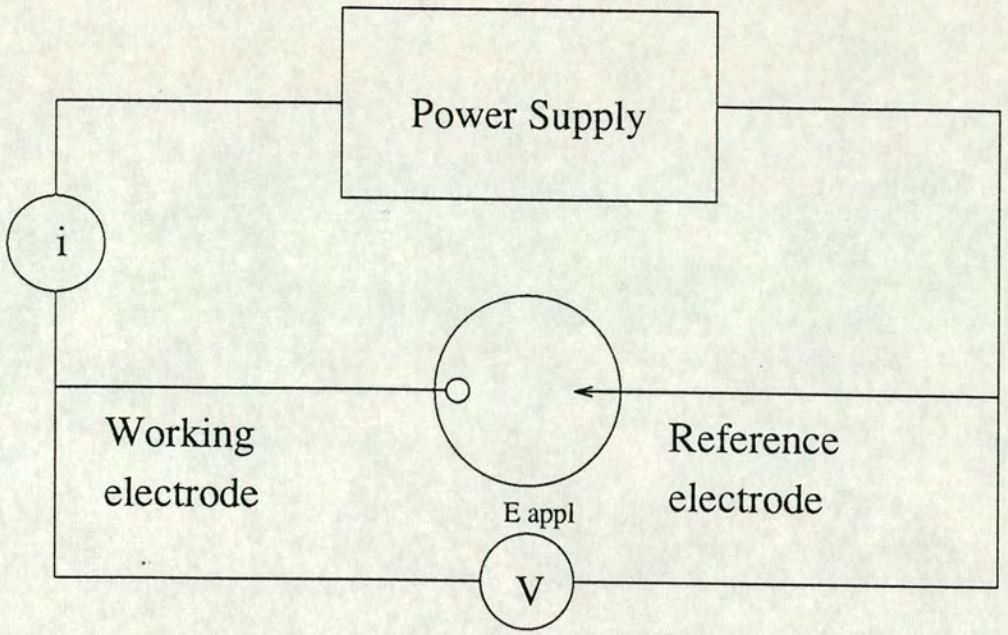

Figure 1.6 : Potential profile for three electrode cell

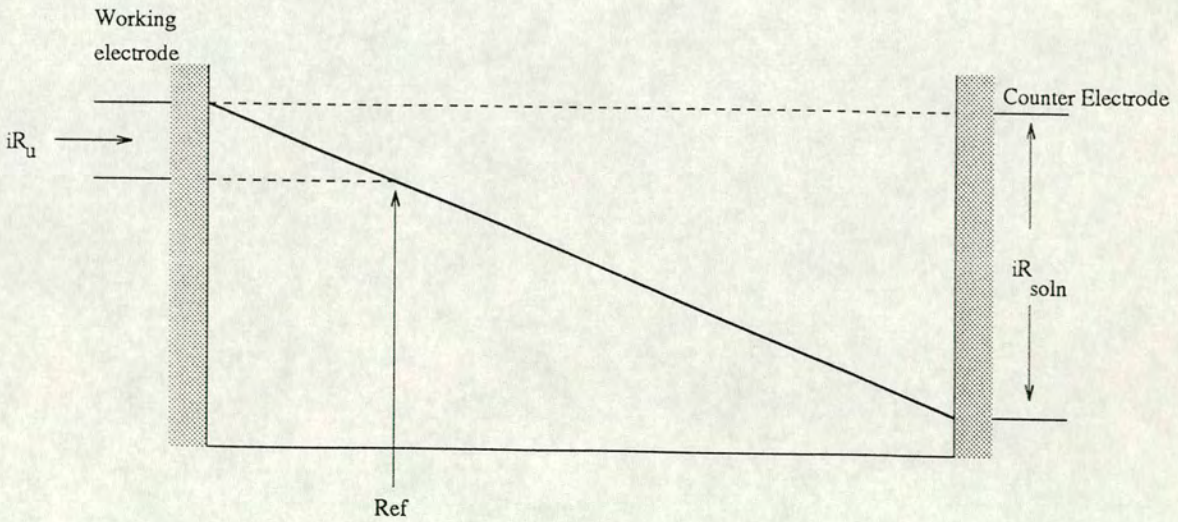

potential profile is detailed schematically in figure 1.6. If the reference electrode is placed anywhere bar the surface of the working electrode, a fraction of iR_S, denoted iR_U (R_U is the uncompensated solution resistance) will appear in the measured potential. The equation relating the applied potential to the potential at the w.e then becomes

$$E_{appl} = E + iR_U$$

For practical reasons, it is impossible to place the reference electrode on the working electrode surface. Too close a placement may result in non-uniform current densities at the electrode surface. Also, it may be desirable for the reference electrode to be protected from either the species under study, or that generated at the working electrode. Modern electrochemical experiments compensate for or suppress R_U by a number of methods, for example convolutive (semi-integral) methods or the use of positive feedback circuitry.

The minimisation of current flow through the reference electrode should leave it unpolarisable and stable. For these conditions to be applied, the reference electrode must fulfil certain requirements:

1. The redox process occurring within the electrode must be fully reversible, and hence follow the Nernst equation.
2. The potential must be independent of time or temperature.
3. The resistance of the component must be suitably high.
4. The electrode must neither contaminate, nor be contaminated by, the test solution.

In practice a salt bridge between the reference electrode and the solution is frequently used.

In this research, the reference electrode of choice was Ag/AgCl. The reference electrode was kept in a separate compartment in a dichloromethane solution containing 0.45M TBA BF_4 and 0.05M TBA Cl. In a small number of cases where this electrode was unsuitable, a platinum 'pseudo-reference' electrode was used. To standardise results and compensate for junction potentials due to the various solvents used, all electrochemical experiments were corrected against ferrocene (E^0 Fc/Fc^+ = 0.55 V vs. Ag/AgCl).

In all voltammetric experiments, a micro-platinum working electrode was used. Typically the surface area was 1 mm^2, the disk being set in soft glass. In coulometric experiments, a platinum basket electrode was used, to ensure rapid current flow and generation of the species of interest. Platinum was also used for the counter electrode. Platinum is used because it is stable over a wide range of potentials, is inert, and has a low impedance. In the case of the working electrode, the platinum surface is frequently polished using fine emery paper, then washed with distilled water. The electrode is then electrochemically conditioned by scanning to positive and negative potentials in the solvent/electrolyte system to be employed.

1.2.3 : Solvent

The choice of solvent is another important factor in the design of an electrochemical experiment. The sample to be studied must be sufficiently soluble in the solvent. The solvent should be liquid over the temperature range of interest. There should also be a suitably large potential 'window' in which the solvent undergoes no redox behaviour of its own.

Other factors that may be taken into consideration are vapour pressure, dielectric constant, toxicity and donor or co-ordinating properties. In this research a range of solvents have been used, with the most common being dimethylformamide (DMF) and acetonitrile.

1.2.4 : Supporting Electrolyte

The supporting electrolyte's primary function is to raise the conductivity of the test solution so that it does not act as a limiting factor in current flow. It is typically used in concentrations between 0.1M and 0.5M, depending on the solvent used. The reduced resistance lowers the value of iR_U, thus minimising the difference between applied and actual voltage (see 1.2.2).

The electrolyte also governs the structure of the electrical double layer at the electrode/solution interface, and the vast excess of electrolyte over test species ensures that the mass transport of the test species will be diffusion controlled.

An ideal supporting electrolyte should be highly soluble in the chosen solvents, be electrochemically and chemically inert, and be easily prepared and purified. In this work, the electrolyte of choice was tetrabutylammonium tetrafluoroborate (TBA BF_4) which was usually used at a concentration of 0.1 M, except for experiments in dichloromethane, when a concentration of 0.5 M was employed.

1.3 : Electrochemical Techniques

Before discussing the actual experimental techniques utilised, it is necessary to consider the types of process that can occur at the electrode surface and the stability of the species formed there.

If we firstly consider what can happen to the redox active species as a result of the electron transfer process, there are three possibilities:

1. The redox pair formed is, on the time scale of the experiment, stable under the prevailing conditions. The reaction fits the equation

$$[Ox] + ne^- \leftrightarrow [Red]$$

Such a system is chemically reversible.

2. The species formed undergoes a rapid chemical reaction after the redox process. The species may isomerise, decompose or react with other moieties present in the solution. This type of reaction fits the equation

$$[Ox] + ne^- \rightarrow [Red] \rightarrow [X]$$

This kind of system is described as chemically irreversible.

3. The species formed undergoes a slow chemical reaction after the redox process. Thus some of the product decomposes. In cyclic experiments, such a system will exhibit a partial return peak. This system is described as partially or semi- reversible.

For the second two cases the experimental conditions may be varied in order to attempt to make the system more reversible. In cyclic techniques the scan rate may be increased, in order to give the redox product less time to react. Alternatively, the temperature of the test solution may be lowered, in order to inhibit the following chemical reaction.

The other factor that can affect the nature of the process observed is the electron transfer step at the working electrode surface. Again, three possibilities exist, all of which will be discussed with respect to a chemically reversible redox system.

1. The charge transfer occurs at a rate faster than that with which the test species diffuses up to the electrode surface. Such a system is electrochemically reversible. It is also known as a Nernstian process, as it will obey the modified Nernst equation,

$$E - E^0 = (RT/nF)\ln(C_O/C_R)$$

where C_O and C_R are the concentrations of oxidised and reduced species respectively, E is the potential at the working electrode and E^0 is the standard potential for the redox couple involved.

2. The charge transfer process occurs at a rate comparable with the rate of diffusion. Thus the rate of electron transfer is affected by both the diffusion and charge transfer kinetics. Such a situation is described as quasi-reversible. This kind of behaviour often yields results which initially resemble reversible processes, but can easily be distinguished by variation of the experimental parameters.

3. The charge transfer process occurs considerably slower than the diffusion of the test species, thus making the electron transfer rate dependant on diffusion kinetics. Such a system is electrochemically irreversible, but should not be confused with a chemically irreversible process.

It is also desirable to define the standard terms used when discussing mass transport in test solutions.

1. Migration - movement of charged bodies due to the influence of an electric field.

2. Diffusion - movement of a species along a concentration gradient.

3. Convection - stirring (forced convection) or hydrodynamic transport (natural convection).

1.3.1 : Cyclic Voltammetry

Cyclic voltammetry is perhaps the most commonly employed electrochemical technique. The ease of use, coupled with the minimal amount of test species required (typically 10 to 20 mg) make it ideal for preliminary investigation of new products. The data gained can be used to give an indication of the exact nature of the species, or for many other purposes (e.g. reaction rates, dissociation constants and other physical properties can be determined by use of the appropriate experiment).

Cyclic voltammetry is typically carried out in a simple three electrode cell (see Figure 1.3). The solution is 'quiet' (unstirred) during the experiment. The large excess of supporting electrolyte and carefully chosen experimental conditions ensure that convection and migration effects are eliminated for the test species, thus leaving diffusion as the only means of mass transport.

In a cyclic voltammetric experiment, the potential applied to the test solution is varied linearly with time, starting at a potential E', and moving to a switching potential, E_λ, whereupon the potential is reversed to return to E'. The potential profile of this procedure is shown in Figure 1.7. The rate of potential change or scan rate, ν, is usually in the range 20 - 500 mVs^{-1}. The current, i, is recorded as a function of E.

A typical cyclic voltammagram for a fully reversible process is shown in figure 1.8. The current response for this type of process yields an asymmetric peaked pattern. The reasons for this trace shape can be outlined as follows:

The potential firstly sweeps 'forward'. As E approaches $E^{o'}$ (the formal potential of the redox process under study) reactant at the electrode starts to be either reduced or oxidised, as appropriate, and a current starts to flow. As the potential continues to

Figure 1.7 : Potential profile for cyclic voltammetry

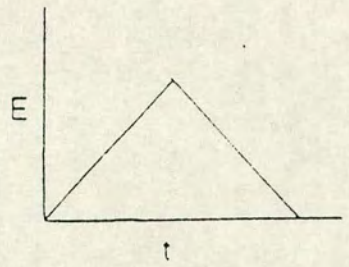

Figure 1.8 : Typical cyclic voltammagram for a reversible system

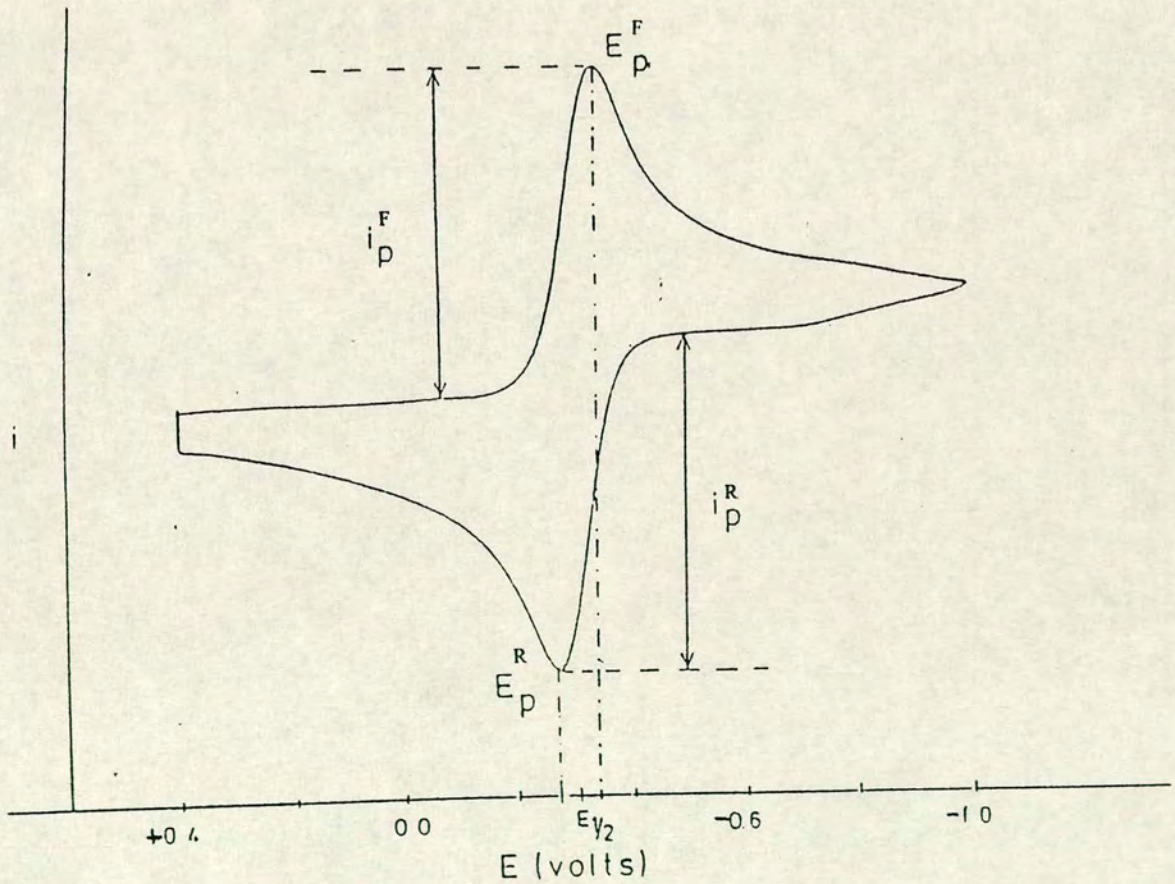

move towards $E^{0'}$, depletion of test species at the working electrode induces diffusion of more test species to the electrode surface. Due to the rapid charge transfer inherent in a reversible system, as E passes $E^{0'}$ the concentration of unreacted test species at the electrode surface falls towards zero, and the current flow reaches a maximum. As the depletion of the test species becomes more widespread throughout the test solution, the current falls off until it reaches a level determined by the diffusion of fresh test species to the electrode surface. At this point the current is 'diffusion controlled'. As a result, the observed current rises sharply as E approaches $E^{0'}$, reaches a maximum shortly after $E^{0'}$, and then falls off to a diffusion controlled current, i_d.

Upon reaching the pre-set 'switching potential' E_λ, the potential begins to sweep back towards the initial voltage. The resulting current flow is essentially that seen for the forward scan, only in reverse, and starting from the current at E_λ, rather than zero current. Thus the maximum current on the reverse sweep is the other side of $E^{0'}$ than that seen for the forward scan.

As previously stated (see section 1.3), a fully reversible process conforms to the Nernst equation. It is therefore possible to treat the current/potential trace for such a system in a purely mathematical manner. The most useful and interesting parameters that can be derived from such a system are the peak current and potential at the maximum of the forward wave (i_P^F and E_P^F respectively) and the corresponding parameters for the return wave (i_P^R and E_P^R). By measuring these parameters for a number of scan rates, we can determine the nature of the process at the electrode. The variations seen for non-reversible processes are detailed in Table 1.1.

For a Nernstian system, equations to determine E_P^F and i_P^F can be derived. It can be shown that the half-wave potential can be represented by

$$E_{½} = E^{0'} + (RT/nF) \ln(D_O/D_R)^{½}$$

where D_O and D_R are the diffusion constants of the oxidised and reduced species respectively. Usually the value of D_O/D_R is close to unity, and thus $E_{½} \approx E^{0'}$. Thus

$$E_P^F - E_{½} = E_P^F - E^{0'} - (RT/nF) \ln(D_O/D_R)^{½}$$

The current at any point on the forward scan can be shown to be

$$i = nFAC_O^*(\pi D_O \sigma)^{½}\chi(\sigma t)$$

where $\sigma = (nFV/RT)$ and $\chi(\sigma t)$ is a dimensionless function representing the normalised current. The value of $\sqrt{\pi}\chi(\sigma t)$ can be determined as a function of $n(E - E_{½})$. This can be shown to reach a maximum of 0.4463 at $n(E - E_{½}) = -28.5$ mV[15]. Thus i_P can be expressed as

$$i_P = 0.4463nFAC_O^*(nF/RT)^{½}\nu^{½}D_O^{½}$$

At 298 K, this becomes

$$i_P = (2.69 \times 10^5)n^{3/2}AD_O^{½}\nu^{½}C_O^*$$

and

$$E_P - E_{½} = -28.5/n \text{ mV} = -1.109(RT/nF)$$

therefore, for a reversible process, E_P is independent of scan rate, and i_P is proportional to $\nu^{½}$.

Table 1.1: Cyclic Voltammetry parameters for different classes of charge transfer process at 298K

Reversible	E_P independent of ν
	$E_P^F - E_P^R = 59/n$ mV, independent of ν
	$\frac{1}{2}[E_P^F + E_P^R] = E_{\frac{1}{2}}$, independent of concentration
	$i_P/\nu^{\frac{1}{2}}$ constant
	$i_P^F/i_P^R = 1$
Quasi-reversible	E_P shifts with ν
	$E_P^F - E_P^R$ increases as ν increases
	$i_P/\nu^{\frac{1}{2}}$ is not independent of ν
	i_P^F/i_P^R generally = 1
Semi-reversible	At low ν, E_P increases by 30/n mV per ten fold increase in ν
	$i_P/\nu^{\frac{1}{2}}$ is not independent of ν
	$i_P^F/i_P^R < 1$, increases as ν increases
Irreversible	E_P shifts with ν
	$i_P/\nu^{\frac{1}{2}}$ is not independent of ν
	No current on reverse scan

ν = scan rate in mVs^{-1}

n = number of electrons involved in the redox process under consideration

1.3.2 : Stirred Linear Voltammetry

It is not possible to tell directly from a cyclic voltammagram whether an observed process is an oxidation or a reduction. Often stirred linear voltammetry is used. Figure 1.9 shows typical cyclic and stirred voltammagrams for a reversible process.

This technique involves stirring the solution in a standard three electrode cell, allowing mass transport by diffusion and convection. Thus the concentration of oxidised and reduced forms of the test species are even throughout the solution, and no reduction in current is seen (only a small fraction of the total amount of test species is consumed). The scan rate used is typically 20 mVs^{-1}. The diffusion limited current, i_d, is proportional to n, the number of electrons involved in the process. Therefore, this technique may be used to deduce the relative number of electrons involved in a process, by comparison of i_d for all observed processes. By convention, traces with positive i_d represent reductions, while those with negative i_d are oxidations. A rotating disc electrode is usually employed as a working electrode in this experiment as it achieves the most efficient method of stirring the solution.

1.3.3 : Alternating Current (AC) Voltammetry

Alternating current voltammetry uses a linear direct current (dc) potential scan, with a small sinusoidal component imposed. The frequency of the alternating potential, ω, is typically 10 - 100 Hz. Because of the sinusoidal voltage, an alternating current flows in addition to the expected dc response. The net ac component is recorded against the linear applied potential.

Figure 1.9 : Typical stirred and unstirred voltammagram

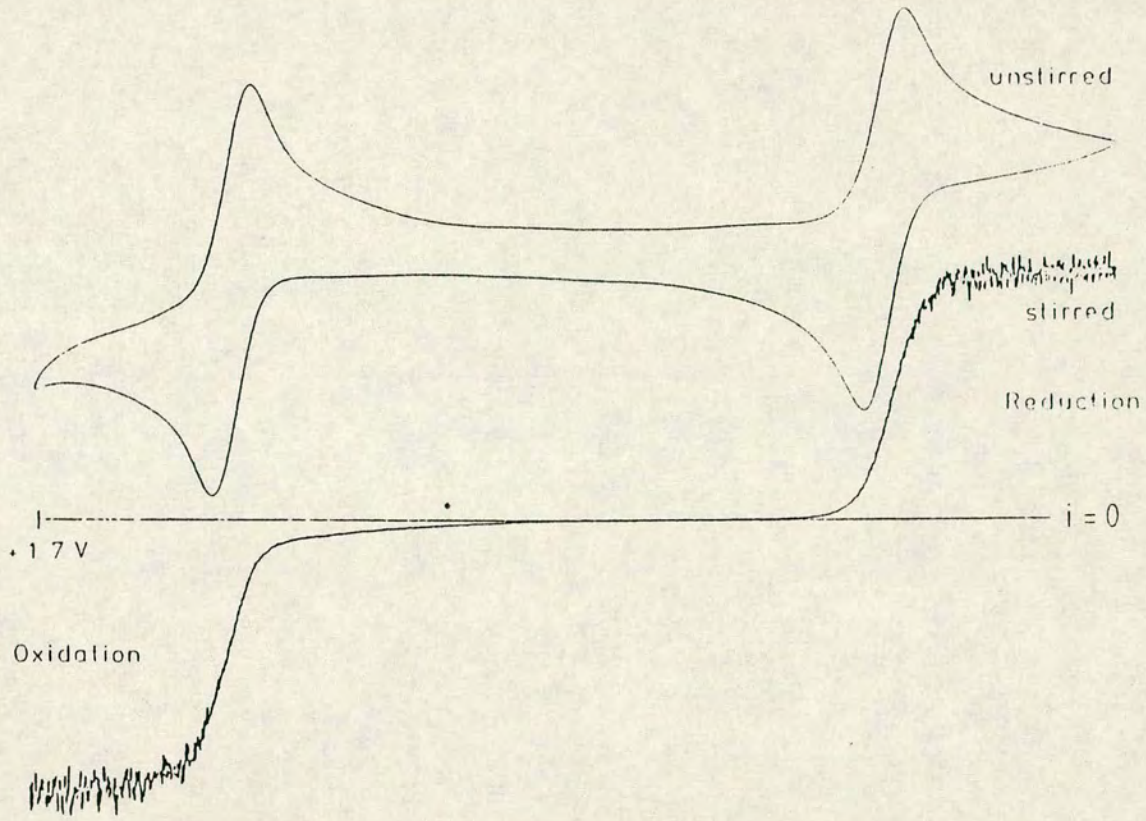

Figure 1.10 : Typical ac voltammagram for a reversible process

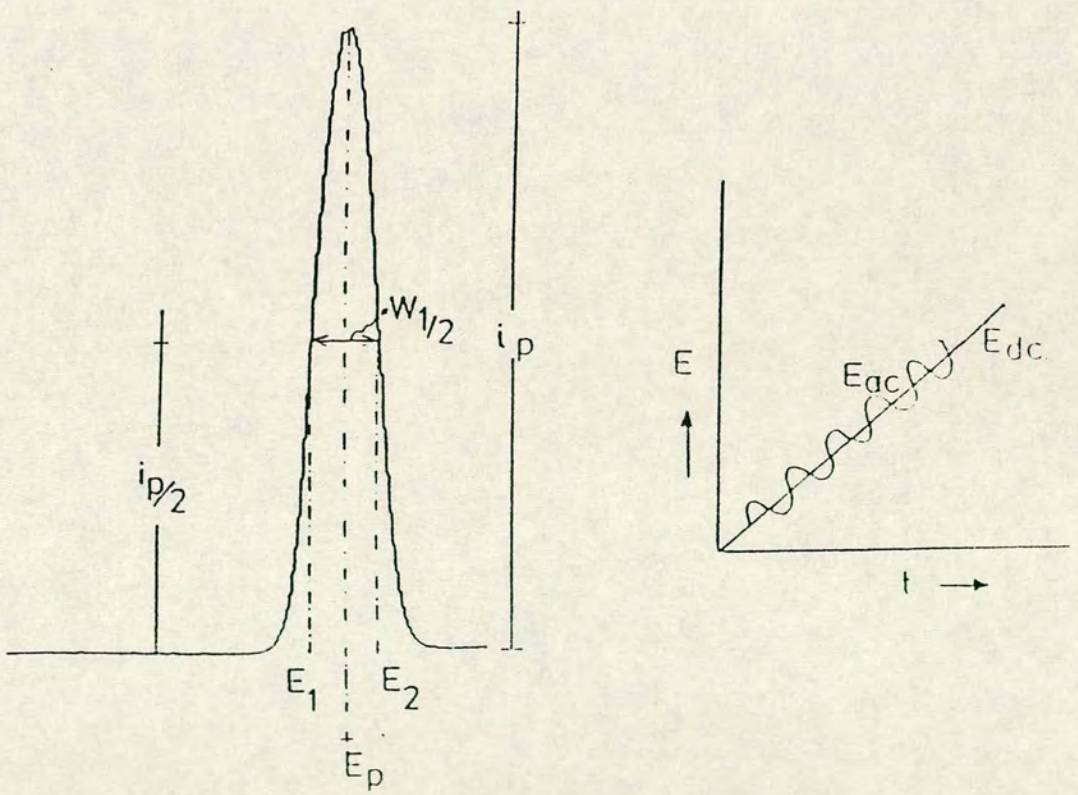

The typical response for an ac voltammetry experiment involving a reversible system is shown in figure 1.10. The peak is symmetric, and has maximum current, i_p, at $E = E_{½}$ for the system under consideration. In this technique, i_p is proportional to the square of the number of electrons involved, as can be seen from the equation

$$i_p = n^2F^2A\omega^{½}D_O^{½}C_O^{*}\Delta E/4RT$$

where A is the area of the electrode, D_O is the diffusion coefficient of the species, C_O^{*} is the bulk concentration of the test species, and ΔE is the magnitude of the superimposed alternating potential.

In a simple view, the ac trace can be thought of as a 'first derivative' of the related dc wave, and indeed this analogy is useful for considering the shape of the ac trace. It is, however, incorrect to view the ac voltammagram only in this light. The experiment provides more information than cyclic voltammetry, through the addition of another variable, ω, which effectively controls the 'timescale' of the experiment. The simple 'first derivative' model fails to explain the relationship between i_p and ω.

Alternating current voltammetry is also more sensitive than dc alternatives, as it can discriminate against background current. This is because the capacitative (background) and faradaic (due to the test species) currents have different phase relationships with the applied voltage. Therefore by phase sensitive detection, the faradaic current can be recorded. The resolution of separate processes is also better for ac voltammetry. Processes with half wave potentials separated by as little as 40mV may be distinguished, whereas dc techniques usually require a separation of 150mV for complete elucidation.

Ac voltammetry can also be used to investigate the reversibility of a process. A reversible process will fit the following criteria.

1. E_p independent of ω; $W_{½}$ (half peak width) is 90/n mV at 298K and is also independent of ω.

2. A plot of i_p vs. $\omega^{½}$ yields a straight line through the origin.

1.3.4 : Electrosynthesis - Coulometry

Preparative scale electrosynthesis can be performed by two methods, either galvanostatic (controlled current) or potentiostatic (controlled potential). During this research, all electrosynthetic processes were carried out by potentiostatic methods.

In coulometry, the cell previously detailed (see Figure 1.4) is used. A constant potential is maintained at the working electrode. For the electrogeneration to go to completion, the applied potential must be at least 60mV beyond $E_{½}$ for the process under consideration.

The current is measured as a function of time, and the solution is stirred throughout the experiment. A typical i vs. time trace is shown in figure 1.11. The area under the curve yields the total charge, Q, passed during the experiment. Thus, assuming 100% efficiency in conversion, we can calculate n by using the equations

$$Q = \int_0^t i\, dt \qquad \text{and}$$

$$Q = nFM$$

where M is the number of moles of starting material.

Figure 1.11 : Current-time response for controlled potential electrolysis

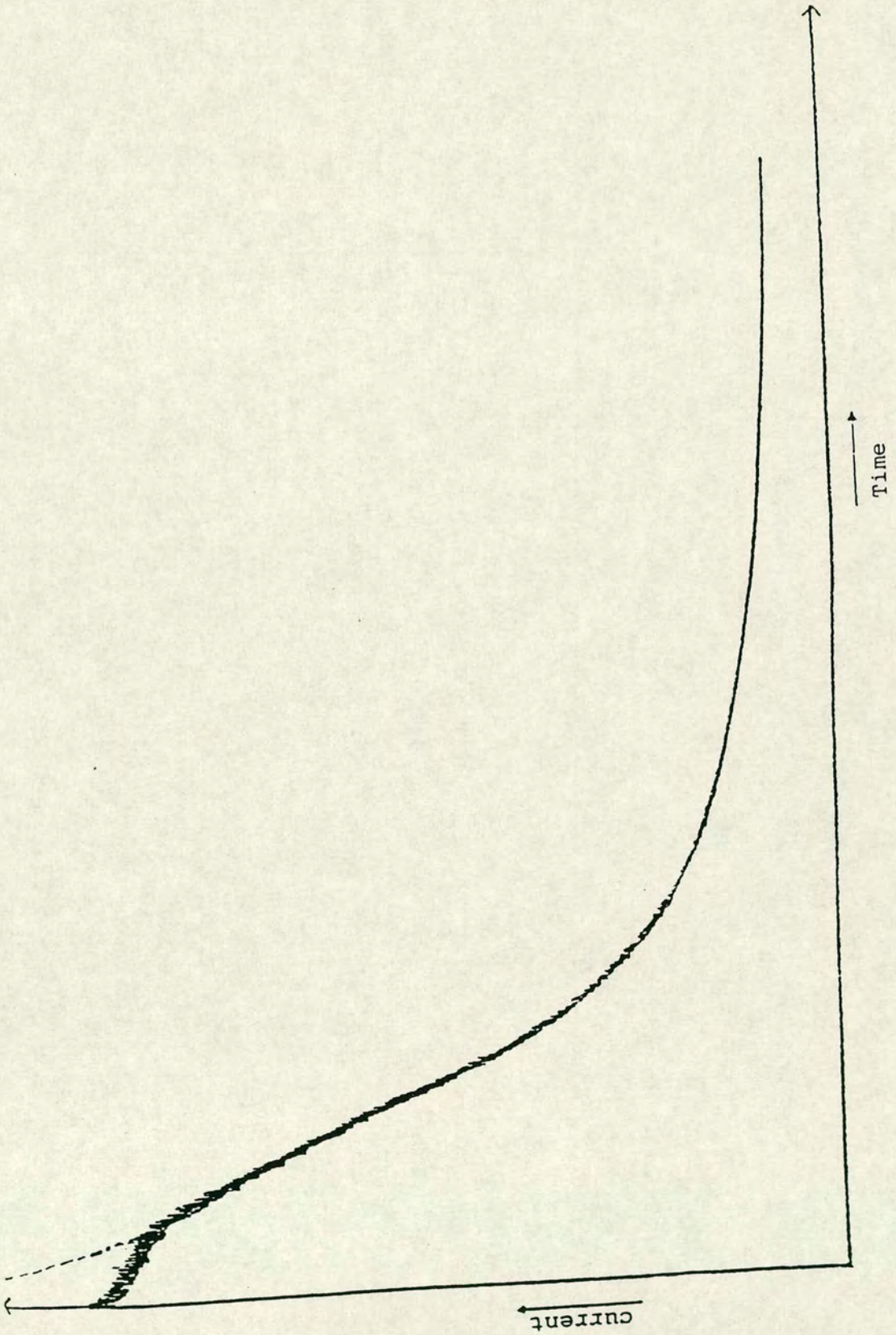

1.4 : Spectroelectrochemistry

Although some electrosynthetic experiments are carried out to investigate or confirm the number of electrons involved in a given electrochemical process, many are carried out with the aim of studying the product generated. This is usually achieved by the use of various spectroscopic techniques. The interest in studying the electrogenerated species becomes greater when the starting material contains more than one redox active site (in which case interest often revolves around which site was actually involved), or when the electrosynthesis has been carried out to induce a subsequent chemical reaction (in which case identification of the products is of paramount importance).

Unfortunately, in many cases the generated species is subject to decomposition, perhaps from oxygen, moisture, heat or other source. For whatever reason, this means that the transfer of the generated species from the electrochemical cell to the spectroscopic one, and then transfer to the spectrometer, can allow the species of interest time and opportunity to decompose. In order to overcome this problem, spectroelectrochemical techniques have been developed, essentially involving generation of the species of interest within the cavity of the spectrometer. Hence a spectroelectrochemical cell is a coulometric three electrode cell designed to fit the requirements of a certain type of spectroscopy.

1.4.1 : Electronic Absorption Spectroelectrochemistry

A cell suitable for UV/VIS/NIR spectroelectrochemistry must fulfil two main criteria.

1. It must be able to perform rapid electrogeneration within the light beam path of the spectrometer.
2. The working electrode cannot have a significant effect on the spectrum observed (i.e. it must be optically transparent).

Within this department, an Optically Transparent Electrode (OTE) cell was designed and built[16], keeping these requirements in mind, and adhering to the principles described by Murray and co-workers[17]. A schematic diagram of the OTE cell is given in figure 1.12.

The working electrode consists of a fine platinum gauze, reinforced with 10% rhodium. This allows light to pass through, whilst giving a large surface area to facilitate rapid electrogeneration. The resulting small drop in transmittance is dealt with by background correction. The small path length of the quartz cuvette (typically 0.5 mm) also aids rapid electrogeneration. The counter and reference electrodes are separated from the test solution by frits, and are locate within the upper reservoir of the cell.

The cuvette/cell assembly sits in a gas tight PTFE block with two sets of quartz windows, as seen in the figure. A constant flow of nitrogen passes between the inner windows, ensuring that the atmosphere surrounding the cell is free from oxygen and moisture. This set up also allows convenient temperature control. By passing the nitrogen flow through a coil immersed in liquid nitrogen, and carefully controlling the

Figure 1.12 : Schematic of the OTE cell

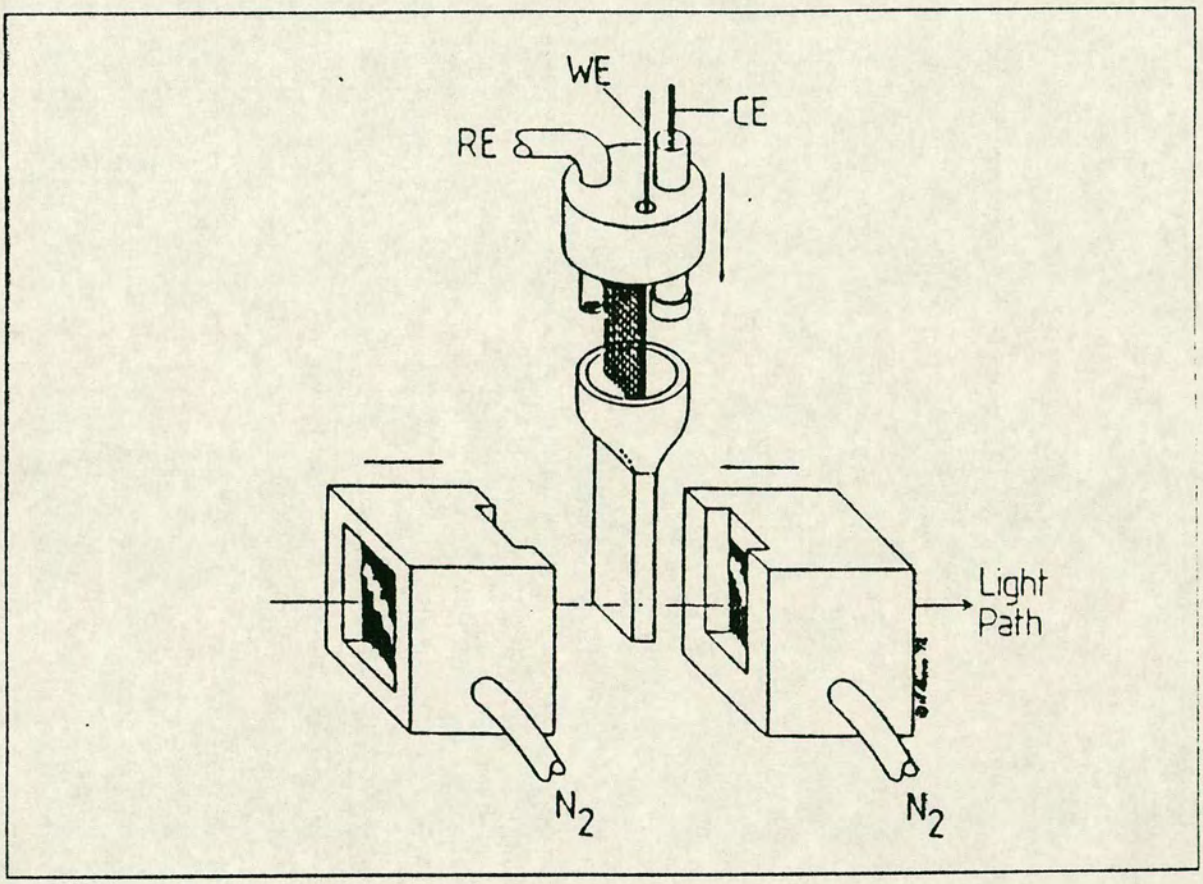

gas pressure, temperatures can be accurately controlled. To prevent fogging of the inner windows by moisture condensing and freezing on the outside, a stream of dry, room temperature nitrogen is passed between the inner and outer windows.

During this work, two types of spectroelectrochemical experiments were carried out utilising the OTE cell.

1. A potential, usually 100 - 200 mV beyond $E_{½}$ for the system under investigation, was selected. A series of spectra were recorded, overlaid upon each other, as a function of time, until the reaction had achieved equilibrium and no more changes in the spectrum were seen.

2. A series of potentials, from one side of $E_{½}$ to the other, were selected. The system would be allowed to equilibrate at each potential before the spectrum was recorded. This type of experiment allows the determination of $E_{½}$ for a Nerstian system.

The Nernst equation is

$$E = E^{0'} + (RT/nF)\ln(C_O/C_R)$$

Experimentally, C_O/C_R is equal to the absorbance ratio, $r(\varepsilon)$, given by

$$r(\varepsilon) = [A(E) - A_R]/[A_O - A(E)]$$

where, for a chosen wavelength, A(E) is the absorbance at potential E, A_R is the absorbance for the fully reduced form and A_O is the absorbance for the fully oxidised form. Thus, for a Nerstian system, a plot of E vs. ln $r(\varepsilon)$ will yield a straight line of slope RT/nF and intercept $E_{½}$.

When performing such an experiment, it is important that the supporting electrolyte has no significant absorptions in the window studied. As such, TBA BF_4 is

ideal for this application as well, and was employed in the same amounts as for electrochemical experiments.

As a final point, it should be noted that, when carrying out spectroelectrochemical experiments on systems believed to be Nerstian, that the process should be reversed and the starting species regenerated. Successful regeneration of the initial spectrum is an excellent test for the chemical reversibility of the process.

An example of the results obtained using the OTE cell is shown in figure 1.13. This shows the oxidation of dicyanobis(bipyridyl)iron(II), in MeCN, at a potential of +0.8 V versus Ag/AgCl. In this case, oxidation results in the collapse of the MLCT bands at around 16000 and 25500 cm^{-1}, and the lessening of the intensity of the intraligand transition at 33000 cm^{-1}. The presence of isosbestic points at 28500, 32500 and 36000 cm^{-1} indicates that no intermediates were formed which absorbed at these energies, and suggests that the oxidation process is a simple one step process, with the product undergoing no further reaction.

Figure 1.13 : Absorption spectral monitoring of $[Fe(bpy)_2(CN)_2]$ in MeCN

E_{appl} = + 0.8 V, T = 243 K

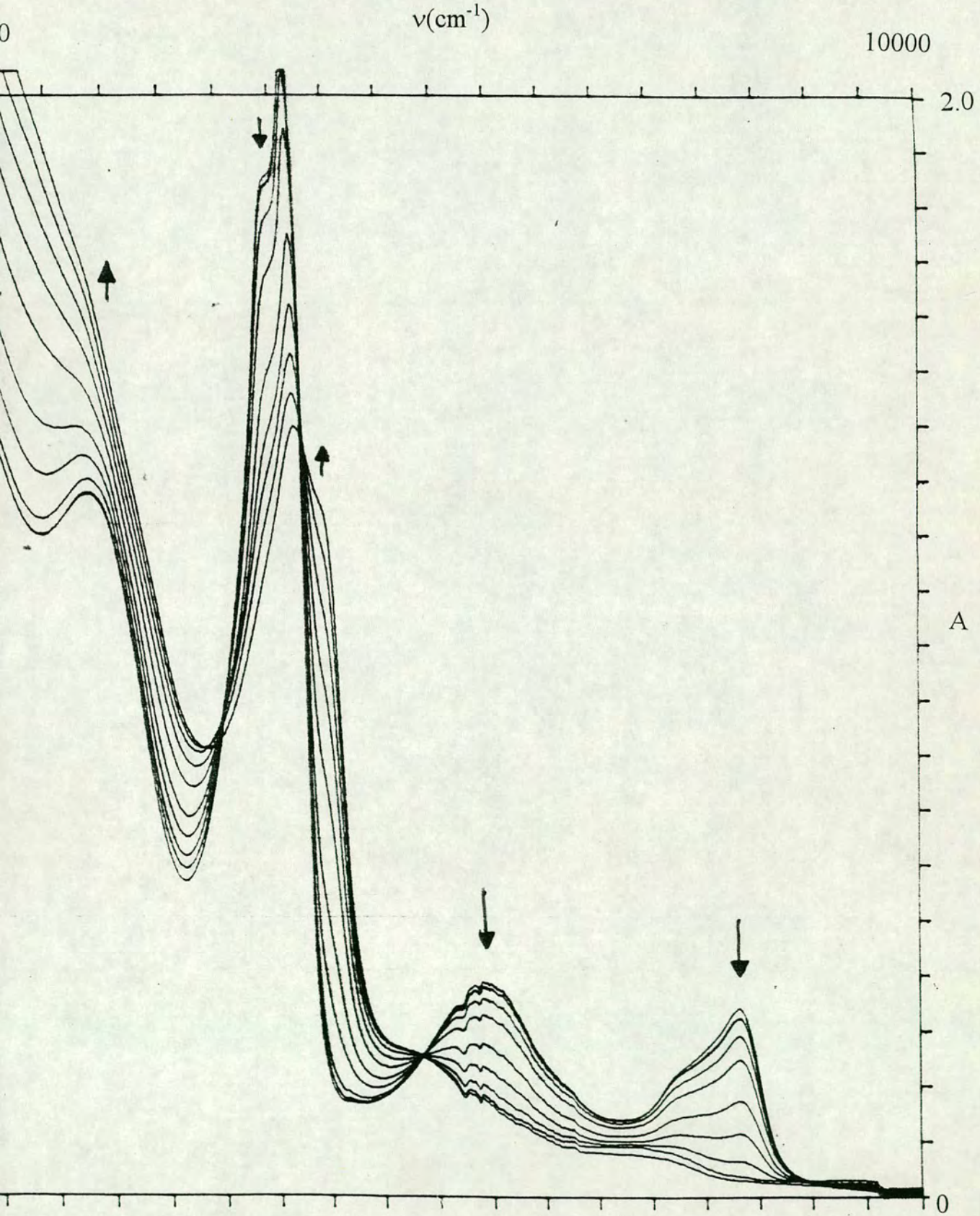

1.5 : References

1. J.F. Hunsberger, *Handbook of Chemistry and Physics, 59th edition*, CRC Press, **1978**, D-193
2. D.F. Shriver, P.W. Atkins, C.H. Langford, *Inorganic Chemistry, 2nd Edition*, Oxford University Press, **1994**
3. G.A Heath, L.J. Yellowlees, P.S. Braterman, *J. Chem. Soc. Chem. Comm.*, **1981**, 287
4. J.N. Demas, A.W. Adamson, *J. Am. Chem. Soc.*, **1971**, 93, 1800
5. L.J. Yellowlees, Ph.D. thesis, University of Edinburgh, **1982**
6. C. Creutz, N. Sutin, *Inorg. Chem.*, **1976**, 15, 496
7. B. Durham, W.J. Dressick, T.J. Meyer, *J. Chem. Soc. Chem. Comm.*, **1979**, 381
8. V. Balzani, F. Bolletta, M.T. Gandalfi, M. Maestri, *Top. Curr. Chem.*, **1978**, 75, 1
9. D.F. Shriver, P.W. Atkins, C.H. Langford, *Inorganic Chemistry*, Oxford University Press, **1994**, Chapter 19, 782
10. C.A. Bignozzi, F. Scandola, *Inorg. Chem.*, **1984**, 23, 1540
11. Y. Lei, T. Buranda, J.F. Endicott, *J. Am. Chem. Soc.*, **1990**, 112, 8820
12. B. Boitrel, A. Lecasnawrocka, E. Rose, *Tetrahedron Letters*, **1992**, 33(2), 227
13. T.K. Jones, C. McPherson, H.L. Chen, M.J. Kendrick, *Inorg. Chim. Acta*, **1993**, 206(1), 5
14. C.A. James, W. Woodruff, *Inorg. Chim. Acta*, **1995**, 229(1-2), 9
15. W.H. Reinmuth, *J. Am. Chem. Soc.*, **1957**, 79, 6358

16. V.T. Coombe, Ph.D. thesis, University of Edinburgh, **1985**

17. W.R. Heinemann, R.W. Murray, G.W. O'Donn, *Anal. Chem.*, **1967**, 39, 1666

The following works were also referenced extensively during the preparation of this introductory chapter.

A.J. Bard, L.R. Faulkner, *Electrochemical Methods, Fundamentals and Applications,* Wiley, **1980**

J. Koryta, J. Dvorak, L. Kavan, *Principles of Electrochemistry, 2nd Edition,* Wiley, **1993**

Chapter 2 : Solvent dependent behaviour of $M(bpy)_2(CN)_2$ (M = Fe, Ru or Os)

2.1 : Introduction

This chapter discusses the UV/VIS/NIR absorption spectra, electrochemistry, spectroelectrochemistry, and, where possible, EPR spectra of complexes of the form $M(bpy)_2(CN)_2$ (M = Fe, Ru, Os) and their oxidised and reduced analogues, paying particular attention to the effect of solvent upon these properties.

The iron complex, dicyanobis(2,2'-bipyridine)iron(II) ($Fe(bpy)_2(CN)_2$), was first reported in 1934[1], and further discussed in 1960 when Schilt reported the synthesis and properties of a range of iron complexes with mixed cyanide and aromatic diimine ligands[2]. Although many of these complexes appeared to show solvent dependent behaviour in their visible absorption spectra, very little further investigation has been carried out. Work by Burgess[3], involving $Fe(bpy)_2(CN)_2$ and a range of related species, indicated that this solvent dependent behaviour often gave a reasonable correlation with the solvent parameter E_T, although results from hydroxylic and non-hydroxylic solvents were treated separately. Other work described the effect of mixed solvent systems on the complexes visible absorption spectrum[4]. Later work by Toma and Takasugi[5] also investigated this behaviour, and noted the effect changing the composition of the mixed solvent system had on the $iron^{II/III}$ oxidation potential, namely that the potential increases linearly with the Acceptor Number (A.N.) of the water/acetonitrile solvent mix used.

In contrast, dicyanobis(2,2'-bipyridyl)ruthenium(II) ($Ru(bpy)_2(CN)_2$) has been investigated in much greater depth. Much of this interest stems from expected similarities in behaviour for this complex and tris(2,2'-bipyridyl)ruthenium(II). As noted in chapter 1, $[Ru(bpy)_3]^{2+}$ has a long lived, readily accessible excited state, and is one of the most studied inorganic species in recent years. As a result, there has been a great deal of interest in related species, often as 'building blocks' for supramolecular assemblies allowing transfer of the promoted electron away from the absorption site,

with the aim of extending the lifetime of the excited state, and using the species as a solar dye.

The complex was first prepared by Schilt[6], and further initial investigations were carried out by Demas *et al*[7] and Bryant *et al*[8]. Demas' work described the effect of changing the solvent from methanol to DMF on the visible spectrum of the complex, whereas Bryant's work describes the spectrum in DMSO and methanol. Much of the further work on the complex has investigated its' excited state properties[9,10] and its' usefulness as a building block in supramolecular species[11,12]. However, work by Fung and co-workers[9] did investigate the solvent dependence of the complex, although the main part of the work was concerned with the emission spectra of the complex and its' reduction products.

The related osmium species, dicyanobis(2,2'-bipyridyl)osmium(II) ($Os(bpy)_2(CN)_2$), was also first prepared by Schilt[6]. As for the iron analogue, further work has been significantly less than for the ruthenium complex, although osmium bpy unit is often used as a 'building block'[13-16], frequently in conjunction with the ruthenium centre[15,16]. However, little work has been carried out investigating the effect of the solvent on the electrochemistry and spectrochemistry of the complex.

2.2 : Solvent Parameters

Over the years, a number of different approaches have been taken in an attempt to correlate the observed behaviour of compounds in different solvents with properties of the solvents themselves. Some methods use measurable physical properties of the different solvents. Others use a standard property of a single compound in a range of solvents. We generally consider this second kind of approach in this work. In all cases, the aim of the resulting scale is to predict the behaviour of other species in the range of solvents the parameter has been established for.

In the course of this work we considered five different solvent parameters :- D_S, Z, E_T, Acceptor Numbers (A.N.) and Donor Numbers (D.N.). These parameters are determined by the following methods.

2.2.1 : D_S

D_S is the bulk dielectric constant of the solvent, and is a unitless quantity. The dielectric constant is given by Coulomb's law, describing the force acting on two electric charges, of magnitude e_1 and e_2, as in

$$F = e_1e_2/D_Sr^2$$

where r is the distance between the charges.

The value of D_S can be determined by use of a capacitor with capacitance C_0 when the cavity of the capacitor is evacuated. If the capacitance is C when the cavity is filled with the solvent in question, then D_S is given by

$$D_S = C/C_0.$$

More commonly, D_S is determined by comparing the capacitance when the solvent is in the cavity, with that when a standard is used, often benzene (D_S = 28.2). The relationship then becomes

$$D_1/D_2 = C_1/C_2$$

where D_1 and D_2 are the dielectric constants of the experimental and standard solvents respectively, and C_1 and C_2 are the appropriate capacitances.

2.2.2 : Z

Z values were defined by Kosower[17]. They are an extension of the Y values proposed by Grunwald and Winsten[18]. The Z values are based on the UV spectrum of 1-ethyl-4-carbomethoxypyridinium iodide in a wide range of solvents. The Z value for a solvent is actually the energy of the solvent dependent band, expressed in kcal. The values obtained, however, are usually expressed as unitless. Kosower theorised that the energy of the charge transfer band due to this compound was characteristic of the 'solvent polarity' or 'ionising' properties of the solvent.

2.2.3 : E_T

The E_T scale for solvents was proposed by Dimroth and Reichardt[19]. This scale is based on the energy of an intramolecular charge transfer of a substituted pyridinium phenol betain, shown as figure 2.1. As for Kosower's Z values, the E_T

scale is the expression of the energy of the solvent dependent maximum in kcal. It too is usually given as unitless. However, while there is a reasonable linear correlation between E_T and Z values, there are sufficient discrepancies between the two to make a direct relationship untenable.

2.2.4 : Donor Number (D.N.)

This system of solvent parameters, along with Acceptor Numbers (A.N.), was proposed by Gutmann[20]. The Donor Number is defined as the molar enthalpy of the formation of the 1:1 adduct between the donor (D) and a 10^{-3} M solution of $SbCl_5$ in 1,2-dichloroethane, measured in kcal mol^{-1}. This is usually expressed as unitless, however. For some solvents, Donor Numbers have been extrapolated from nmr experiments, using the ^{23}Na chemical shift of sodium perchlorate, which has been shown to have a linear relationship with the value of D.N. for a range of solvents[21].

2.2.5 : Acceptor Numbers (A.N.)

This parameter was proposed by Gutmann[22], but is based on work by Mayer[23]. It is based on the ^{31}P nmr shift of triethyl phosphine oxide dissolved in pure solvent. To scale the results, hexane is used as a reference and assigned a value of 0, and the $Et_3PO \rightarrow SbCl_5$ complex is assigned a value of 100. The chemical shift in any solvent is extrapolated to infinite dilution and corrected for the difference in volume susceptibility between the solvent and hexane. This gives a corrected value δ_{corr}. The unitless Acceptor Number is then obtained from

$$A.N. = \frac{\delta_{corr}.100}{\delta_{corr(Et3PO.SbCl5)}} = \delta_{corr}.\ 2.348$$

The values of these five parameters for the range of solvents used in this work are given in table 2.1. From the table, it is clear that the different parameters lead to different orderings of the solvents, and thus each will give better correspondence with different systems. While the D.N. and A.N. scales have been designed to be as wide ranging as possible, and D_s is a purely physical measurement, we would expect the Z

and E_T scales to give best results with interactions similar to those used in the initial determination of the scale.

Table 2.1 : Solvent parameters for solvatochromic behaviour

Solvent	D_s	E_T	Z	D.N.	A.N.
Acetone	20.7	42.2	65.7	17.0	12.5
Pyridine	12.3	40.2	64.0	33.1	14.2
DMF	36.7	48.3	68.5	26.6	16.0
DMSO	49.0	45.0	71.1	29.8	19.3
MeCN	36.2	46.0	71.3	14.1	19.3
$MeNO_2$	38.6	46.3	N/A	2.7	20.5
CH_2Cl_2	8.9	41.1	64.2	N/A	23.1
EtOH	24.3	51.9	79.6	20	37.1
MeOH	32.6	55.5	83.6	19	41.3

Figure 2.1 : Structure of compound used to determine Z values

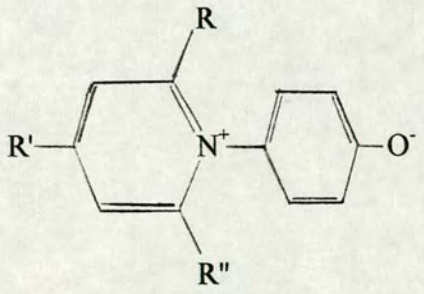

2.3 : Results and Discussion

2.3.1 : $Fe(bpy)_2(CN)_2$

The solvent dependent behaviour of bis(2,2'-bipyridyl)dicyanoiron(II) was first reported by Schilt in 1960[2]. This work noted the variation of the energy of the ^{1}MLCT band in the electronic absorption spectrum with solvent. The exact electronic nature of this transition was not known at the time, and so no firm conclusions about the relationship between band position and solvent could be drawn. Later work by Burgess[3] examined this phenomenon in a much larger range of solvents, and a correlation between MLCT band position and the solvent parameter E_T[20] was established for the related complex $Fe(4,7\text{-diMeophen})_2(CN)_2$.

After these early studies, attention appears to have shifted to the analogous ruthenium complex, due to its potentially more useful photochemistry.

A typical electronic spectrum for bis(2,2'-bipyridyl)dicyanoiron(II) in acetonitrile is shown in figure 2.2. Four transitions in the UV/VIS range may be observed. These transitions are generally assigned as a ^{1}MLCT band ($d \rightarrow \pi^*(1)$) at lowest energy, another ^{1}MLCT band ($d \rightarrow \pi^*(2)$), a bpy internal transition ($\pi \rightarrow \pi^*(1)$) and, at highest energy, a second bpy internal transition ($\pi \rightarrow \pi^*(2)$). The two highest energy bands are observed at slightly different energies in the spectrum of free bpy in solution. The presence of d-d bands would normally be expected for a low-spin d^6 transition metal species at modest energies. The intensities of such transitions are very low due to their nature, and so they are hidden by the much more intense MLCT and internal ligand transitions. The positions of the various absorption bands in a large range of different solvents are detailed in table 2.2. In a number of these solvents, the higher energy transitions are masked by absorptions of the solvent itself.

Figure 2.2 : Electronic Absorption Spectrum of $Fe(bpy)_2(CN)_2$ in MeCN

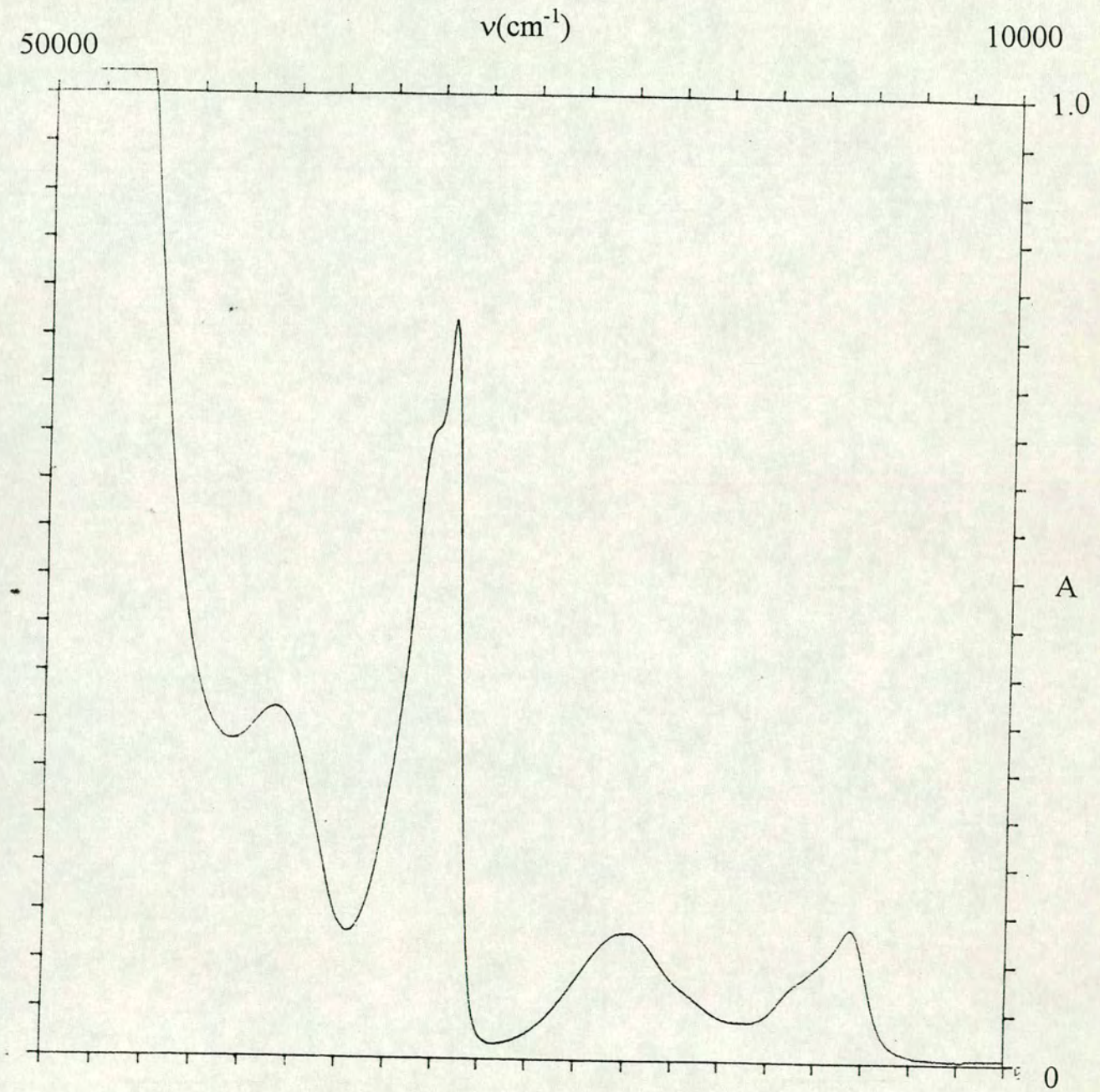

Table 2.2 : UV/VIS/NIR Results for $Fe(bpy)_2(CN)_2$

	Band position (cm^{-1})			
Solvent	MLCT(1)	MLCT(2)	$\pi \rightarrow \pi^*(1)$	$\pi \rightarrow \pi^*(2)$
Pyridine	16031	25523	-------	-------
DMF	16087	25510	33157	-------
Acetone	16255	25988	33971	-------
DMSO	16404	25853	-------	-------
MeCN	16556	26015	33423	40719
CH_2Cl_2	16578	26512	33289	40455
$MeNO_2$	16903	26540	-------	-------
EtOH	17656	27116	33344	40371
MeOH	18038	27488	34440	41263

We can attempt to fit the experimental data to a number of solvent parameters, described earlier. Figures 2.3 to 2.7 show graphically any relationship between MLCT band position and solvent parameter.

It can be seen that the best linear relationship between the experimental results and the solvent parameters is obtained using the Acceptor Numbers (A.N.) devised by Gutmann, although Kosower's Z values and the E_T values also give reasonable linear correlations. This result is not surprising as Gutmann noted a close relationship between A.N., Z and E_T in his initial work[23].

The lowest energy MLCT transition involves excitation of an electron from a metal based $d\pi$-orbital to an unoccupied bpy π^* orbital. Therefore we decided to study the electrochemistry of the complex in various solvents since oxidation of the complex involves removal of an electron from the HOMO and the reduction process involves addition of an electron to the LUMO. Thus the difference between the

Figures 2.3 - 2.5 : Plots of MLCT Position for $Fe(bpy)_2(CN)_2$ against D_s, D.N., E_T

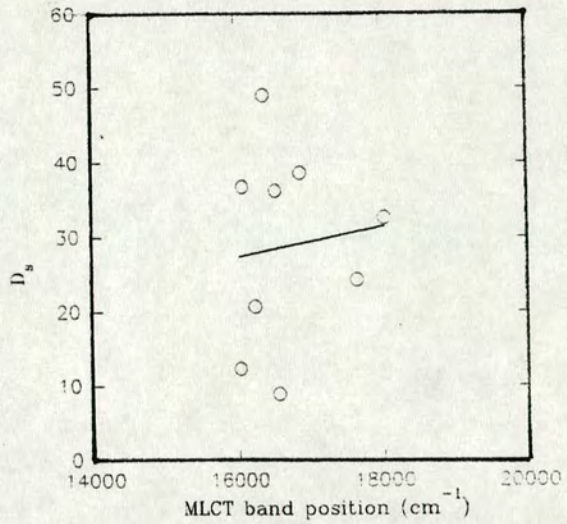

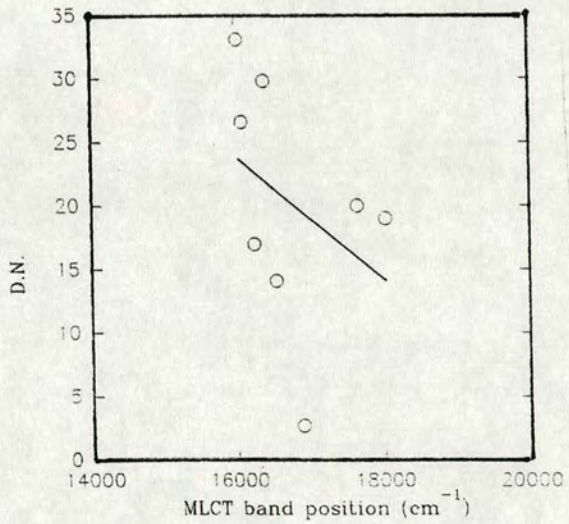

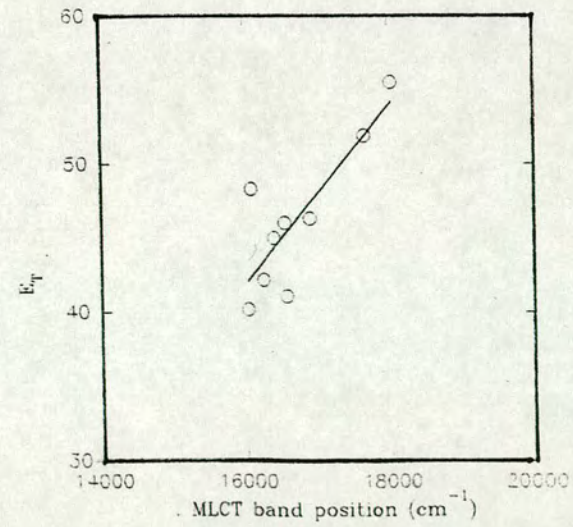

Figures 2.6 & 2.7 : Plot of MLCT position for $Fe(bpy)_2(CN)_2$ against Z and A.N.

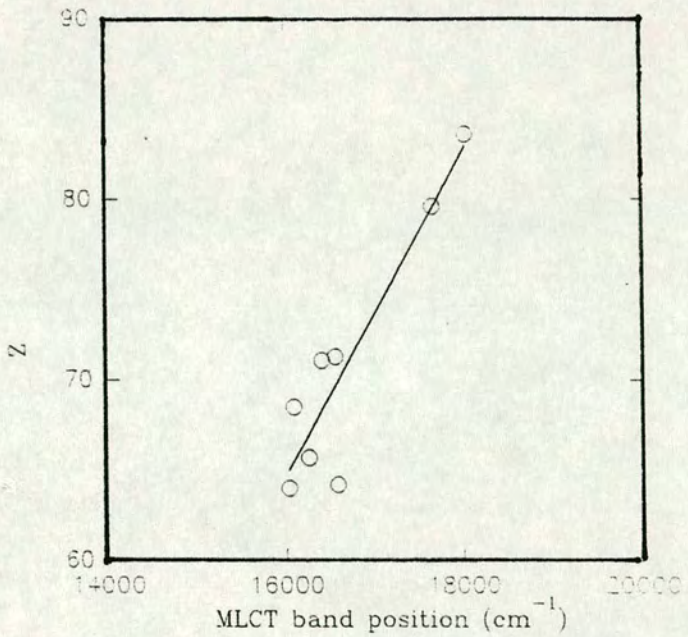

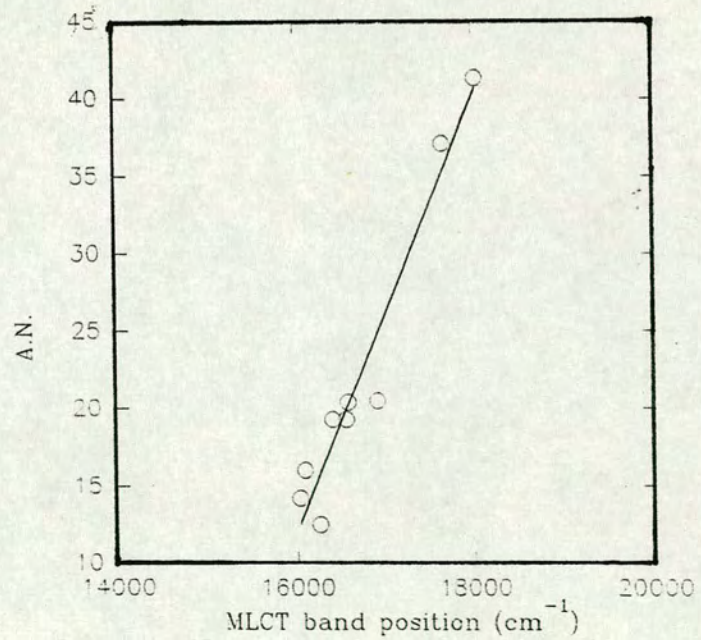

oxidation and reduction potentials could be expected to be related to the lowest energy MLCT where an electron is promoted from the metal d-orbitals (cf oxidation) to a ligand π^* orbital (cf reduction). A schematic representation of this relationship is shown in figure 2.8.

The complex typically shows two reductive processes and one oxidative process, providing the solvent allows observation of all redox processes before undergoing redox processes of its own. The oxidative process is usually observable. This oxidative process is fully reversible at room temperature and is assigned as the Fe(II)/Fe(III) couple, i.e. removal of a $d\pi$ electron, d^6 electronic configuration oxidised to a d^5 electronic configuration. The two one-electron reductive processes are semi-reversible at room temperature, but they are fully reversible at 240 K. These processes are assigned as sequential reductions of the two bpy ligands. A typical cyclic voltammetric response for the complex is shown in figure 2.9 and the half-wave potentials of the complex in various solvents are given in table 2.3. All potentials are corrected versus Fc/Fc^+ at +0.55 V.

Figure 2.8 : Simple Orbital diagram for $Fe(bpy)_2(CN)_2$

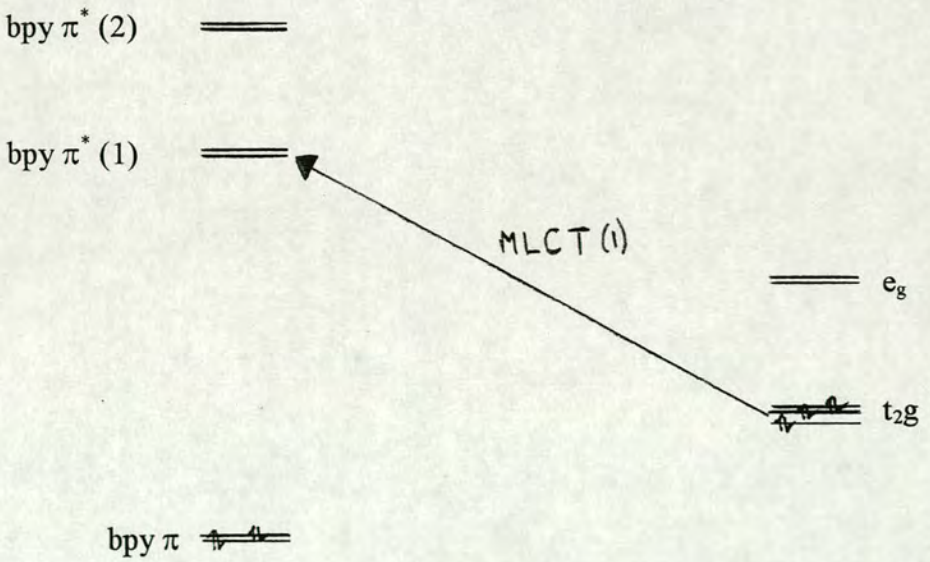

Figure 2.9 : Cyclic voltammagram of $Fe(bpy)_2(CN)_2$

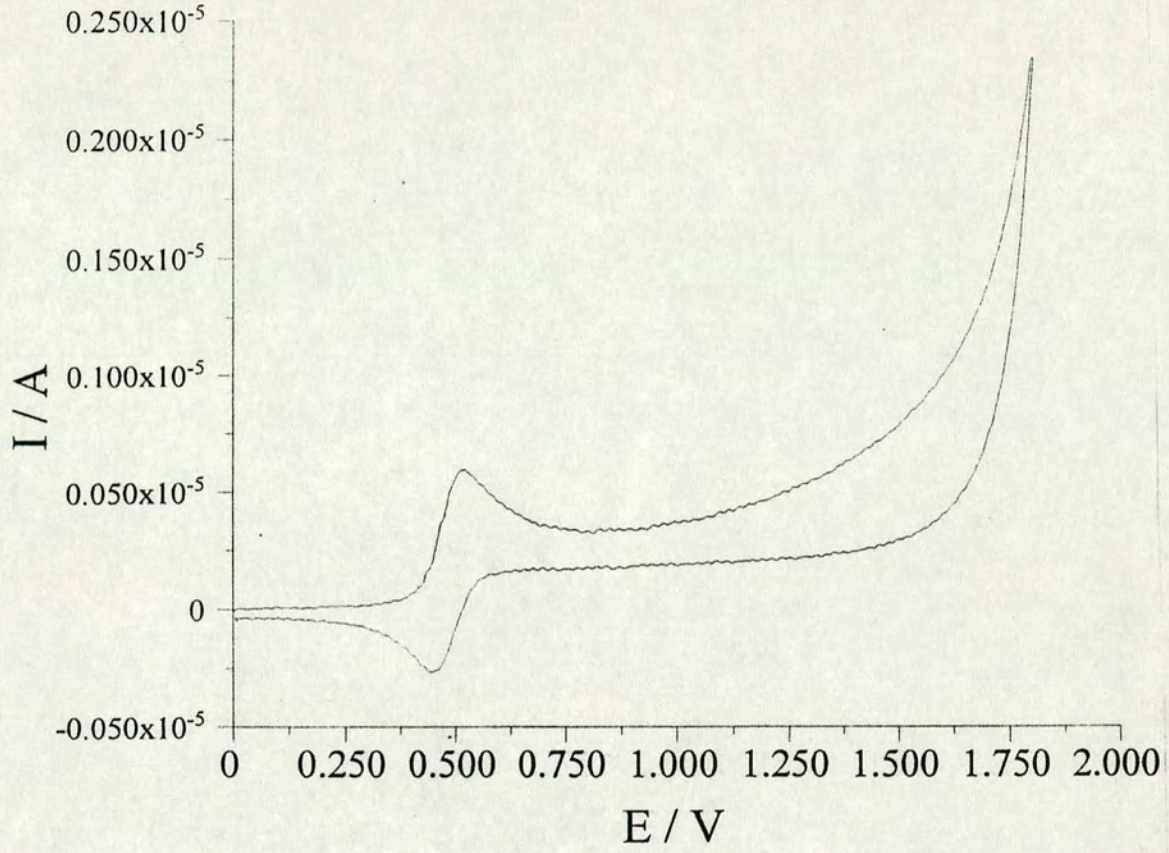

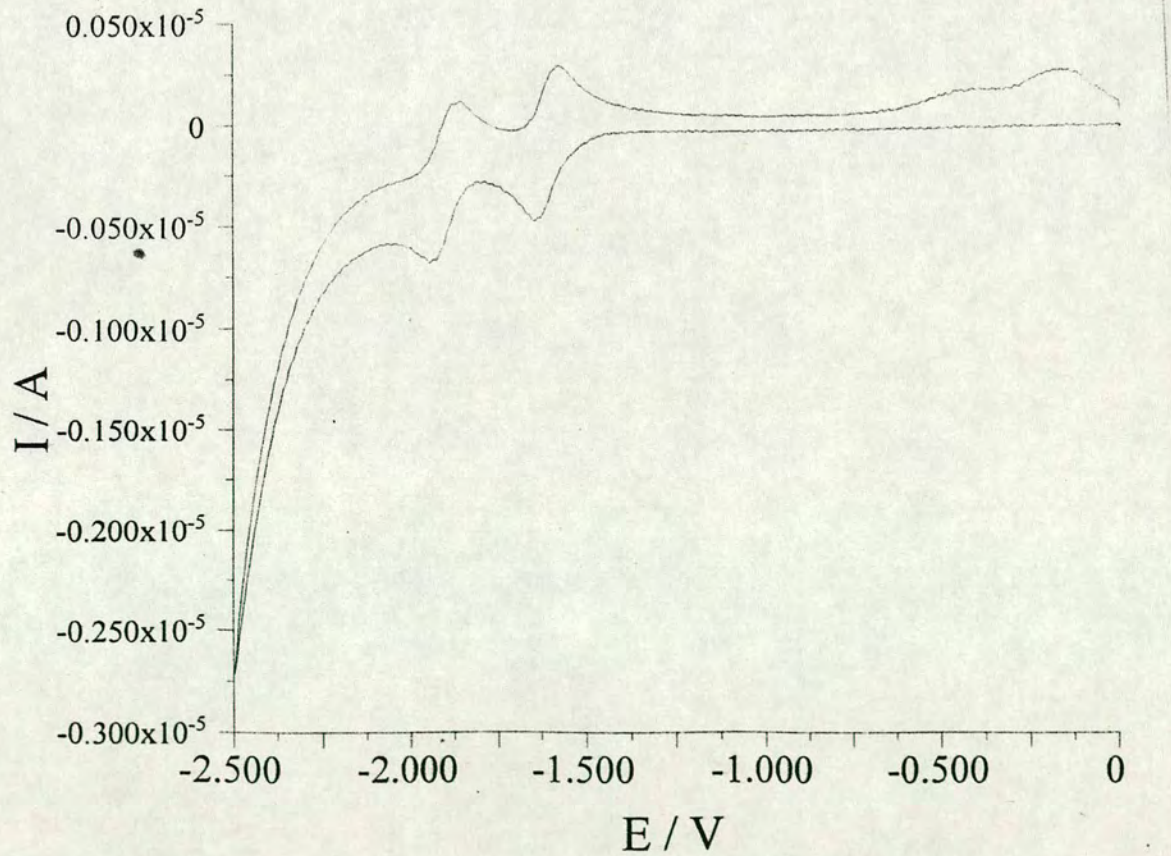

Table 2.3 : $E_{1/2}$ values of $Fe(bpy)_2(CN)_2$ in various solvents

Solvent	$E_{1/2}$ ($Fe^{II/III}$)	$E_{1/2}$ ($bpy^{0/-}$) (1)	$E_{1/2}$ ($bpy^{0/-}$) (2)
Pyridine	+0.575 V	~ -1.58 V	-------
DMF	+0.565 V	-1.535 V	-1.825 V
DMSO	+0.60 V	-1.54 V	-1.82 V
MeCN	+0.615 V	-1.535 V	~-1.8 V
CH_2Cl_2	+0.64 V	-1.55 V	-1.83 V
$MeNO_2$	+0.655 V	-------	-------
MeOH	+0.78 V	-------	-------

There is a clear variation of the potential of the metal-based process with solvent, but the ligand-based reductions appear to remain almost solvent invariant. Indeed, a linear relationship between MLCT energy and $Fe^{II/III}$ potential is evident from figure 2.10.

Figure 2.10 : Relationship between MLCT position and $E_{1/2}$(Fe(II)/Fe(III))

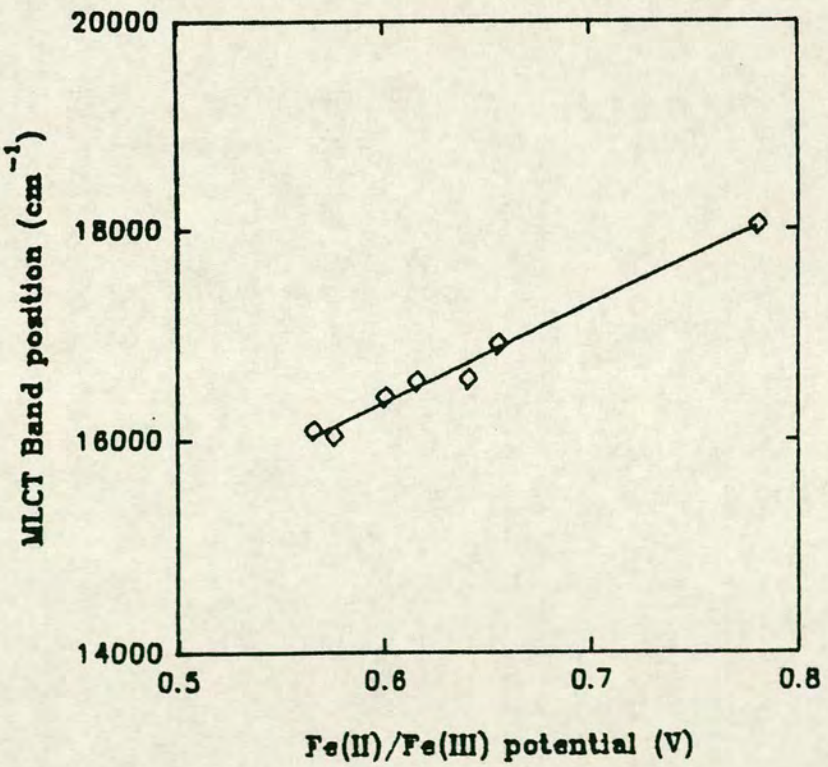

We can rationalise this relationship by considering the solvent to be interacting with the electron density associated with the cyanide ligands, especially the lone pair of electrons present on each ligand. Experimentally, we observe no solvent dependence on the equivalent MLCT band when the cyano ligands are replaced by bpy. Thus we suggest that the solvent interaction with the complex must be via the cyanide ligand and not the bpy ligand. As we observe a correlation with Acceptor Numbers, it is reasonable to assume that the solvent molecule interacts with the complex by accepting some of this electron density.

The magnitude and nature of this interaction are obviously dependent on the exact nature of the solvent molecule. In general, the withdrawal of electron density from the lone pair on the ligand will cause a shift in electron density along the carbon-nitrogen bond. This will in turn lessen the amount of electron density available for σ-donation to the metal centre. The decreased σ interaction means that there will be an increase in the length of the iron/cyanide carbon bond. This in turn means there is less overlap between the metal d-orbitals and the cyanide ligand π^* system, thus lessening the $d \rightarrow \pi^*$ back-bonding. These changes in electron density and bonding will perturb the relative energies of the d-orbitals, and hence a variation in associated properties is seen. Such a perturbation should be seen in the IR spectrum of the complex, in a range of solvents. Unfortunately, the relevant IR absorbances are difficult to observe in many of the solvents being used, being obscured by bands due to the solvent itself. As a consequence of these observed variations, we wanted to study whether the oxidised and reduced compounds also exhibit solvent dependent behaviour.

2.3.2 : $[Fe(bpy)_2(CN)_2]^+$

The electronic absorption spectrum of the Fe^{III} complex has been recorded previously[2], but only in water, ethanol and dilute sulphuric acid, and only those bands occurring in the visible region have been reported.

However, with the availability of spectroelectrochemical techniques, such as the OTE cell, it is possible to generate the oxidised species *in situ* and record its

electronic absorption spectrum in a wide range of solvents. It is also feasible to chemically generate the cation, using an oxidising agent such as concentrated nitric acid, although the validity of results obtained in such a manner may be questionable due to the possibility of preferential solvation of the complex by the water or excess acid from the oxidising agent. Other chemical oxidising agents are not soluble in all the solvents used in this study. Nevertheless, results obtained in this manner, where possible, are presented as an alternative to bulk electrogeneration of the product.

Electrogeneration of the oxidised complex can be monitored spectroscopically by use of the OTE cell in conjunction with the UV/VIS/NIR spectrometer. The results of such an experiment are shown in figure 2.11. The collapse of both MLCT bands is clearly demonstrated, as is the shift to lower energy of the bpy internal transitions, as the bonding between the bpy ligands and the iron centre is altered by the removal of an electron from the Fe $d\pi$ orbitals. We expect the Fe(III) to π^* bpy MLCT transition to be at higher energy than the Fe(II) MLCT transition and it will probably lie under the more intense intraligand transitions. However, unlike the oxidation of tris(2,2'-bipyridyl)iron(II)$^{2+}$ to tris(2,2'-bipyridyl)iron(III)$^{3+}$, a LMCT band is not observed growing in, although Schilt noticed a band at 18900 cm^{-1} in water, with a much lower extinction coefficient than is seen for the original iron(II) moiety.

Although no information about the perturbation of the metal d-orbitals can be gained from these results, the presence of an unpaired electron on the d^5 metal centre allows us to utilise epr spectroscopy as a probe on the Fe(III) centre. Fortunately, this complex yields an epr signal at 77K, even though this is not always possible with a low-spin d^5 iron complex. Reiff and DeSimone[24] recorded the spectrum of the complex in a DMA-H_2O mix at 77K, but results in other mediums have never been published. We were unable to record any solution epr spectra.

A typical spectrum is shown in figure 2.12, and the positions of the *g*-values are indicated. The results determined from samples prepared by bulk electrosynthesis

Figure 2.11 : Absorption spectrum monitoring of $[Fe(bpy)_2(CN)_2]$ in DMF

T = 243 K, E_{appl} = +0.8 V

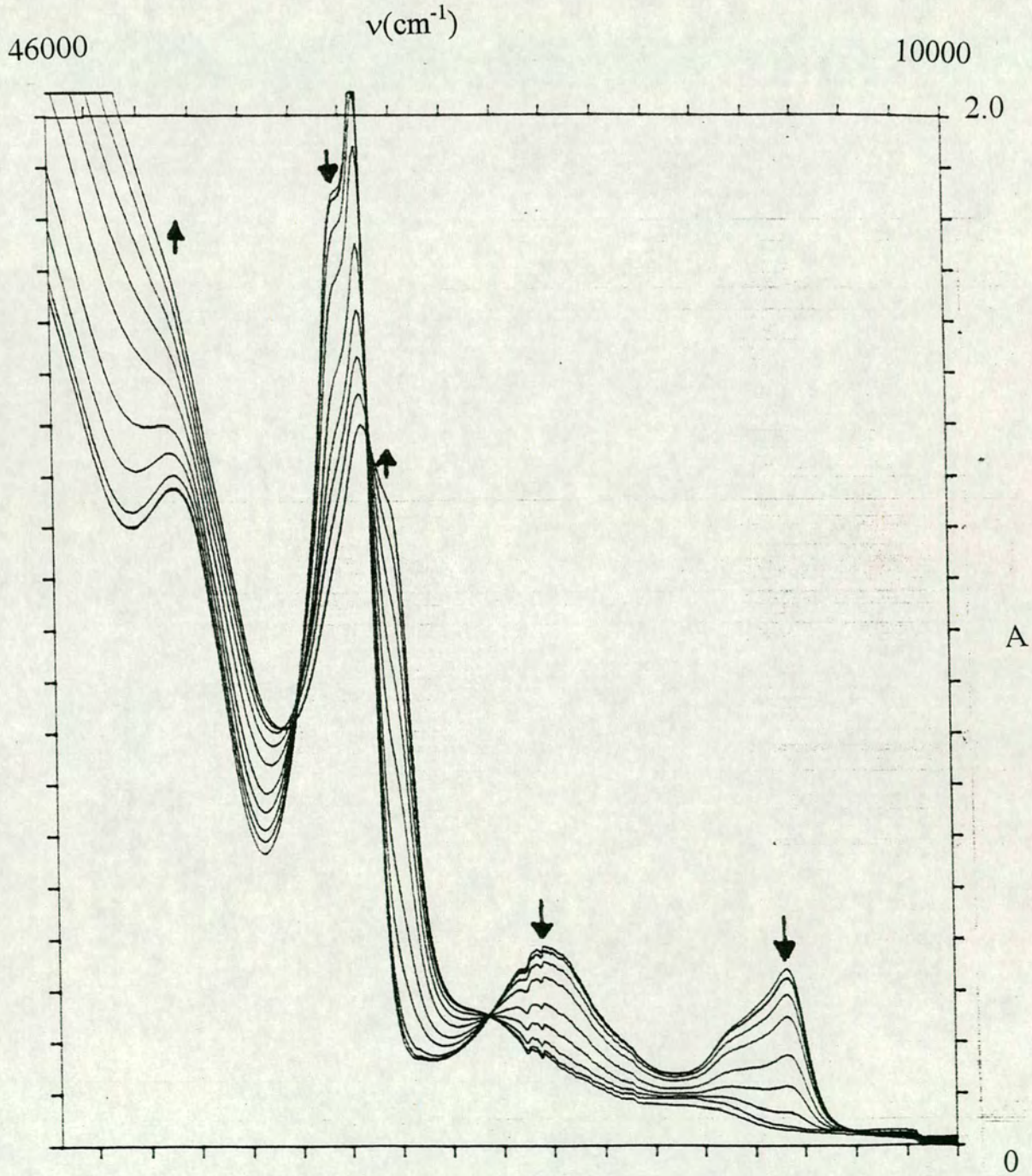

Figure 2.12 : EPR spectrum of $[Fe(bpy)_2(CN)_2]^+$ in DMF, T = 77 K

Electrogenerated E_{appl} = +0.8 V

Centre Field : 2500 G
Sweep Width : 3000 G
Frequency : 9.35 GHz

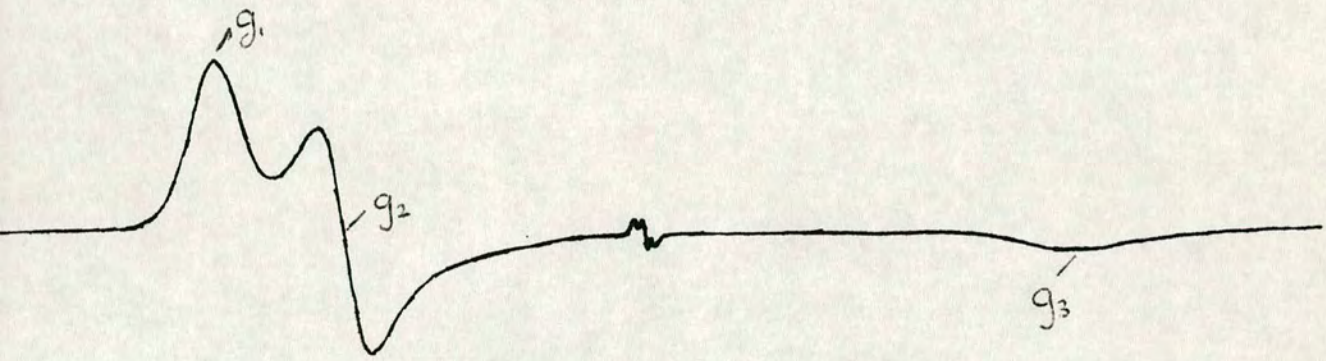

Table 2.4 : EPR data for electrochemically generated $[Fe(bpy)_2(CN)_2]^+$

Solvent	g_1	g_2	g_3
DMF	2.802	2.515	1.567
DMSO	2.780	2.523	1.563
MeCN	2.774	2.528	1.567
$MeNO_2$	2.774	2.523	1.558

Table 2.5 : EPR data for chemically generated $[Fe(bpy)_2(CN)_2]^+$

Solvent	g_1	g_2	g_3
DMF	2.790	2.513	1.571
DMSO	2.762	2.505	1.565
MeCN	2.765	2.530	1.546
$MeNO_2$	2.765	2.530	1.518

Figure 2.13 : Effects of axial and rhombic distortion on metal d-orbitals

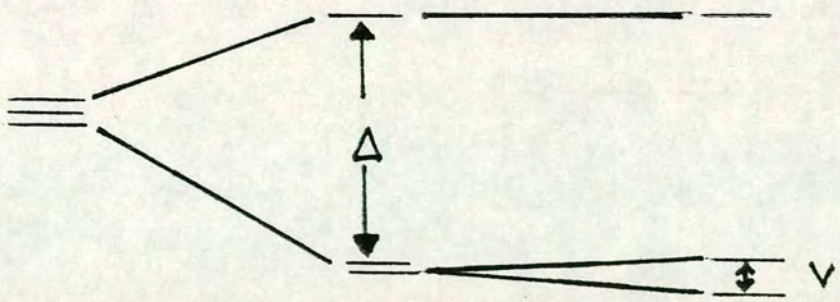

are given in table 2.4, while those from chemical oxidation by concentrated nitric acid are given in table 2.5

The epr spectra obtained are all rhombic in nature, typical for a low spin d^5 transition metal complex of such low symmetry. As can be seen from table 2.4, the *g* values for the electrogenerated complexes are almost completely independent of the solvent used, in contrast to the electrochemistry and electronic absorption spectra associated with the parent material.

A common method of analysing the raw epr data for low-spin d^5 complexes is that proposed by Hill[25], which is based on work by Griffith[26]. This method of analysis has been used for similar systems to those under consideration[27,28] and theoretical parameters derived using it give a good correlation with experimental results. The procedure works for *pseudo*-octahedral complexes with axial and rhombic distortions. The effect these distortions have on the metal d orbitals is shown in figure 2.13. The axial splitting parameter is Δ, the rhombic splitting parameter is V and λ is the spin-orbit coupling constant for the metal in question. A purely axial distortion can only be considered by reducing the rhombic factor to zero.

The analysis takes all five electrons on the metal centre into explicit consideration. This method yields three different five electron functions T_2^0, T_2^+ and T_2^-, which may also be written as ^2A, $^2E_+$ and $^2E_-$, the labels A and E describing the parenthood of the state in a purely axial field. These then split into three Kramers doublets, represented by two identical 3 x 3 matrices, one of which is shown below.

		$\lvert T_2^- \rangle$	$\lvert \bar{T}_2^0 \rangle$	$\lvert T_2^+ \rangle$
		$\lvert \bar{T}_2^+ \rangle$	$\lvert T_2^0 \rangle$	$\lvert \bar{T}_2^- \rangle$
$\lvert T_2^- \rangle$	$\lvert \bar{T}_2^+ \rangle$	$\lambda/2$	0	V/2
$\lvert \bar{T}_2^0 \rangle$	$\lvert T_2^0 \rangle$	0	$-\Delta$	$-\lambda/\sqrt{2}$
$\lvert T_2^+ \rangle$	$\lvert \bar{T}_2^- \rangle$	V/2	$-\lambda/\sqrt{2}$	$-\lambda/2$

The epr active ground state Kramers doublets can then be written as

$$\Psi = p|T_2^{+}\rangle + q|T_2^{0}\rangle + r|T_2^{-}\rangle$$

$$\Psi' = p|T_2^{-}\rangle + q|T_2^{0}\rangle + r|T_2^{+}\rangle$$

The three components of the g tensor are then described by

$$g_x = 2[2pr - q^2 + kq\sqrt{2}(r - p)]$$

$$g_y = 2[2pr + q^2 + kq\sqrt{2}(r + p)]$$

$$g_z = -2[p^2 - q^2 + r^2 + k(p^2 - r^2)]$$

where $p^2 + q^2 + r^2 = 1$. The orbital reduction factor, k, is ideally a measure of covalency, but, when determined by this method of epr analysis, the value of k acts as a combination of various factors[26,29].

Unfortunately, the epr experiment only yields the absolute magnitudes of the g values, not their signs. It also yields no information on the correspondence between g_1, g_2 and g_3 with g_x, g_y and g_z. Each combination of $\pm g_1$, g_2 and g_3 with g_x, g_y and g_z can, in theory, yield a unique solution for p, q, r and k. To reduce the number of solutions under consideration, only those which yield reasonable values of k are considered further ($0 < k < 1.5$).

The actual method used to solve the equations was as follows. Firstly, an iterative computer solver[30] was used to solve for all forty-eight combinations of g_x, g_y and g_z. Only twelve solutions were found which yielded reasonable values of k. These form six pairs which differ only in the sign of r.

A program for matrix diagonalisation and calculation of eigenvalues[31] was used to evaluate λ, Δ and V. The program, known as eigen, and which is freely available, also gave values of E_1 and E_2, the low energy ligand field transitions. E_1 and E_2 can be measured by NIR spectroscopy of the d^5 complex and therefore allow correlation between theory and experiment. Initially, guestimates for λ, Δ and V were introduced to the program which then produced values for p, q and r as well as energies for the three orbitals under consideration, from which values for E_1 and E_2

could be calculated. The values of Δ and V were varied until matches for p, q and r previously determined were obtained.

The values of Δ, V, E_1 and E_2 are directly proportional to the value of λ. However, we may only measure λ by experimental observation of E_1 or E_2. As such, it is normal to quote the results of this analysis in the form of the ratios Δ/λ, V/λ, E_1/λ and E_2/λ. All results will therefore be presented as these ratios.

Table 2.6 gives the twelve acceptable k value solutions arising from the analysis of the electrogenerated epr spectrum of $[Fe(bpy)_2(CN)_2]^+$ in DMF. Only the first two sets of values for p, q and r from Table 2.6 gave reasonable values for Δ/λ and V/λ. Thus we consider further only the first two solutions. For all other systems under study, similar results eventuate and therefore only the two plausible solutions are presented in tables 2.7 and 2.8.

Table 2.6 : Analysis of epr spectrum for $[Fe(bpy)_2(CN)_2]^+$ in DMF

g_x	g_y	g_z	p	q	r	k
-2.802	2.515	1.567	0.263	0.964	-0.035	1.11
-2.802	2.515	-1.567	0.741	0.671	-0.027	1.25
-2.802	1.567	-2.515	0.831	0.543	-0.118	1.25
-2.802	-1.567	-2.515	0.796	0.211	-0.568	1.11
-2.515	1.567	-2.802	0.858	0.505	-0.091	1.25
-2.515	-1.567	-2.802	0.831	0.161	-0.533	1.11
-2.515	2.802	1.567	0.263	0.964	0.035	1.11
-2.515	2.802	-1.567	0.741	0.671	0.027	1.25
-1.567	2.802	-2.515	0.831	0.543	0.118	1.25
1.567	2.802	-2.515	0.796	0.211	0.568	1.11
1.567	2.515	-2.802	0.831	0.161	0.533	1.11
-1.567	2.515	-2.802	0.858	0.505	0.091	1.25

Table 2.7 : Derived parameters for electrogenerated $[Fe(bpy)_2(CN)_2]^+$

Solvent	p	q	r	k	Δ/λ	V/λ	E_1/λ	E_2/λ
DMF	0.263	0.964	-0.035	1.11	2.96	0.97	2.63	3.87
DMF	0.741	0.671	-0.026	1.25	0.36	0.11	1.42	1.65
MeCN	0.264	0.964	-0.030	1.10	2.94	0.82	2.66	3.80
MeCN	0.741	0.671	-0.023	1.25	0.36	0.10	1.42	1.65
$MeNO_2$	0.267	0.963	-0.031	1.09	2.90	0.82	2.62	3.76
$MeNO_2$	0.741	0.671	-0.024	1.24	0.36	0.11	1.42	1.65
DMSO	0.265	0.964	-0.031	1.10	2.93	0.85	2.64	3.80
DMSO	0.741	0.671	-0.024	1.24	0.36	0.11	1.42	1.65

Table 2.8 : Derived parameters for chemically generated $[Fe(bpy)_2(CN)_2]^+$

Solvent	p	q	r	k	Δ/λ	V/λ	E_1/λ	E_2/λ
DMF	0.262	0.964	-0.034	1.107	2.98	0.96	2.65	3.88
DMF	0.742	0.670	-0.026	1.246	0.36	0.12	1.42	1.65
MeCN	0.271	0.962	-0.029	1.079	2.84	0.75	2.60	3.68
MeCN	0.740	0.672	-0.022	1.239	0.37	0.10	1.42	1.65
$MeNO_2$	0.280	0.960	-0.029	1.060	2.76	0.72	2.54	3.59
$MeNO_2$	0.738	0.675	-0.022	1.233	0.38	0.10	1.42	1.65
DMSO	0.265	0.964	-0.032	1.073	2.93	0.88	2.64	3.81
DMSO	0.742	0.670	-0.024	1.235	0.36	0.10	1.42	1.65

Table 2.7 details the values obtained for electrogenerated samples, while table 2.8 gives those obtained for chemically generated samples. Similar results are obtained regardless of the method of generation of the oxidised product.

Although we do not know absolutely the value of λ for the complex under consideration, we can estimate the energies of the expected crystal field transitions, E_1 and E_2, using previously determined values for λ. For iron(II) the value of λ is estimated at 400 cm^{-1}, and for iron(III) it is 460 cm^{-1}. This leads to estimated energies for E_1 of 1050 to 1220 cm^{-1} depending on the exact value of λ. The estimated energy of E_2 is 1560 to 1750 cm^{-1}. We therefore predict that for $[Fe(bpy)_2(CN)_2]^+$ there should be two low energy absorption bands in the IR region of the spectrum. Unfortunately the expected low extinction coefficients and nature of the solvents used make study by conventional IR spectrometry very difficult.

Comparison of the results obtained from the oxidation product of $[Fe(bpy)_3]^{2+}$ i.e. $[Fe(bpy)_3]^{3+}$ are possible. The higher symmetry of this related complex leads to an axial type of spectrum, from which a value of Δ/λ was calculated to be 3.03[24]. This value is obviously close to our larger value of Δ/λ, thus implying that the rhombic splitting is less important in the overall electronic structure than the axial splitting, and also implying that the ligand field due to the four nitrogen and two carbon donor atoms is very similar to that for the six nitrogen donors in $[Fe(bpy)_3]^{2+}$.

If we consider the chemically generated samples, we obtain very similar results, although some variation in measured *g* values is observed. Even though the *g* values are not as consistent as those obtained for the electrogenerated species, this has very little effect on the parameters derived as above. Differences between electrogenerated samples and chemically generated samples may result from residual amounts of paramagnetic chemical reductant used.

Thus the solvent used appears to have a negligible effect on the energies of the metal d-orbitals in the oxidised form. This suggests that the energy of the metal based

orbitals in the oxidised Fe(III) complex are not sensitive to interaction with solvent. We offer the following explanation to account for the observed results :-

The removal of an electron from the metal d-orbitals upon oxidation will considerably reduce the d(π) to cyanide π^* back-bonding interaction, thus increasing the metal to cyanide carbon distance. This in turn will lead to a decreased σ-type interaction between the ligand and the metal d-orbitals. The net result of this will be a decreased electronic interaction between the metal and ligand, through both the σ- and π- type interactions present. Thus any interaction between the solvent and the electron density on the cyanide ligand, which we have proposed causes the observed solvent dependent behaviour in the parent complex, will not perturb the d-orbitals to the same extent. As a result the epr spectrum, dependent on the relative energies of the d-orbitals, is independent of the solvent used, and so this interaction can be assumed to be minimised. This can be seen in the consistency of the *g* values, derived parameters and energies.

2.3.3 : $[Fe(bpy)_2(CN)_2]^-$

The reduction product of the complex is also of interest. While the metal-based oxidation appears to remove the solvent dependent behaviour of the complex, the ligand-based reduction should, in theory, superimpose the already observed behaviour of the complex on that seen for a reduced bipyridyl ligand.

The absorption spectrum of reduced bipyridyl, both free and chelated to a metal centre, is well known[32,33]. The UV/VIS/NIR spectrum of reduced bpy is shown in figure 2.14. Often, reducing a complex containing the bpy ligand results in the superimposition of this spectrum on the spectrum of the starting complex, although any MLCT bands associated with the bpy ligand may suffer a loss in intensity.

The epr spectrum of free bpy[34] shows hyperfine and superhyperfine structure due to the nitrogen and hydrogen atoms in the molecule. This leads to a spectrum consisting of up to 81 lines, depending on the resolution obtained under various experimental conditions.

Figure 2.14 : UV/VIS/NIR spectrum of bpy$^{\cdot}$

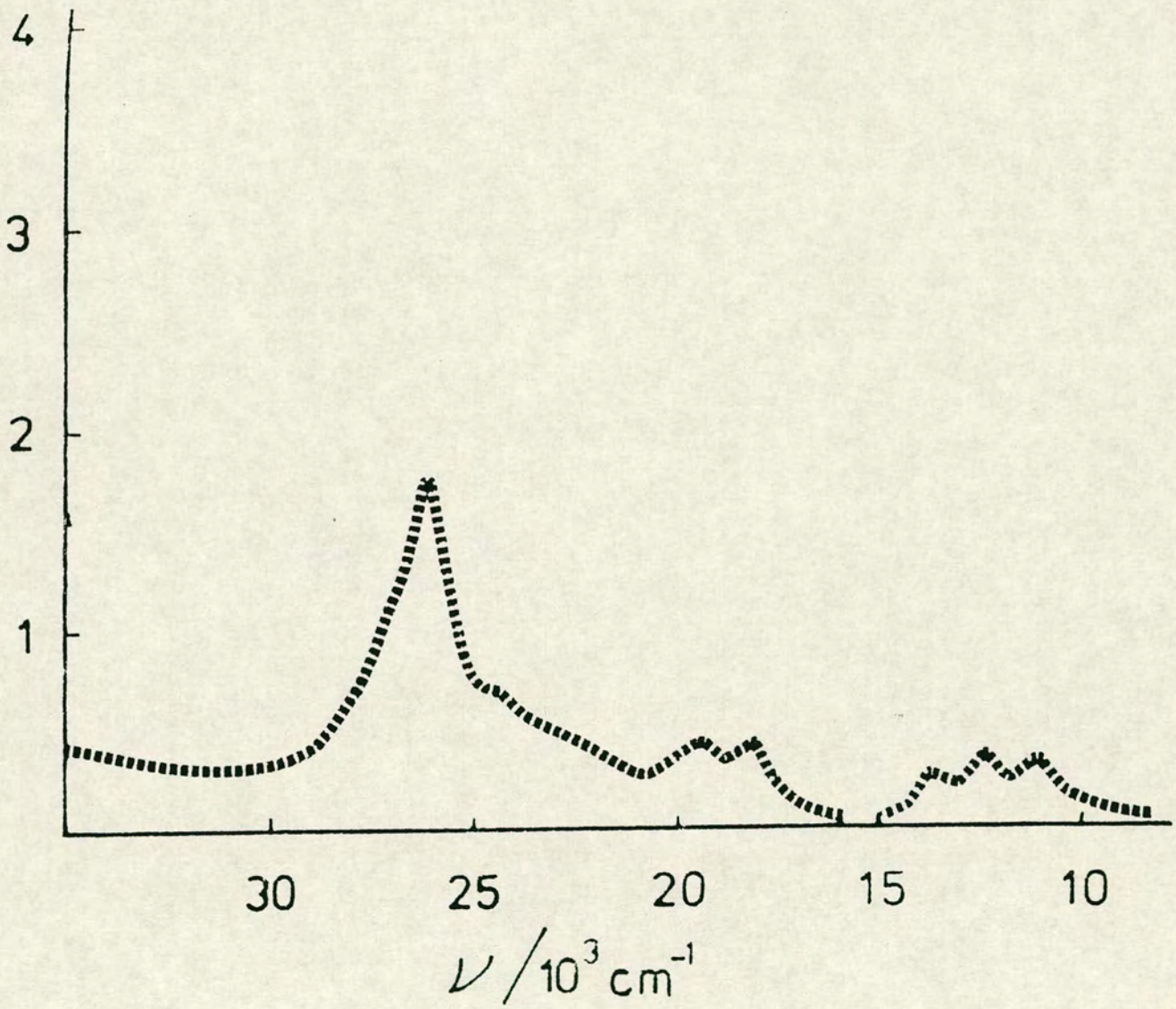

Figure 2.15 : Absorption spectrum monitoring of $[Fe(bpy)_2(CN)_2]$ in DMF

T = 243 K, E_{appl} = -1.7 V

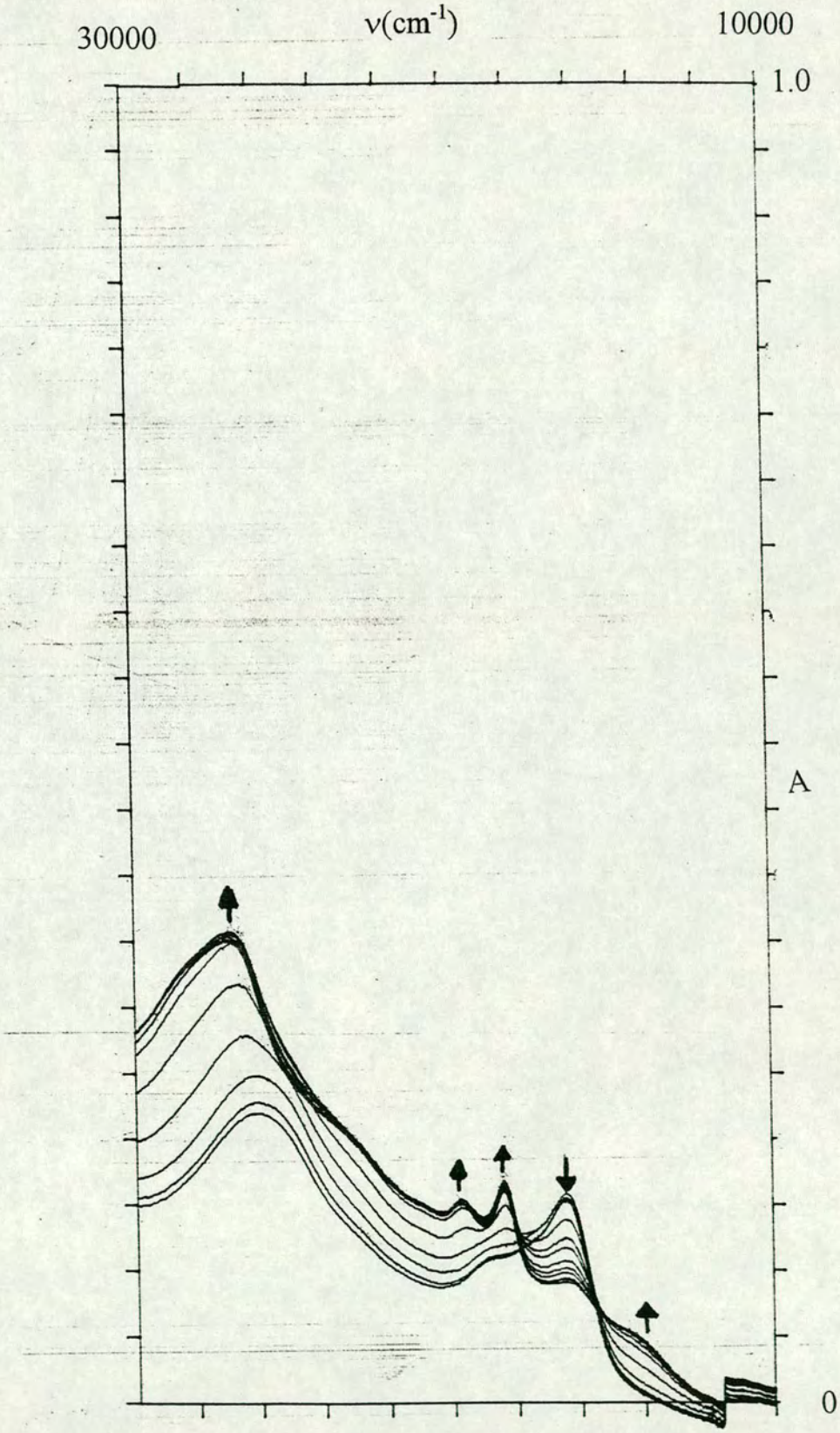

Figure 2.16 : EPR spectrum of $[Fe(bpy)_2(CN)_2]^-$ in DMF, T = 77K

Centre Field : 3300 G
Sweep Width : 400 G
Frequency : 9.35 GHz

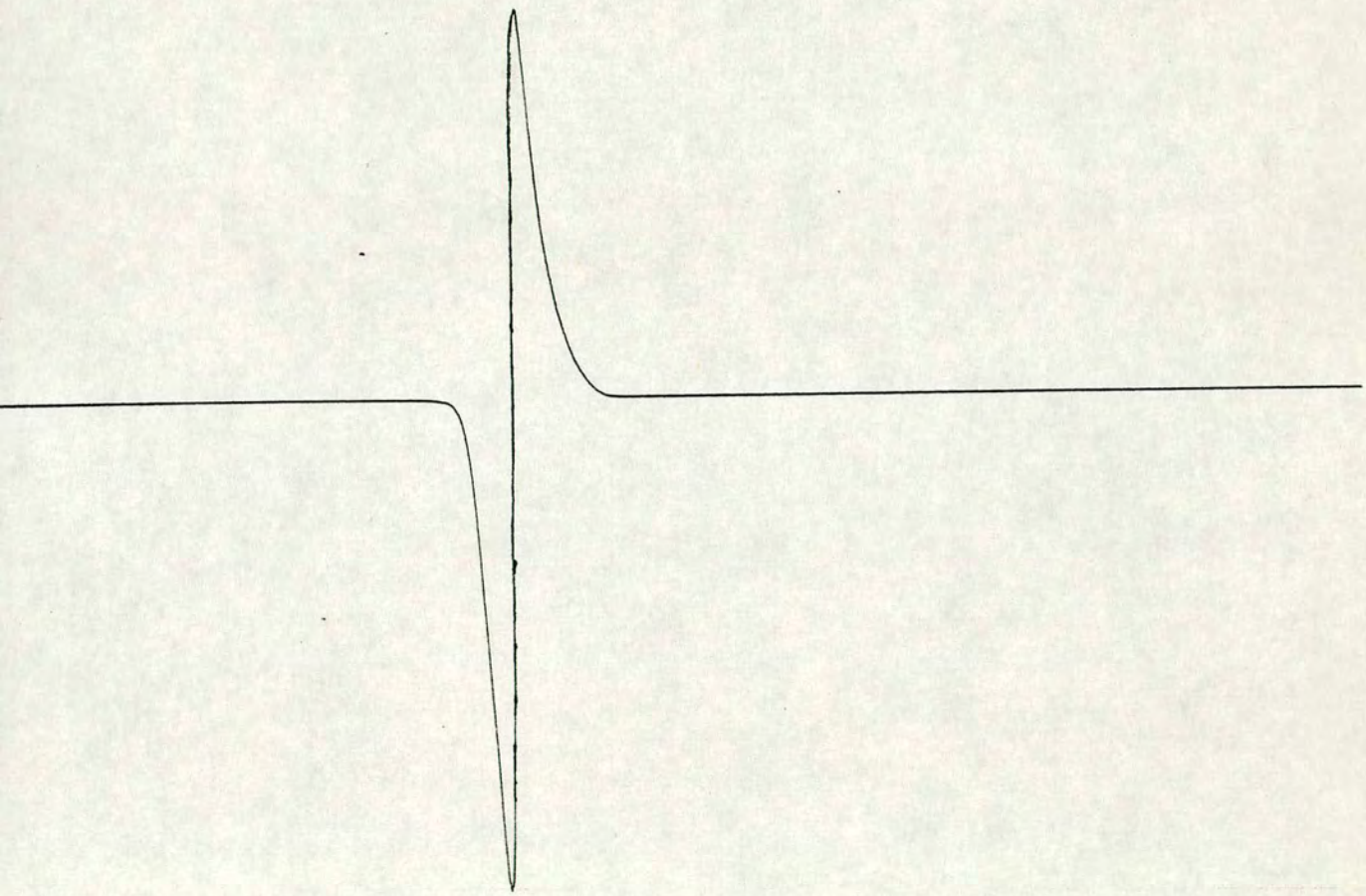

The epr spectrum typically seen for a chelated, reduced bipyridyl ligand is far simpler. The reductions of tris(bipyridyl)iron(II) and tris(bipyridyl)ruthenium(II) have been extensively investigated using epr spectroscopy[35]. The singly reduced forms of these complexes yield a single resonance, very close to the free electron value. No hyperfine coupling is observed to either the ligand nitrogens or the metal centre.

We can monitor the reduction of the complex via use of the OTE cell. The results of such an experiment are shown in figure 2.15. We observe the growth of several bands associated with a reduced bpy unit as potential of -1.7 V is applied to the system, as well as a reduction in intensity of the first MLCT process, to around half of its initial intensity. This is to be expected, as there is now only one unoccupied bpy π^* orbital for the iron d-electrons to be excited into. Upon return of the applied potential to zero, the initial spectrum is regenerated.

As the reduced species $[Fe(bpy)_2(CN)_2]^-$ has an unpaired electron we should also observe an epr spectrum. This is indeed the case and a typical spectrum measured at 77 K is shown in figure 2.16. This spectrum is very similar to that seen for the singly reduced tris(bipyridyl)iron species mentioned previously[35]. The *g* value of 2.008, measured in DMF, is indicative of the unpaired electron being predominantly on the ligand π^* orbital, and not on the metal d-orbitals. This behaviour matches exactly that seen for the analogous tris(bipyridyl) complex.

The question of whether the electron is localised on a single ligand π^* orbital or delocalised over the entire π^* network for both bipyridyl ligands is best addressed by looking at the epr spectrum at various temperatures. As in Motton, Hanck and DeArmond's work on reduced forms of tris(bipyridyl)iron(II)[35], if temperature dependent line broadening is observed, then this is liable to be due to electron 'hopping' from one ligand to the other, on a time scale comparable to that of the epr experiment. Unfortunately, time constraints prevented this experiment from being performed.

2.3.4 : *cis*-$Ru(bpy)_2(CN)_2$

The electronic absorption spectrum of bis(2,2'-bipyridyl)dicyanoruthenium(II) in acetonitrile is shown in figure 2.17. As for the analogous iron complex, the observed bands are generally assigned as a MLCT band ($d \rightarrow \pi^*$ (1)) at lowest energy, a second MLCT band ($d \rightarrow \pi^*$ (2)), a bpy internal transition ($\pi \rightarrow \pi^*$ (1)) and, at highest energy, a second intraligand transition ($\pi \rightarrow \pi^*$ (2)). As before, any d-d transitions are not observed, presumably because they are obscured by the more intense charge transfer processes.

The solvent dependent behaviour of the complex was first reported by Demas and co-workers in 1986[7]. This work noted the variation in energy of both MLCT transitions on changing the solvent from methanol to DMF. This was used as evidence for the assigned *cis* configuration of the complex. Later works[36,37] were concerned with the effects of protonation of the cyanide ligands, in particular the study of the absorption and emission characteristics of the complex.

In 1988 Fung and co-workers[9] investigated the complex in a range of different solvents, and correlated $Ru^{II/III}$ potential, the energy of the lowest energy MLCT band and the maximum of the emission band with Gutmann's Acceptor Numbers (AN)[23]. This work went on to conclude that a specific solvent-solute interaction in the second co-ordination sphere was responsible for the solvatochromsim observed. Since this work investigations concerning this complex have tended to be more concerned with the reduction of the complex than the oxidation.

Figure 2.17 :Electronic Absorption Spectrum of $Ru(bpy)_2(CN)_2$ in MeCN

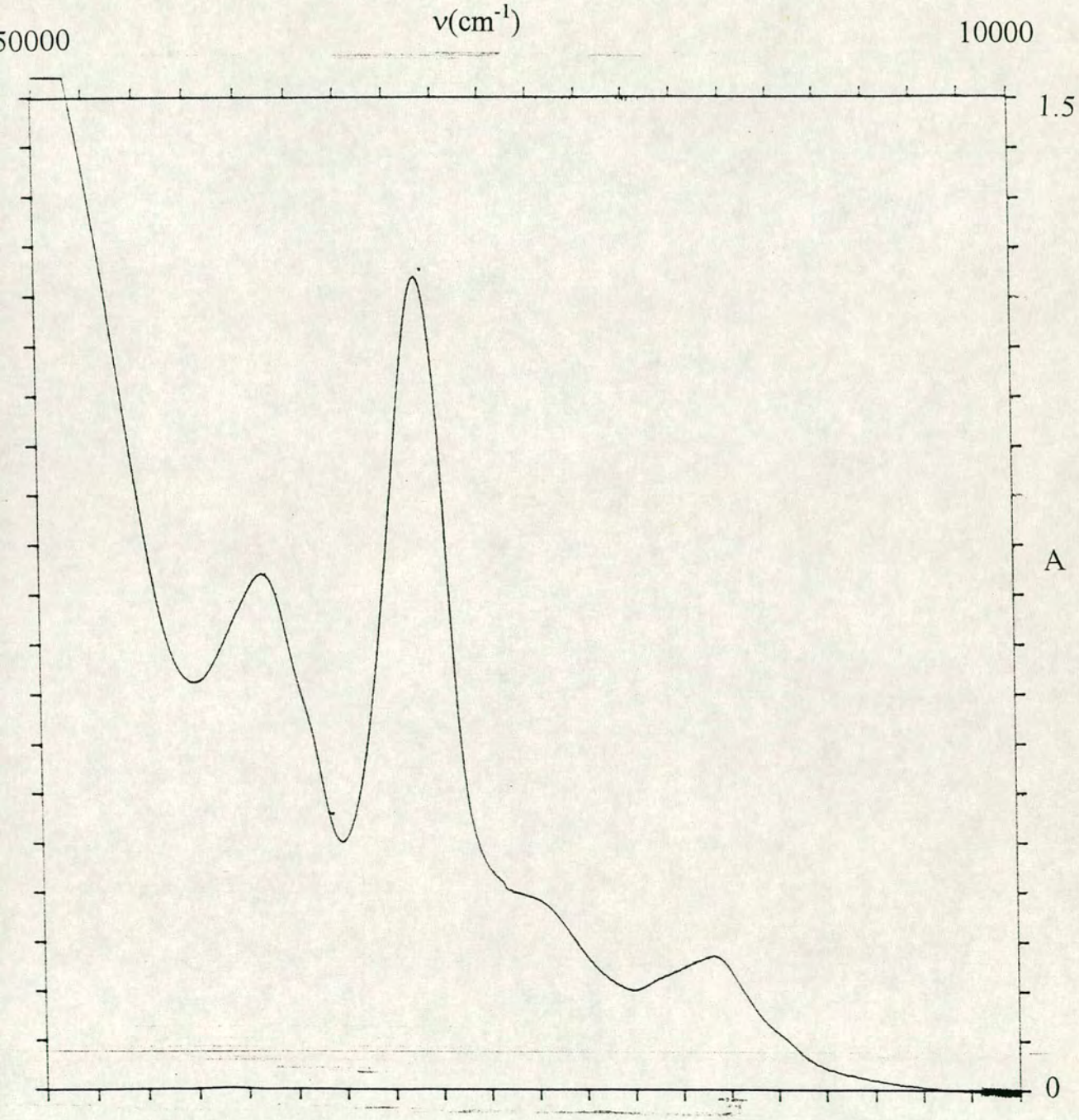

The variation in the energies of the observed absorptions in a range of solvents are shown in table 2.9. These results compare well with those obtained by Fung *et al*, and, as such, give a good linear correlation with A.N.

The complex shows an oxidative process and two reductive processes, dependent on the solvent window. The oxidative process is always observed, is fully reversible at ambient temperature and is assigned as the Ru(II)/Ru(III) couple. The two reductive processes are quasi-reversible at room temperature, but the first can be made fully reversible by cooling to 230K. These processes are assigned as sequential reduction of the two bipyridyl ligands.

Table 2.9 : UV/VIS/NIR Results for $Ru(bpy)_2(CN)_2$

	Band position (cm^{-1})			
Solvent	MLCT(1)	MLCT(2)	$\pi \rightarrow \pi^*(1)$	$\pi \rightarrow \pi^*(2)$
Pyridine	19841	-------	-------	-------
DMF	19904	28441	34015	-------
Acetone	20000	28500	-------	-------
DMSO	20193	28802	33969	-------
MeCN	20610	29172	34437	41257
CH_2Cl_2	20128	28670	34154	40785
$MeNO_2$	20445	-------	-------	-------
EtOH	21556	-------	34530	40984

Figure 2.18 : Cyclic Voltammagram of $Ru(bpy)_2(CN)_2$

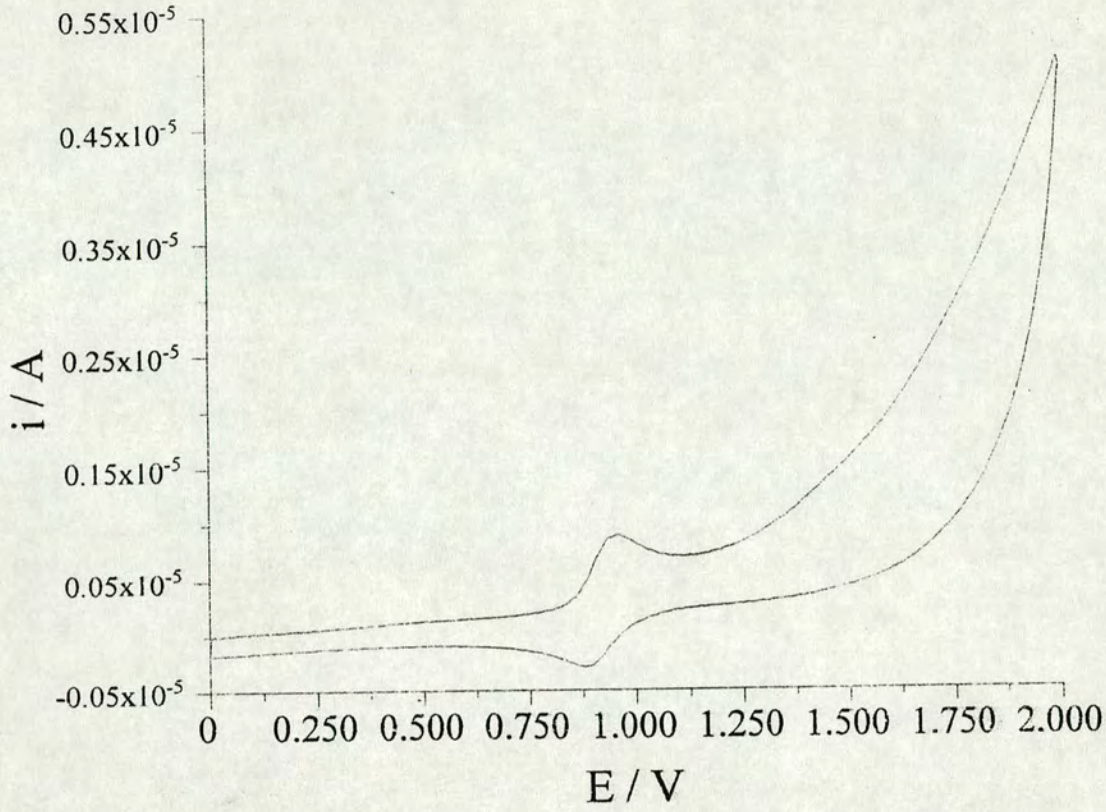

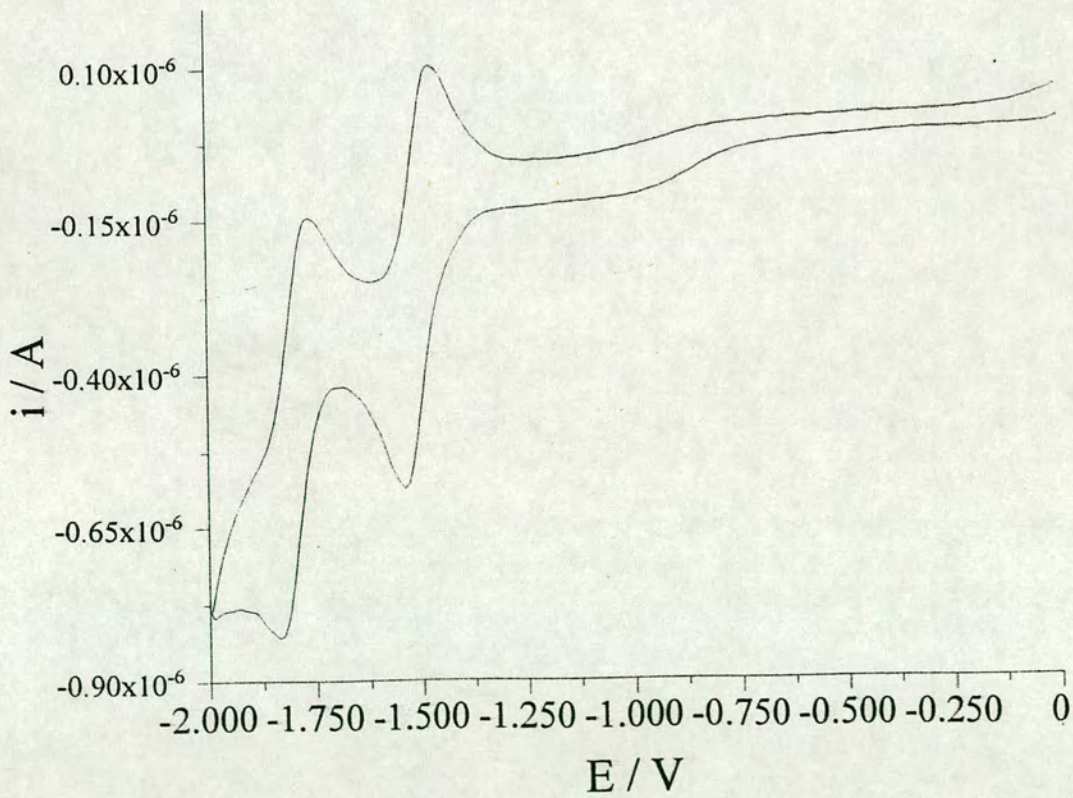

Table 2.10 : $E_{1/2}$ values of $Ru(bpy)_2(CN)_2$ in various solvents

Solvent	$E_{1/2}$ ($Ru^{II/III}$)	$E_{1/2}$ ($bpy^{0/-}$) (1)	$E_{1/2}$ ($bpy^{0/-}$) (2)
Pyridine	+0.92 V	-1.51 V	-------
DMF	+0.93 V	-1.50 V	-1.78 V
DMSO	+0.98 V	-1.51 V	-1.79 V
MeCN	+0.98 V	-1.50 V	-------
CH_2Cl_2	+1.025 V	-1.51 V	-------
$MeNO_2$	+1.003 V	-------	-------

Figure 2.19 : Relationship between MLCT position and $E_{1/2}$ (Ru(II)/Ru(III))

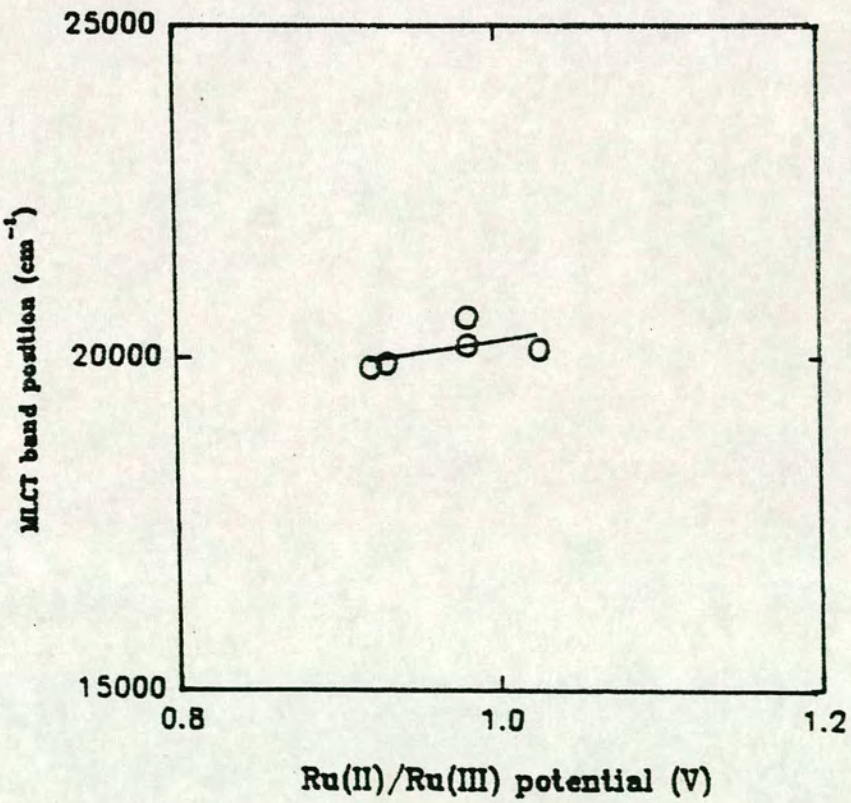

A typical voltammetric response for the complex is shown in figure 2.18 and the half-wave potentials in various solvents are shown in table 2.10. All potentials are corrected versus Fc/Fc^+ at +0.55V.

There is an obvious variation of Ru(II)/Ru(III) potential with solvent, but the ligand based reductions, like those for the analogous iron complex, are independent of the solvent used. A linear relationship between $Ru^{II/III}$ potential and the energy of the first MLCT band is evident from figure 2.19.

We rationalise this relationship in the same manner as for the relationship previously seen for the analogous iron complex. Once again, the interaction of the solvent molecule with the lone pair of electrons on the cyanide ligand perturbs the relative energies of the metal d-orbitals and gives rise to the observed behaviour.

As a result of these variations, it was desirable to study both oxidised and reduced forms of the complex to see if these also display solvent dependent characteristics.

2.3.5 : $[Ru(bpy)_2(CN)_2]^+$

The electronic absorption spectrum of this species has, surprisingly, not been reported in the literature. However, the availability of the OTE cell and other spectroelectrochemical techniques allows us to study this species *in situ*.

Unlike the corresponding iron species, chemical oxidation is only possible using iron(III) trichloride, no reaction occuring when using concentrated nitric acid or sodium nitrite as the oxidising agent. Results obtained in this manner are again similar to those generated by bulk electrogeneration.

Electrogeneration of the oxidised species can be conveniently monitored in the UV/VIS/NIR region by use of the OTE cell. The results of such an experiment are

Figure 2.20 : Absorption spectrum monitoring of $Ru(bpy)_2(CN)_2$ in DMF

$T = 243$ K, $E_{appl} = + 1.1$ V

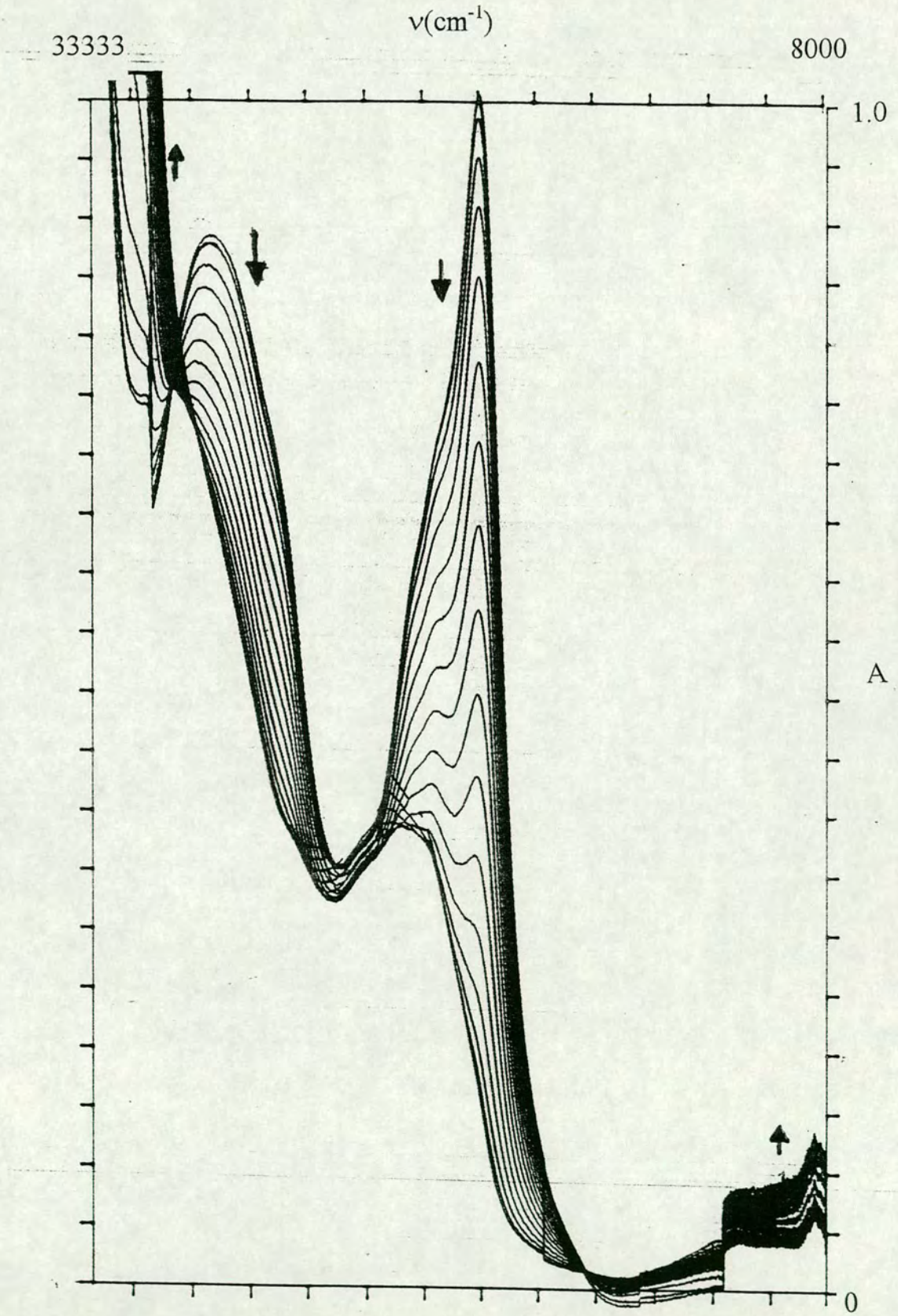

shown in figure 2.20. This demonstrates the collapse of the two MLCT bands and, as for the iron complex, no LMCT process is seen growing in, although such a transition might be observed. In this case, the LMCT band lies outwith the range studied, and can be observed under different experimental conditions (see page 72). The Ru(III) $\rightarrow$ bpy MLCT, expected at higher energy, will be masked by the bpy intraligand transitions. Both this and the LMCT band would be expected to be much less intense than the original MLCT process.

The presence of an unpaired electron on the d^5 metal centre makes this species an ideal candidate for further study using epr spectroscopy. Unfortunately, iron(III) trichloride is epr active, and so chemically generated samples cannot be used to gain any meaningful results due to overlap of the two signals. Study of electrogenerated samples is still viable, however. A typical epr spectrum for the oxidised complex is shown in figure 2.21.

This spectrum shows the rhombic line shape typically associated with a low spin d^5 metal centre with C_2 symmetry. The g values obtained by bulk electrogeneration of the complex in various solvents are given in table 2.11.

The values obtained from these experiments appear solvent independent. Indeed, the variation in g_3 is only ± 0.003, which is well within experimental error.

We can analyse the data from the epr experiments can be examined using the method described by Hill[25]. The results obtained are quite similar to those for the analogous iron complex, and are detailed in table 2.12.

Again, we do not know the absolute values of λ for Ru(II) and Ru(III). We can, however, use previously determined values to estimate the energies of the crystal

Figure 2.21 : EPR spectrum of $[Ru(bpy)_2(CN)_2]^+$ in DMF, T = 77 K

Electrogenerated, E_{appl} = + 1.1 V

Centre Field : 3300 G
Sweep Width : 2000 G
Frequency : 9.35 GHz

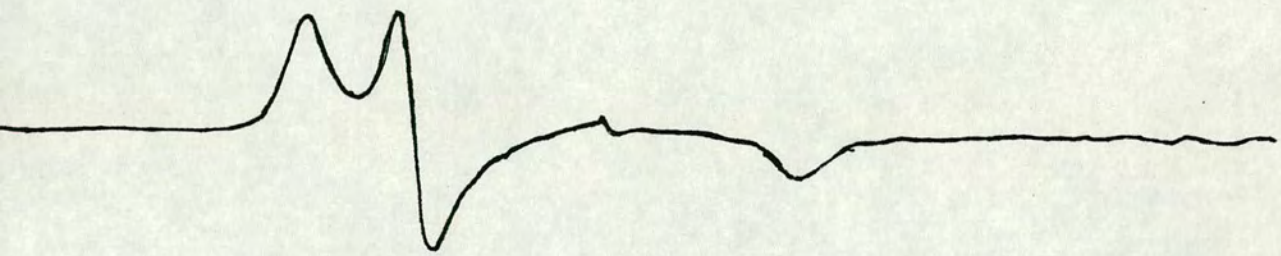

Table 2.11 : EPR data for electrochemically generated $[Ru(bpy)_2(CN)_2]^+$

Solvent	g_1	g_2	g_3
DMF	2.500	2.300	1.789
CH_2Cl_2	2.509	2.310	1.789
MeCN	2.479	2.301	1.786
$MeNO_2$	2.504	2.305	1.786

Table 2.12 : Derived parameters for electrochemically generated $[Ru(bpy)_2(CN)_2]^+$

Solvent	p	q	r	k	Δ/λ	V/λ	E_1/λ	E_2/λ
DMF	0.190	0.981	-0.031	0.90	4.10	1.50	3.46	5.17
DMF	0.775	0.632	-0.019	1.16	0.21	0.08	1.44	1.58
MeCN	0.190	0.981	-0.030	0.90	4.07	1.38	3.47	5.08
MeCN	0.774	0.633	-0.019	1.16	0.21	0.07	1.44	1.58
$MeNO_2$	0.191	0.981	-0.030	0.90	4.09	1.48	3.45	5.14
$MeNO_2$	0.774	0.633	-0.019	1.16	0.22	0.08	1.44	1.58
CH_2Cl_2	0.189	0.981	-0.030	0.90	4.09	1.51	3.49	5.22
CH_2Cl_2	0.774	0.633	-0.019	1.16	0.22	0.08	1.44	1.58

field transitions. For ruthenium(II), λ is approximately 1000 cm^{-1} [27], while for ruthenium(III) λ is 1180 cm^{-1}. We can use these values to obtain limits for E_1 and E_2. Thus we estimate E_1 to be between 3450 and 4080 cm^{-1}, and E_2 between 5140 and 6180 cm^{-1}.

Although E_1 is expected to lie outwith the range of the UV/VIS/NIR spectrometer, it should be possible to observe E_2 and hence obtain a value for λ. However, the low extinction coefficient of such absorbances, expected to be around 30 $mol^{-1}cm^{-1}$, means that it may be difficult to observe the transitions. Using a cell with 1 cm path length allows a greater chance of observation, but also precludes *in situ* electrogeneration of the complex. There are also absorbances due to electrolyte and solvents in the region of interest, which may obscure the very weak ligand field absorptions expected.

A solvent which does not absorb significantly in the near infra-red (4000 cm^{-1} to 10000 cm^{-1}) is propylene carbonate. Therefore, a saturated solution of $Ru(bpy)_2(CN)_2$ in propylene carbonate with 0.1 M TBA BF_4 as electrolyte can be used in an attempt to observe these low energy bands, using the OTE cell. The concentration of test species required precludes the observation of MLCT and intraligand transitions (they become too intense for the spectrometer to measure). However, it should now be possible to observe the very low intensity bands predicted.

The results of such an experiment are shown in figure 2.22. The intense, sharp absorbances between 4000 and 4500 cm^{-1} are due to the solvent, but are very well defined. As they occur in one possible area of interest, where a high value of λ could lead to an observable E_1, it is desirable to subtract the initial spectrum from the final

Figure 2.22 : NIR absorption spectrum monitoring of $Ru(bpy)_2(CN)_2$ in propylene carbonate, T = 243 K, E_{appl} = +1.2 V

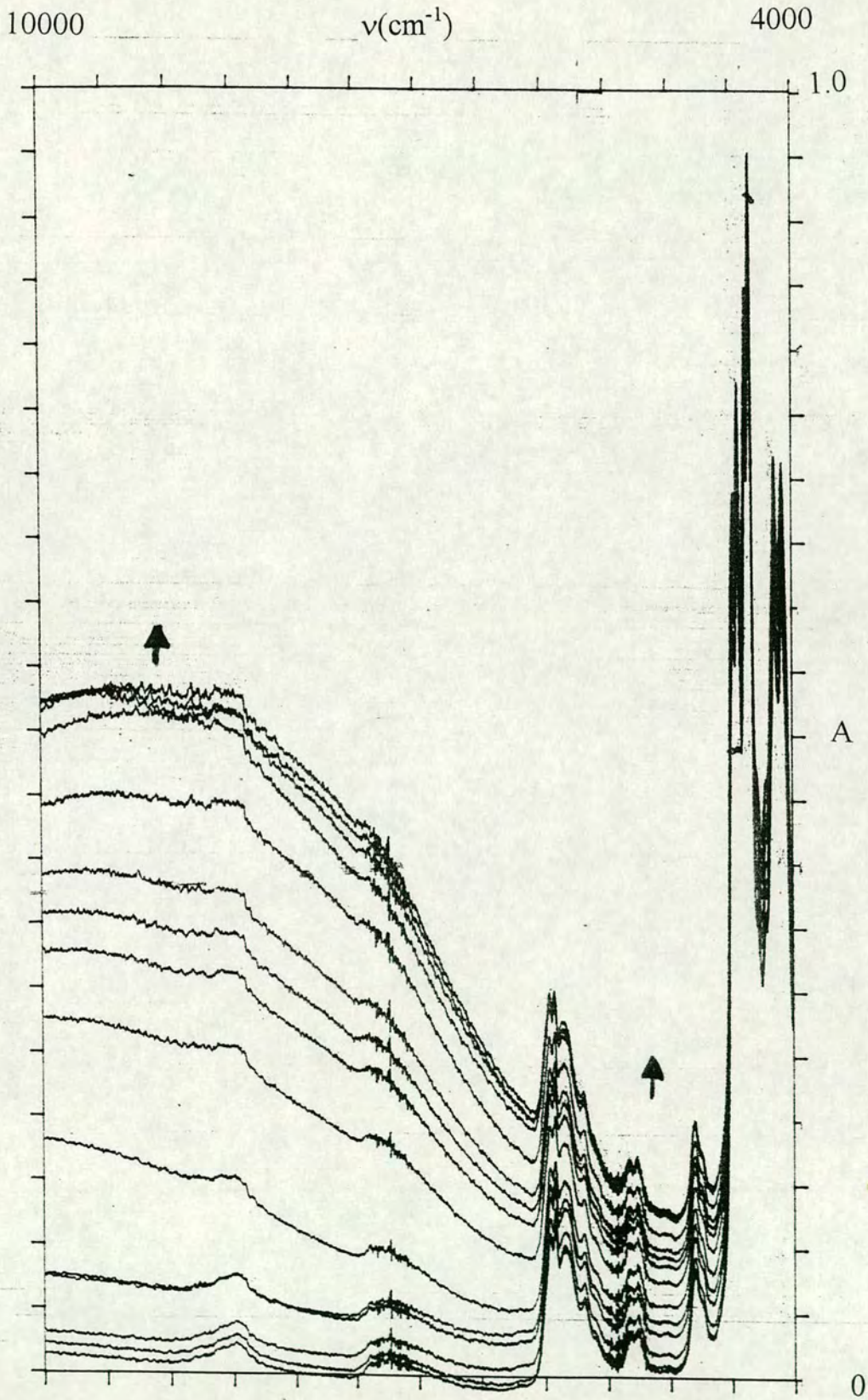

Figure 2.23 : Subtraction of initial spectrum from final spectrum of electrogenerated $[Ru(bpy)_2(CN)_2]^+$ in propylene carbonate

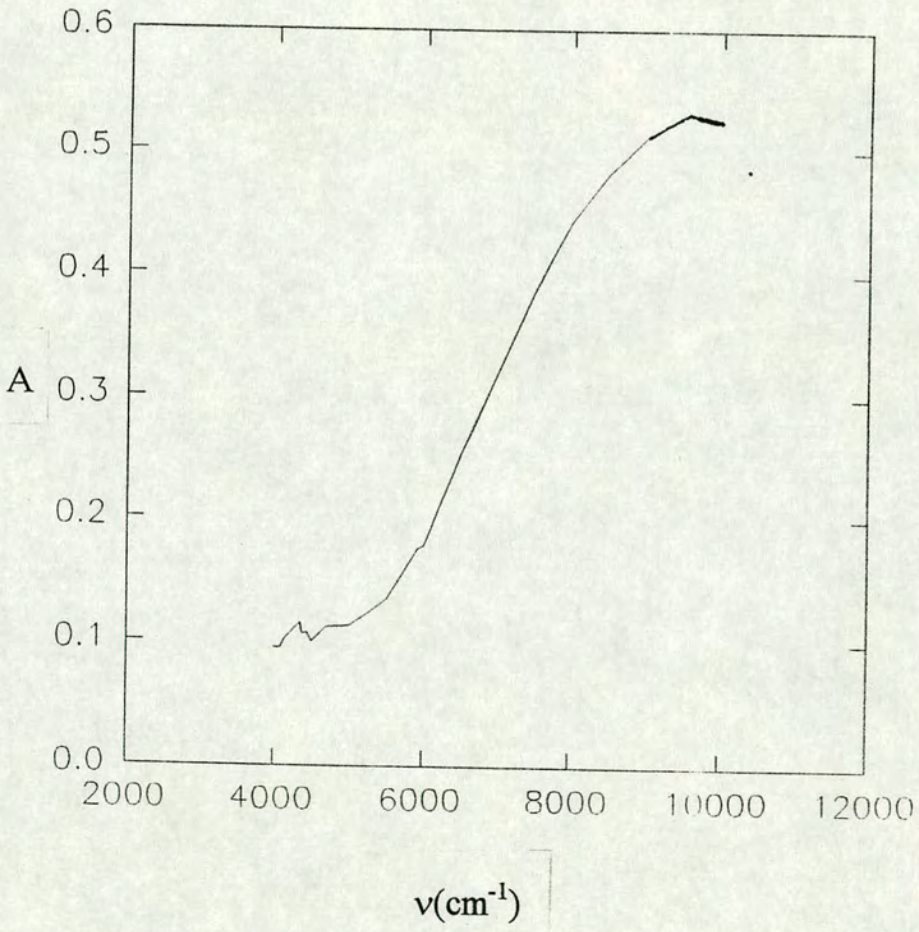

spectrum, in order to see those absorbances not due to the solvent. The result of this is shown in figure 2.23.

The spectrum shows a very weak band at around 4300 cm^{-1}. If we assign this absorption band to the E_1 transition then the experimentally determined value for λ computes at 1240 cm^{-1}. This value of λ is in reasonable agreement with previously determined values of λ for Ru(III). The extinction co-efficient of the transition is between 20 and 100 $mol^{-1}cm^{-1}$, although accurate determination is difficult due to the presence of the much more intense band at 9000 cm^{-1}. This absorption band is assigned as the LMCT process discussed earlier, and has an extinction co-efficient of around 500 $mol^{-1}cm^{-1}$. Unfortunately, it will obscure the predicted, very weak E_2 transition.

An alternative assignment would be to consider the weak absorption at 4300 cm^{-1} as originating from E_2. However this would result in a value of λ of around 840 cm^{-1} which is significantly different from previously reported values of λ for Ru(III).

2.3.6 : $[Ru(bpy)_2(CN)_2]^-$

As for the iron complex previously described, the reduction product of *cis*-$Ru(bpy)_2(CN)_2$ is of interest. Again, we hope to observe the superimposition of the previously seen solvent dependent behaviour, associated with the metal centre, with the expected features of a reduced, chelated bipyridyl.

We can monitor the change in the electronic absorption spectrum on reduction by use of the OTE cell. The results of such an experiment are shown in figure 2.24. This shows the growth of bands associated with a reduced bpy ligand, coupled with the reduction in intensity of the lower energy bpy $\pi \rightarrow \pi^*$ transition. There is a small

Figure 2.24 : Absorption spectrum monitoring of $Ru(bpy)_2(CN)_2$ in DMF

T = 243 K, E_{appl} = -1.7 V

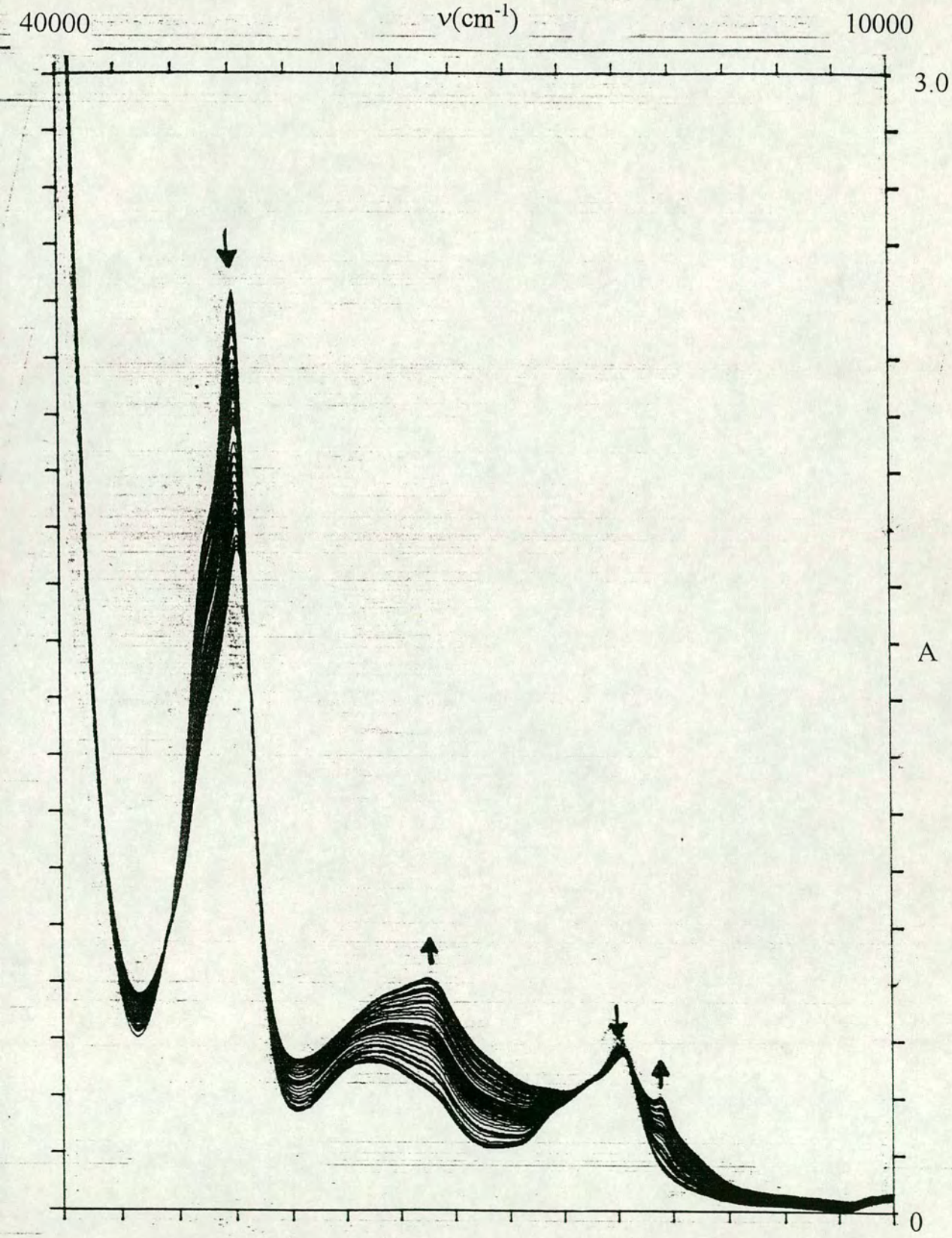

reduction in intensity around the lower energy MLCT band, which we would expect to reduce by half. However, some of the reduced bpy transitions occur in this area, and so new absorbances grow in coincidental with the collapsing MLCT. Thus only a small reduction in intensity is observed. If the potential is returned to zero after generation the initial spectrum is regained. Thus we electronically characterise the first one-electron reduction product of $[Ru(bpy)_2(CN)_2]$ as $[Ru(II)(bpy^0)(bpy^-)(CN)_2]^-$.

Again, the presence of an unpaired electron should lead to the reduced complex yielding an epr spectrum. This is indeed the case, and the epr spectrum of the reduced complex in DMF at 77K is shown in figure 2.25.

This spectrum is typical for an unpaired electron delocalised over the bipyridyl π^* system, and shows no measurable interaction with the metal centre. It is virtually identical to the spectrum for reduced tris(bipyridyl)ruthenium(II), as described in work by Motten *et al*[35]. The *g*-value of 2.008 is very close to that for the free electron, and to that seen for many organic radicals.

As discussed previously, the problem of whether the unpaired electron is delocalised over one ligand or both of them is best investigated by variable temperature epr studies. Again, lack of time prevented this experiment from being carried out.

Figure 2.25 : EPR spectrum of $[Ru(bpy)_2(CN)_2]^-$ in DMF, T = 77 K

Centre Field : 3300 G
Sweep Width : 400 G
Frequency : 9.35 GHz

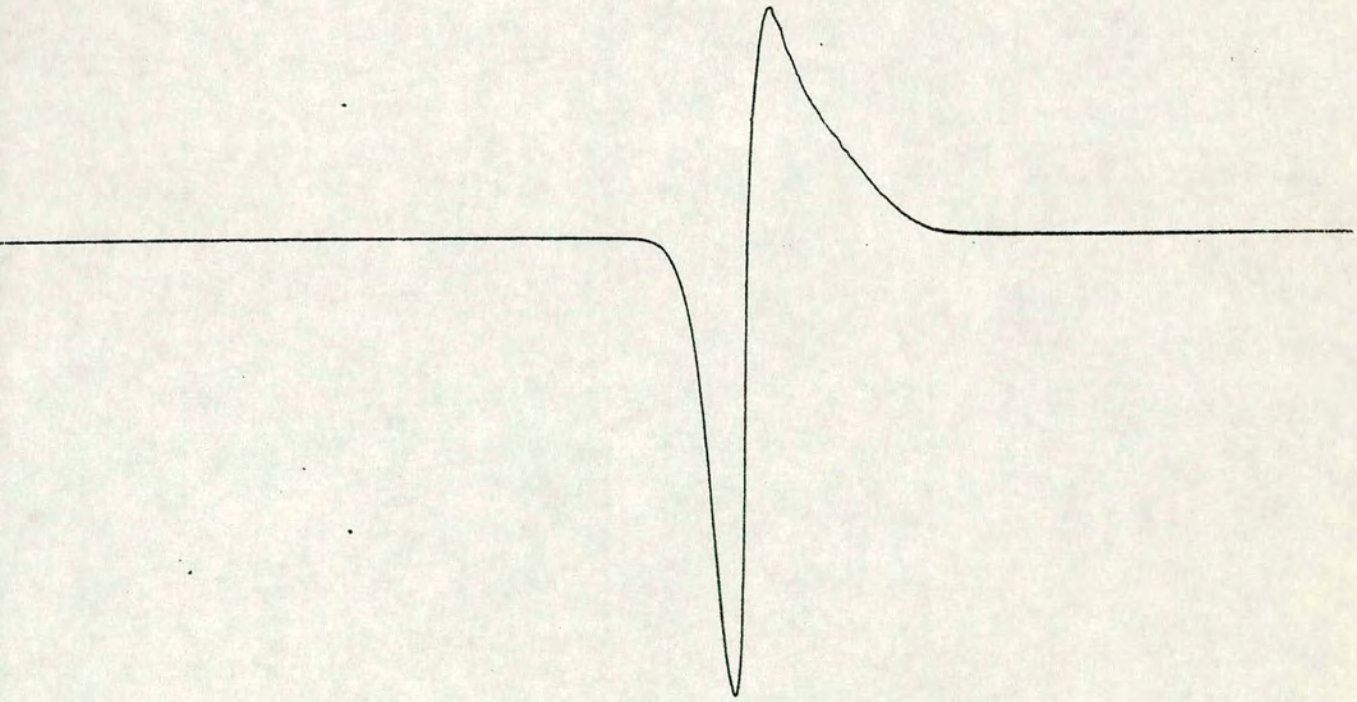

2.3.7 : $Os(bpy)_2(CN)_2$

Solvent dependent behaviour of bis(2,2'-bipyridyl)dicyanoosmium(II) has not been extensively reported in the literature. The electronic absorption spectrum of the complex was recorded by Bryant *et al* in 1971[8]. This spectrum showed the same general features seen for the corresponding iron and ruthenium examples. Thus two ligand $\pi \rightarrow \pi^*$ internal bands were observed at 41180 and 34400 cm^{-1}. However, the MLCT bands expected are more complex than those seen for the related iron and ruthenium species. This is because, as a third row transition metal, osmium complexes have a high degree of spin-orbit coupling. Under these conditions spin labels become meaningless, and transitions which would be forbidden normally, such as spin-triplet transitions, become allowed. Thus a considerably more complex absorption spectrum is seen.

In particular, the region around what could be considered as the higher energy ^{1}MLCT band is particularly complex, and precludes a specific maximum being found and studied. The lower energy MLCT band, formally ($d(\pi) \rightarrow \pi^*$ (1)), is still clearly visible and thus can be investigated in a range of solvents. However, due to the number of extra transitions present, the position of the maximum absorption peak is investigated.

A typical electronic absorption spectrum of the complex in DMF is shown in figure 2.26. The bands that are clearly seen, and which can be accurately assigned are the $d(\pi) \rightarrow \pi^*$ (1) MLCT band and the $\pi \rightarrow \pi^*$ (1) ligand internal transition. A second ligand transition ($\pi \rightarrow \pi^*$ (2)) can be observed in solvents with a suitable UV window, such as methylene chloride.

Figure 2.26 : Electronic Absorption spectrum of $Os(bpy)_2(CN)_2$ in DMF

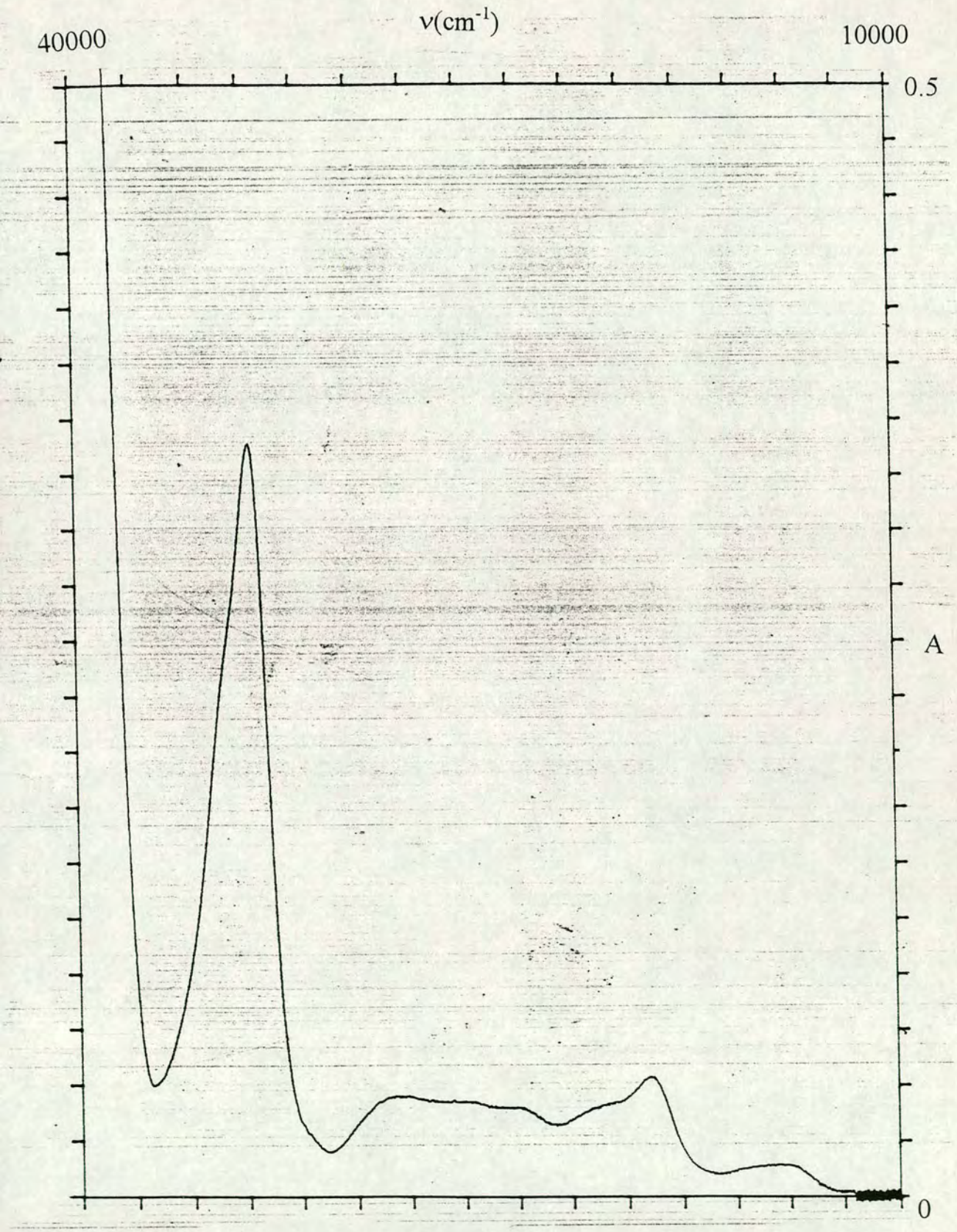

The spectrum of $[Os(bpy)_2(CN)_2]$ is solvent dependent. The energies of the absorptions in a range of solvents are given in table 2.13.

As for the corresponding iron and ruthenium compounds it is possible to plot the variation of the lowest energy MLCT band against the various solvent parameters given in table 2.1 previously. Once again, a plot versus A.N. gives the best linear correlation, and this plot is shown in figure 2.27.

Table 2.13 : UV/VIS/NIR Results for $Os(bpy)_2(CN)_2$

	Band position (cm^{-1})			
Solvent	MLCT(1)	MLCT(2)	$\pi \rightarrow \pi^*(1)$	$\pi \rightarrow \pi^*(2)$
DMF	19365	28936	34061	------
DMSO	19380	28605	33738	------
MeCN	19716	29275	34437	------
CH_2Cl_2	19608	29412	34200	41257
$MeNO_2$	19968	-------	------	------
MeOH	20532	29587	34532	38287

Figure 2.27 : Plot of MLCT position for $Os(bpy)_2(CN)_2$ against A.N.

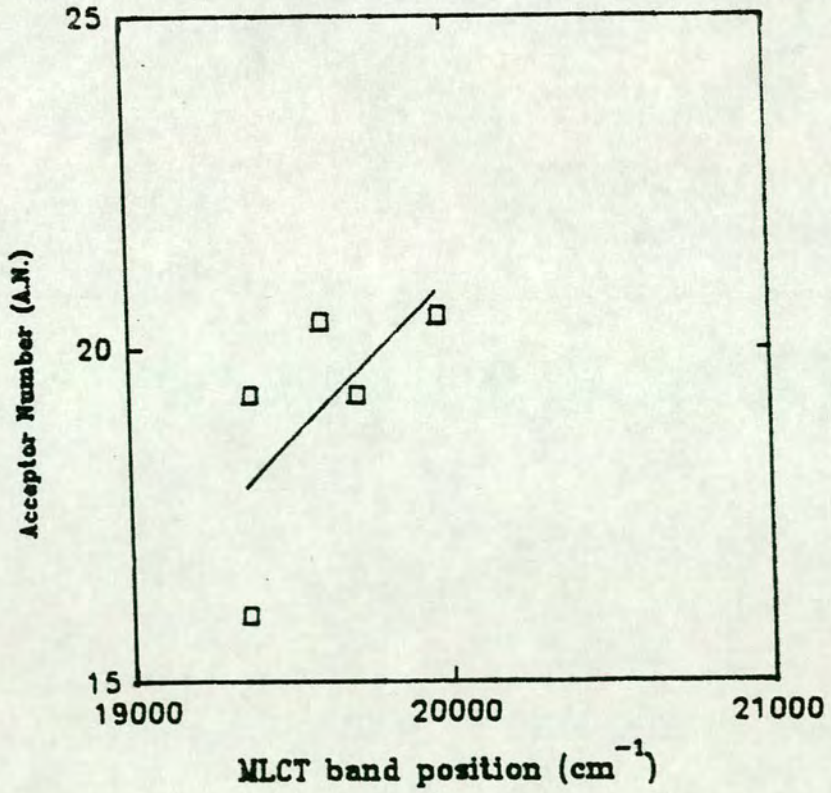

We have investigated the electrochemistry of bis(2,2'-bipyridyl) dicyanoosmium in a range of solvents. Providing the solvent window is large enough, the complex demonstrates one process in the oxidative region, and two processes in the reductive region. The oxidative process appears fully reversible at room temperature, and is assigned as the osmium II/III couple. The first of the reductive processes is quasi-reversible at room temperature, and the second process is irreversible. These processes can be made reversible by cooling to 233K and 218K respectively. These are assigned as sequential reduction of each of the bipyridyl ligands in turn.

A typical cyclic voltammagram for the complex is shown in figure 2.28, and the half-wave potentials in various solvents are shown in table 2.14. All potentials are corrected versus Fc/Fc^{+} at +0.55V.

Once more there is an obvious variation in the metal oxidation potential with the solvent, but the ligand based reduction potentials are solvent independent. This corresponds well with the observed behaviour of the iron and ruthenium complexes seen previously. A linear relationship between the oxidation potential and the energy of the MLCT band is evident from figure 2.29.

The rationale for this behaviour is the same as for the iron and ruthenium complexes examined previously. The solvent interacts with the lone pair of electrons on the cyanide ligand and hence the energies of the metal d-orbitals are perturbed. These perturbations are manifested in the observed variation of MLCT energy and oxidation potential with solvent.

Figure 2.28 : Cyclic Voltammagram of $Os(bpy)_2(CN)_2$

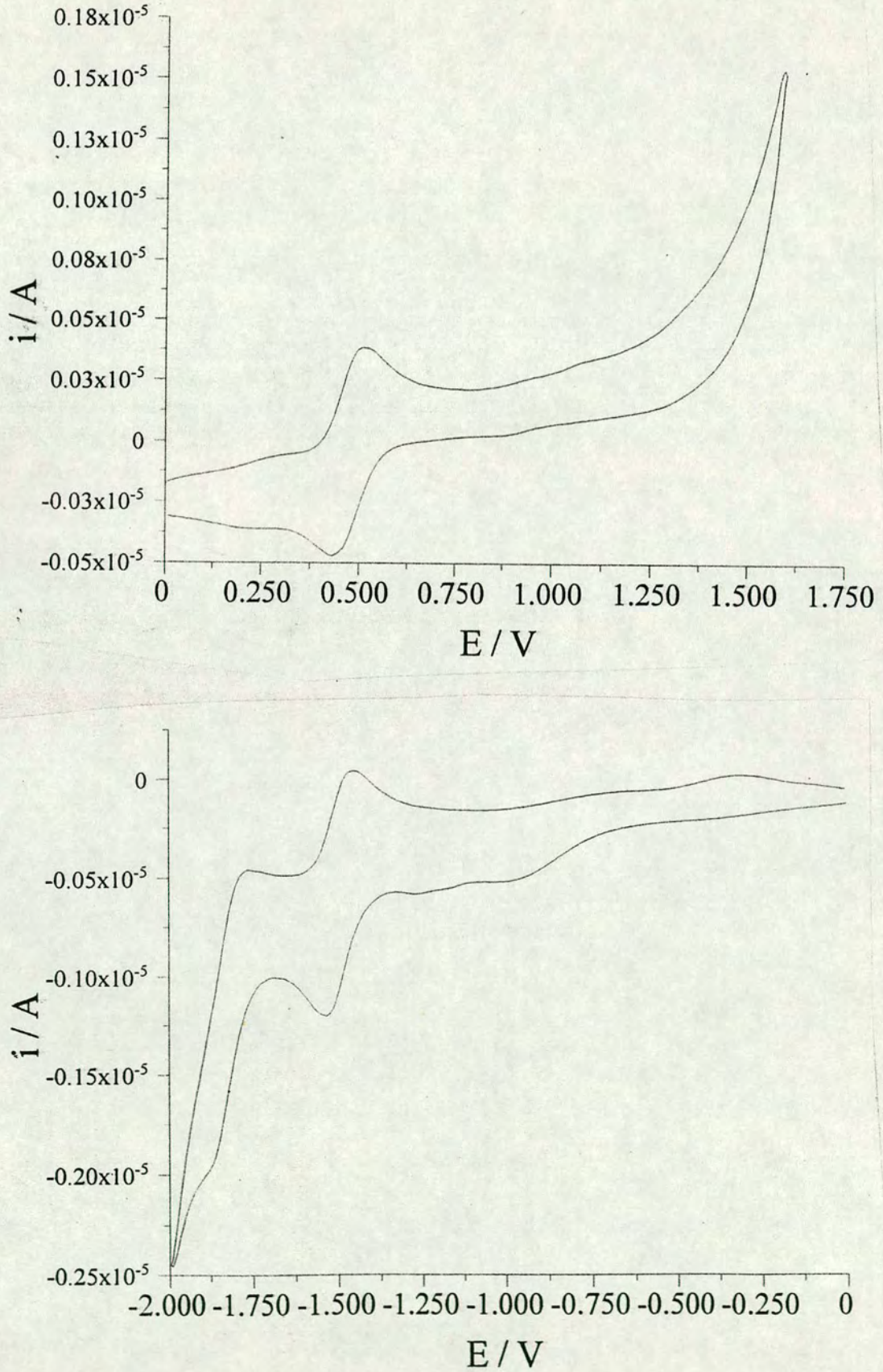

Table 2.14 : $E_{1/2}$ values for $Os(bpy)_2(CN)_2$ in various solvents

Solvent	$E_{1/2}$ ($Os^{II/III}$)	$E_{1/2}$ ($bpy^{0/-}$) (1)	$E_{1/2}$ ($bpy^{0/-}$) (2)
DMF	+ 0.555 V	- 1.435 V	~- 1.72 V
DMSO	+ 0.57 V	- 1.42 V	- 1.70 V
MeCN	+ 0.60 V	- 1.42 V	- 1.71 V
$MeNO_2$	+ 0.625 V	-------	-------
CH_2Cl_2	+ 0.605 V	~- 1.45 V	-------
MeOH	+ 0.78 V	-------	-------

Figure 2.29 : Relationship between MLCT position and $E_{1/2}$ (Os(II)/Os(III))

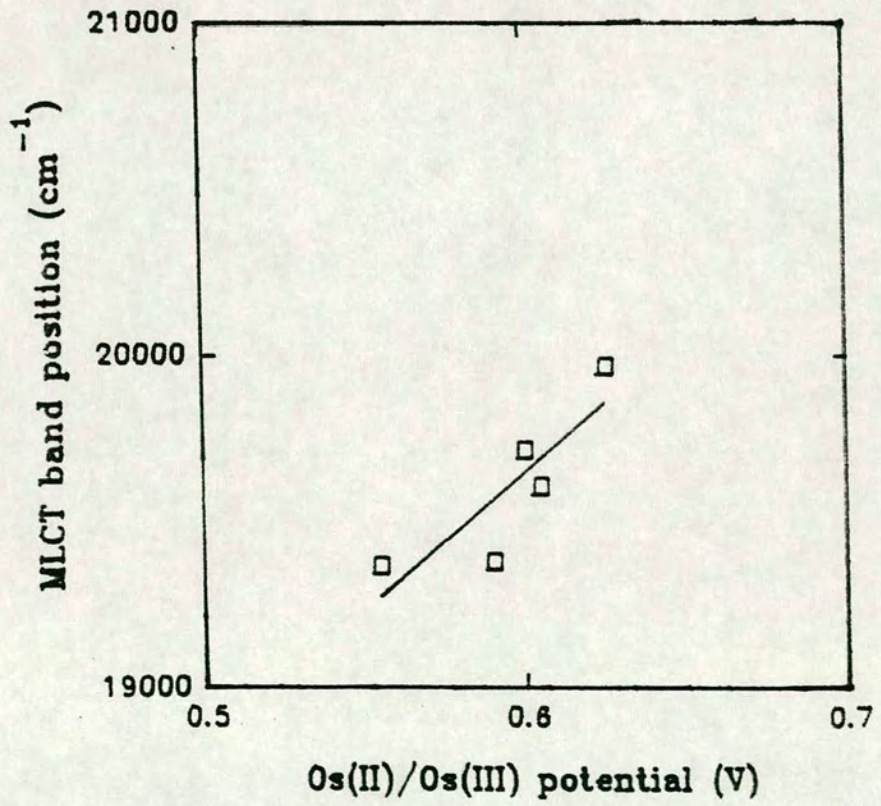

Because of these relationships, it is again desirable to investigate both the oxidised and reduced forms of the complex, to see if they too display this solvent dependent behaviour.

2.3.8 : $[Os(bpy)_2(CN)_2]^+$

There has previously been little investigation of the oxidised form of the complex. The electronic absorption spectrum has not been reported. However, the ease of *in situ* generation, by utilising the OTE cell, allows us to study the complex in a range of solvents.

Like the corresponding iron species, chemical generation with excess nitric acid is possible. Where obtained, such results are presented as an alternative to bulk electrogeneration experiments. Care must be taken, however, as, once more, preferential solvation of the complex by water or excess acid may occur. Thus any solvent dependency seen in these experiments may be due to this effect.

Electrogeneration of the oxidised complex can be easily carried out and monitored by use of the OTE cell. The results of such an experiment are shown in figure 2.30.

Again, we can observe the collapse of the MLCT bands as we oxidise the complex. No new bands grow in the region under investigation, although we might expect a ligand-to-metal charge transfer (LMCT) band to grow in. No such band is observed. It may be that such a band does exist, but that it is obscured by other transitions or it lies outwith the range studied.

Although it cannot be seen in figure 2.30, there is also a shift in the energies of the ligand internal transitions upon oxidation. This is due to the changes brought

Figure 2.30 : Absorption spectrum monitoring of $Os(bpy)_2(CN)_2$ in DMF

$T = 243$ K, $E_{appl} = +0.8$ V

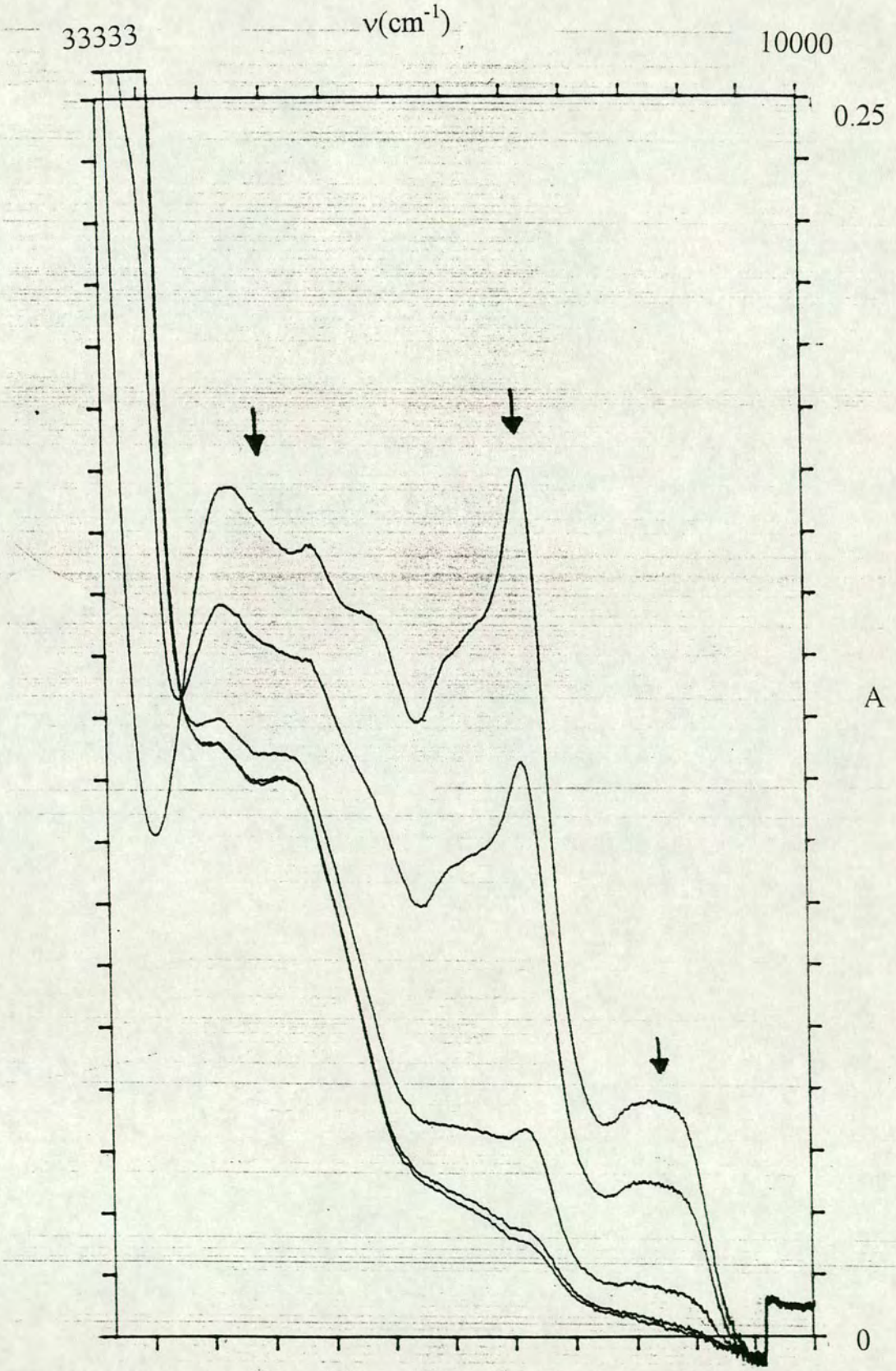

about by oxidation of the metal centre, which has some effect on the ligand orbitals most closely associated with the osmium atom. Unfortunately, no detailed information about the interaction of the complex with the various solvents can be gleaned from these results.

However, the presence of an unpaired electron on the d^5 metal centre means that this species should be a good candidate for study by epr spectroscopy. There are numerous examples of osmium(III) species yielding clear epr spectra[27,28]. Unfortunately, in this case no satisfactory epr signal could be obtained, despite repeated electrogenerations in a wide range of solvents.

2.3.9 : $[Os(bpy)_2(CN)_2]^-$

As in the case of the corresponding iron and ruthenium species, the characteristics of the first reduction product of $[Os(bpy)_2(CN)_2]$ may be of interest. We would expect to see very similar behaviour for this complex when compared with those previously discussed (see 2.3.3 and 2.3.6).

Again, we monitored the reduction by use of the OTE cell, and the results of such an experiment are shown in figure 2.31. This clearly demonstrates the growth of bands associated with a reduced bpy unit, coupled with a 50% reduction in intensity for the MLCT and bpy internal processes. The collapse of the MLCT process is again masked by the growth of these new bands. There are four isosbestic points seen, indicating a reversible process involving no intermediates. Upon return of the potential to zero, the initial spectrum was regenerated.

This complex also yields an epr signal. A typical spectrum, that of the reduced complex in DMF, is shown in figure 2.32. Once more we observe a single line, with a

Figure 2.31 : Absorption spectrum monitoring of $Os(bpy)_2(CN)_2$ in DMF

$T = 243$ K, $E_{appl} = -1.6$ V

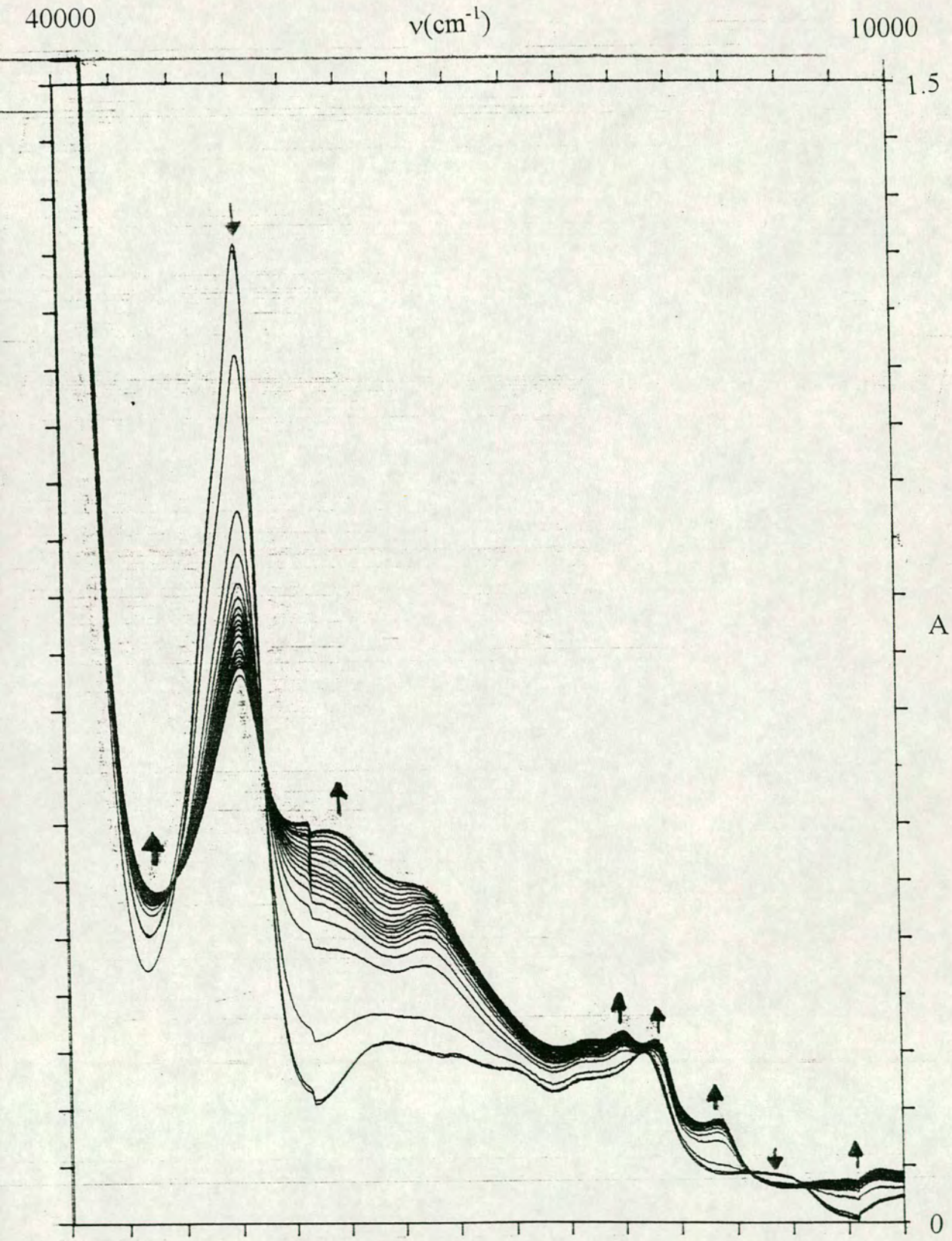

Figure 2.32 : EPR spectrum of $[Os(bpy)_2(CN)_2]^-$ in DMF, T = 77 K

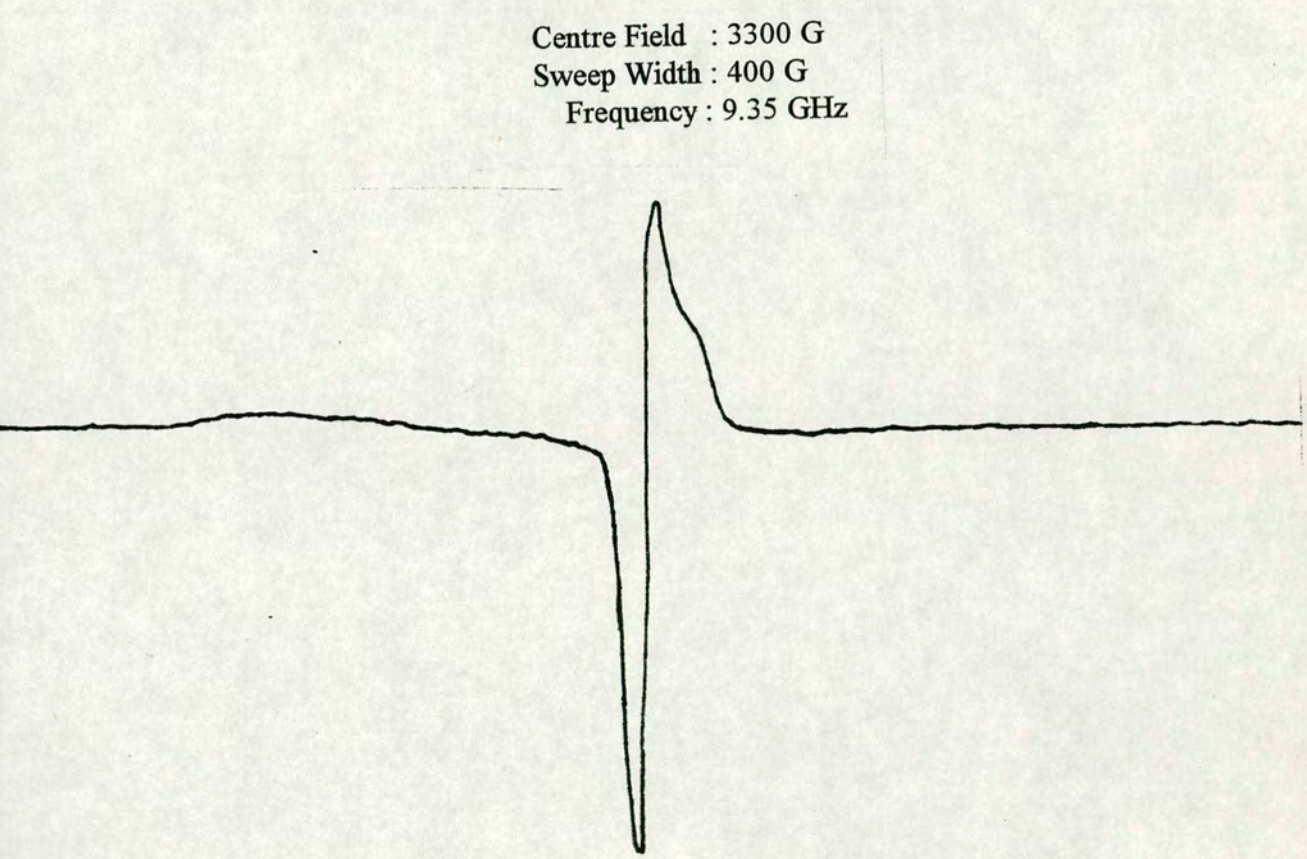

g value of 1.993. Again this is typical behaviour for an unpaired electron on the bpy ligands. Whether this electron is localised on one ligand or 'hopping' between the two is best determined by variable temperature experiments, with line broadening indicating the electron moving between ligands. Lack of time prevented us from attempting this experiment.

2.4 : Conclusions

From the results described in this chapter, it is clear that all three complexes appear to behave in a broadly similar manner. All the M(II) species display solvent dependent MLCT processes in their UV/VIS/NIR spectra, and all show a solvent dependent metal based oxidation, and two solvent independent ligand based reductions (solvent window permitting). The iron complex shows a greater degree of solvent dependence than either the ruthenium or the osmium complex. We can rationalise this by considering that the iron complex is a $3d^6$ species, whilst the ruthenium and osmium are $4d^6$ and $5d^6$ respectively. Thus the orbitals involved in the Fe-cyanide interaction are less diffuse, and so a stronger interaction will occur, and so any perturbation of the cyanide ligand (in this case by the solvent) will have a larger effect.

Upon oxidation of the metal centre, all three complexes demonstrate the collapse of the MLCT bands, and no new bands are observed between 10000 and 50000 cm^{-1} in any case. In the case of the iron and ruthenium species epr spectra may be obtained. The resultant spectra are completely independent of both solvent and method of generation. Analysis of the resultant data predicts the presence of low intensity (20-100 mol^{-1} dm^3 cm^{-1}) bands in the near infra-red, which we have observed

for the oxidised ruthenium complex. This confirms that the rhombic splitting, due to lowering of the symmetry of the system on going from $M(LL)_3$ to $M(LL)_2(X)_2$, is relatively unimportant compared to the axial splitting of the metal d-orbitals. We rationalise the lack of solvent dependent behaviour for the oxidised M(III) containing species by proposing a reduced interaction between the metal centre and the cyanide ligands upon oxidation, thus preventing the solvent from affecting the d-orbitals by perturbation of this system.

Upon reduction all three complexes show the growth of bands in the absorption spectrum due to reduced bpy, along with the partial collapse of MLCT and ligand internal processes. The epr spectra of all three singly reduced species demonstrate a single signal, strongly suggestive of an electron delocalised over the bpy π system, although whether this electron is localised on one ligand, or can 'hop' between the two is not known. As expected, this resonance is not affected by solvent.

2.5 : Preparation of compounds

2.5.1 : $Fe(bpy)_2(CN)_2$

The procedure used was as described in the literature[2]. In a typical preparation, ferrous ammonium sulphate ($Fe(NH_4)_2(SO_4)_2$, 1.565g) and 2,2'-bipyridine (1.932g) were dissolved in 200ml water, and the solution was heated to just below boiling. Potassium cyanide (KCN, 4.05g) was dissolved in approximately 10ml of water, and added to the mixture. On cooling a dark red precipitate was obtained. This precipitate was filtered, washed with water and ether and dried under vacuum. The typical yield obtained was 85-90 %.

Analysis : Calculated for $FeC_{22}H_{16}N_6$: C 62.88 % H 3.84 % N 20.00 %

Found : C 55.09 % H 5.29 % N 17.47 %

Corresponds to $Fe(bpy)_2(CN)_2.3H_2O$ (Calaculated : C 55.71 % H 4.68 % N 17.72 %)

2.5.2 : $Ru(bpy)_2(CN)_2$

The complex was prepared using two different methods from the literature[6,7]. In a typical preparation utilising the first method, bis(bipyridine)dichlororuthenium(II) ($Ru(bpy)_2Cl_2$, 0.18226g) and potassium cyanide (1g) were dissolved in methanol/water. The mixture was refluxed for one hour, then the methanol was removed on a rotary evaporator. Orange crystals were formed on cooling of the aqueous solution and these were filtered and recrystallised from methanol/ether. The yield was typically in excess of 90%.

The other synthetic method ensured that the product had the *cis* configuration. In a typical preparation, oxalatobis(bipyridyl)ruthenium(II) ($Ru(bpy)_2(ox)$, 1g) was dissolved in 100ml of methanol. Potassium cyanide (1g) was dissolved in 25ml of

water and added to the methanolic solution. The resulting mixture was then refluxed for 16 hours. The solution was evaporated to dryness, and the residue was extracted with two 15ml portions of boiling water. The extracts were filtered hot, leaving the product as red crystals on the filter. The crystals were washed with ether and dried under vacuum. Again, yields in excess of 90% were recorded. This method was preferred as the synthesis and purification of the starting material was easier.

Analysis : Calculated for $RuC_{22}H_{16}N_6$: C 56.77 % H 3.46 % N 18.05 %

Found : C 47.64 % H 4.58 % N 14.66 %

Corresponds to $Ru(bpy)_2(CN)_2.6H_2O$ (Calculated : C 46.07% H 4.92% N 14.65 %)

2.5.3 : $Os(bpy)_2(CN)_2$

This complex was prepared by the method described in the literature[8]. In a typical preparation, previously prepared bis(bipyridyl)dichloroosmium(II) ($Os(bpy)_2Cl_2$, 0.09036g) was dissolved in ethanol/water, along with potassium cyanide (1g). This mixture was refluxed for eight hours, filtered, and the ethanol was removed on a rotary evaporator. Green/brown crystals of the product precipitated. These were filtered off, washed with water and ether, and dried under vacuum. The yield was typically 40-50%.

Analysis : Calculated for $OsC_{22}H_{16}N_6$: C 47.64 % H 2.91 % N 15.15 %

Found : C 39.18 % H 4.32 % N 12.70 %

Corresponds to $Os(bpy)_2(CN)_2.6H_2O$ (Calculated : C 39.87 % H 4.26 % N 12.68 %)

2.5.4 : TBA BF_4

Tetrabutylammonium tetrafluoroborate (TBA BF_4) was prepared by a well established method. A 48 wt. % solution of fluoroboric acid (HBF_4, 100ml) was

neutralised by addition of a 40 wt. % solution of tetrabutylammonium hydroxide (TBAOH) until the pH of the solution was 7. This led to a white precipitate, which was filtered off, recrystallised from methanol/water, and dried under vacuum.

2.6 : References

1. G.A. Barbieri, *Atti. Accad. Lincei*, **1934**, 20, 273
2. A.A. Schilt, *J. Am. Chem. Soc.*, **1960**, 82, 3000
3. J. Burgess, *Spectrochimica Acta*, **1970**, 26A, 1369
4. J. Burgess, S.F.N. Norton, *J. Chem. Soc. Dalton Trans.*, **1972**, 1712
5. H.E. Toma, M.S. Takasugi, *J. Soln. Chem.*, **1989**, 18(6), 575
6. A.A. Schilt, *J. Am. Chem. Soc*, **1963**, 85, 904
7. J.N. Demas, T.F. Turner, G.A. Crosby, *Inorg. Chem.*, **1969**, 8(3), 674
8. G.M. Bryant, J.E. Fergusson, H.K.J. Powell, *Aust. J. Chem.*, **1971**, 24, 257
9. E.Y. Fung, A.C.M. Chua, J.C. Curtis, *Inorg. Chem.*, **1988**, 27, 1294
10. A. Juris, F. Barigelletti, V. Balzani, P. Belser, A. Von Zelewsky, *J. Chem. Soc. Faraday Trans.*, **1988**, 27(2), 2295
11. C.A. Bignozzi, S. Roffia, F. Scandola, *J. Am. Chem. Soc.*, **1985**, 107, 1644
12. C.A. Bignozzi, C. Paradisi, S. Roffia, F. Scandola, *Inorg. Chem.*, **1988**, 27(2), 408
13. G. Denti, S. Serroni, L. Sabatino, M. Ciano, V. Recevuto, S. Campagna, *Gazz. Chim. Ital.*, **1991**, 121, 37
14. M.M. Richter, K.J. Brewer, *Inorg. Chem.*, **1993**, 32, 2827
15. M.M. Richter, K.J. Brewer, *Inorg. Chem.*, **1993**, 32, 5762
16. D.A. Reitsma, F.R. Keene, *J. Chem. Soc. Dalton Trans.*, **1993**,18, 2859
17. E.M. Kosower, *J. Am. Chem. Soc.*, **1958**, 80, 3253
18. E.G. Grunwald, S. Winstein, *J. Am. Chem. Soc,*. **1948**, 70, 846
19. K. Dimroth, E. Reichardt, *Z. Anal. Chem.*, **1966**, 215(5), 344

20. V. Gutmann, *Inorg. Nucl. Chem. Lett.*, **1966**, 2, 257

21. R.H. Erlich, A.I. Popov, *J. Am. Chem. Soc.*, **1971**, 93, 5620

22. V. Gutmann, *Electrochim. Acta,* **1976**, 21, 661

23. W. Mayer, *Mh. Chem.*, **1975**, 101, 91

24. W.M. Reiff, R.E. DeSimone, *Inorg. Chem.*, **1973**, 12(8), 1793

25. N.J. Hill, *J. Chem. Soc.Faraday Trans. 2*, **1972**, 68, 427

26. J.S. Griffith, *The Theory of Transition Metal Ions*, Cambridge University Press, **1961**

27. G.K. Lahari, S. Bhaltacharya, B.K. Ghosh, A. Chakravorty, *Inorg. Chem.*, **1987**, 26, 4324

28. S. Bhaltacharya, B.K. Ghosh, A. Chakravorty, *Inorg. Chem.*, **1985**, 24, 3224

29. R.E. DeSimone, *J. Am. Chem. Soc.*, **1973**, 95, 6238

30. TK Solver

31. Module f02abc of the NAG C code available on EUCS systems

32. E. König, S. Kremer, *Chem. Phys. Lett.*, **1970**, 5, 87

33. L.J.Yellowlees, Ph.D. thesis, University of Edinburgh, **1983**

34. E. Koenig, H. Fischer, *Z. Naturforsch.*, **1963**, 17A, 1063

35. A.G. Motten, K.W. Hanck, M.K. deArmond, *Chem. Phys. Lett.*, **1981**, 79, 541

36. S.H. Peterson, J.N. Demas, *J. Am. Chem. Soc.*, **1976**, 98, 7880

37. S.H. Peterson, J.N. Demas, *J. Am. Chem. Soc.*, **1979**, 101, 6571

Chapter 3 : Complexes with Polypyridyl Bridging Ligands

3.1 : Introduction

As mentioned in Chapter 1, it is frequently of interest to place a second metal centre in close proximity to a Ru(bpy) moiety, and then to study any interactions between the metal centres. Such complexes are often mooted as precursors to some form of molecular solar panel, absorbing light and converting it to electricity[1]. As the bipyridyl ligand is particularly good at binding to metal centres as well as being an active participant in the photochemical process, one logical choice for a linking unit between the two metal centres is a ligand based on the bipyridine molecule, but capable of binding two, or more, metal centres.

The advantages to this approach are many. Firstly, the nature of the ligand allows easy synthesis of mono-metallic complexes due to the ready chelation of the metal centre. Secondly, the ligand may add interesting photochemical and electrochemical properties to that already present from the M(bpy) core. Thirdly, if unsaturated or aromatic systems are in use, the π^* system of the ligand may enhance the interaction of the metal centres, or even lead to some unexpected and interesting results. Other advantages include the theoretical use of a wide range of metals, as many co-ordinate strongly to bipyridyl, and, once the behaviour of the ligand is known, we may reasonably predict the properties of the new complexes.

Various ligands have been used to link the different metal centres, including 2,2'-bipyrimidine[2], 2,3,7,8-tetra-2-pyridyl-pyrazino[2,3-*g*]quinoxaline[2], 2,2',3,3'-tetra-2-pyridyl-6,6'-biquinoxaline[2], 2,3-bis(2-pyridyl)pyrazine[3], and

2,5-bis(2-pyridyl)pyrazine[4]. Such complexes show a range of interesting electrochemical and photophysical properties.

This chapter details the properties of a range of such complexes, both mono- and bi-metallic, with a range of bridging ligands.

3.2 : Ligands

3.2.1: 2,3-Dipyridylpyrazine (dpp)

2,3-Dipyridylpyrazine is capable of bridging one or two metal centres in a bidentate manner. This feature has been used to make a wide range of monometallic and bi-metallic complexes[3,5].

The electronic absorption spectrum of dpp in acetonitrile is shown in figure 3.1. No transitions are observed in the visible region. Two absorptions are seen in the UV region, and these are assigned as intraligand $\pi \rightarrow \pi^*$ transitions, analogous to those seen for the bpy ligand.

The electrochemistry of dpp in DMF is shown in figure 3.2. There is a single process at -1.83V, corrected against ferrocene/ferrocinium. This process is semi-reversible at room temperature, and can be made reversible by cooling the solution to -40° C. The lack of oxidative processes is typical of this type of compound. By way of comparison, free bpy is around 200mV more difficult to reduce than free dpp.

3.2.2: 2,3-Dipyridylquinoxaline (dpq)

This ligand is capable of chelating to two metal centres as a bidentate ligand. A range of monometallic and bimetallic species containing dpq have been synthesised and studied. Unfortunately, after preparation of the complex $Ru(bpy)_2(dpq)](BF_4)_2$, there was none of the free ligand left to perform spectroscopic and electrochemical studies on.

We were unable to locate spectroscopic or electrochemical data for the free ligand in the published literature. We would expect its behaviour to be intermediate between that for dpp and dpb.

Figure 3.1 : Electronic absorption spectrum of dpp in MeCN

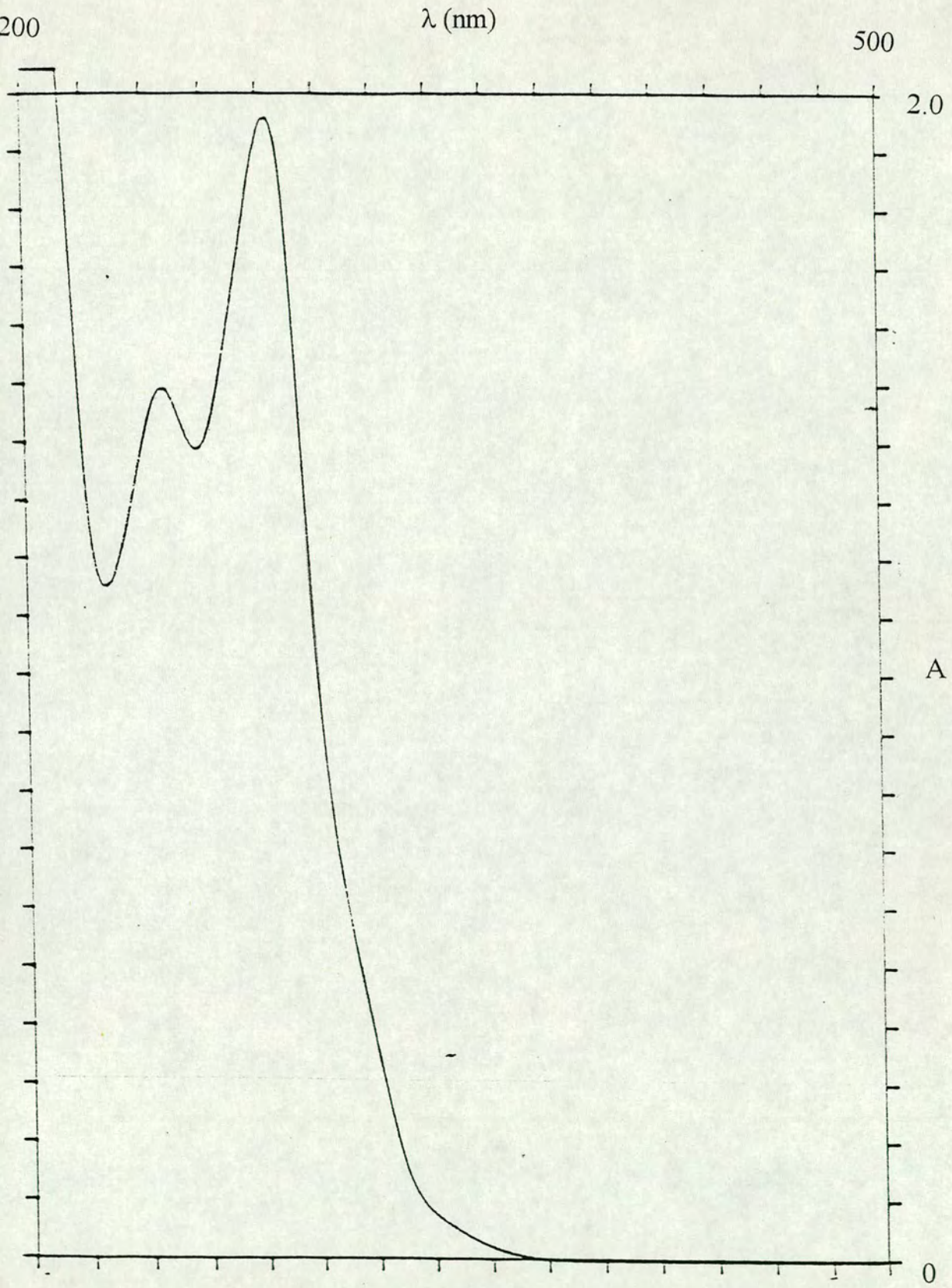

Figure 3.2 : Electrochemistry of dpp in DMF

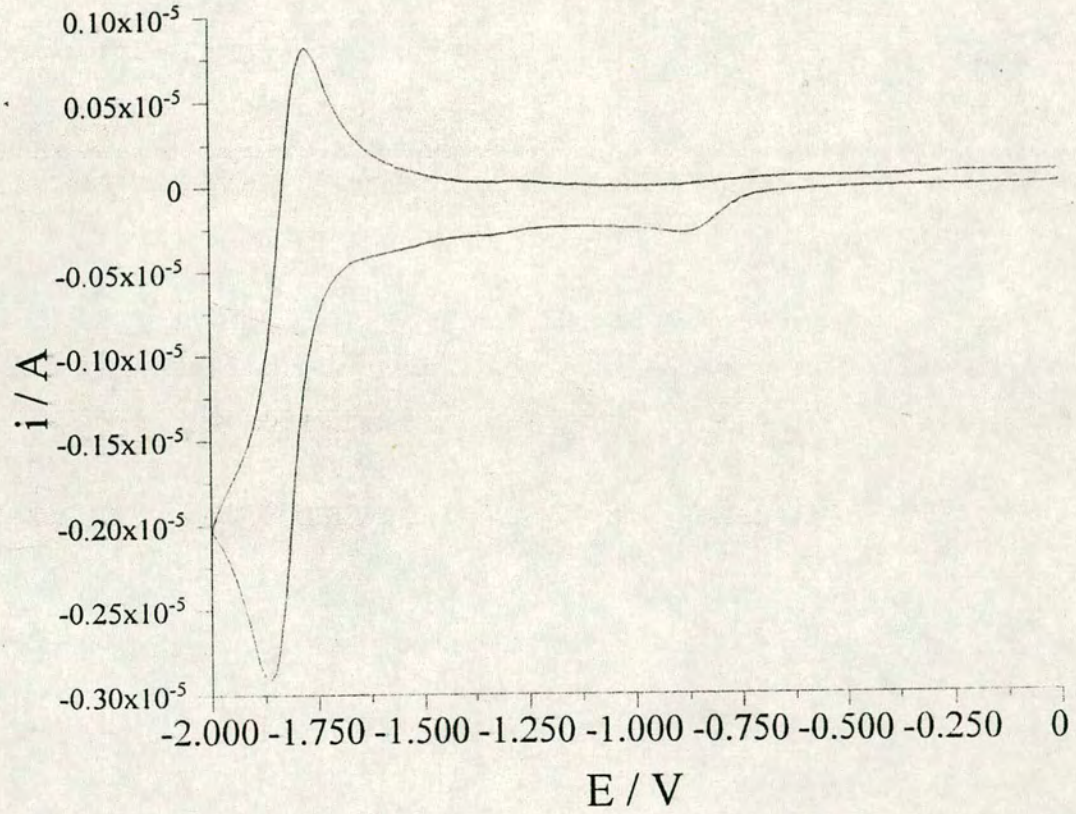

3.2.3: 2,3-Dipyridylbenzoquinoxaline (dpb)

As for the previous ligands, dpb is capable of chelating to one or two transition metal centres as a bidentate ligand. Again, a range of monometallic and bi-metallic complexes have been prepared and studied.[6,7]

The electronic absorption spectrum of dpb in acetonitrile is shown in figure 3.3. The absorptions in the UV region are assigned as $\pi \rightarrow \pi^*$ intraligand transitions. The less intense absorption at 26385 cm^{-1} is also assigned as a $\pi \rightarrow \pi^*$ intraligand transition.

The electrochemistry of dpb in DMF is shown in figure 3.4. The compound demonstrates no electrochemistry in the oxidative range, but two processes can be observed in the reductive range. The first, at -1.19 V, is fully reversible at room temperature, while the second, at -1.74 V is irreversible, even upon cooling. Both the relatively easy first reduction, and the low energy visible absorption are indicative of a readily accessible π^* orbital on dpb.

The three ligands dpp, dpq and dpb differ only in the sequential addition of a benzene ring to the central pyrazine unit. These additional conjugated rings can be used to explain the increasing ease of reduction of the compounds. The increased size of the π system means that the extra electron gained upon reduction can be more easily accommodated due to a larger amount of delocalisation of charge.

To illustrate this, the energy of the of the ultra-violet absorption band and the reduction potentials of the free ligands are given in table 3.1. This clearly shows the increasing ease of reduction and the lowering in energy of the $\pi \rightarrow \pi^*$ transition as the conjugation of the ligand is increased.

Figure 3.3 : Electronic absorption spectrum of dpb in MeCN

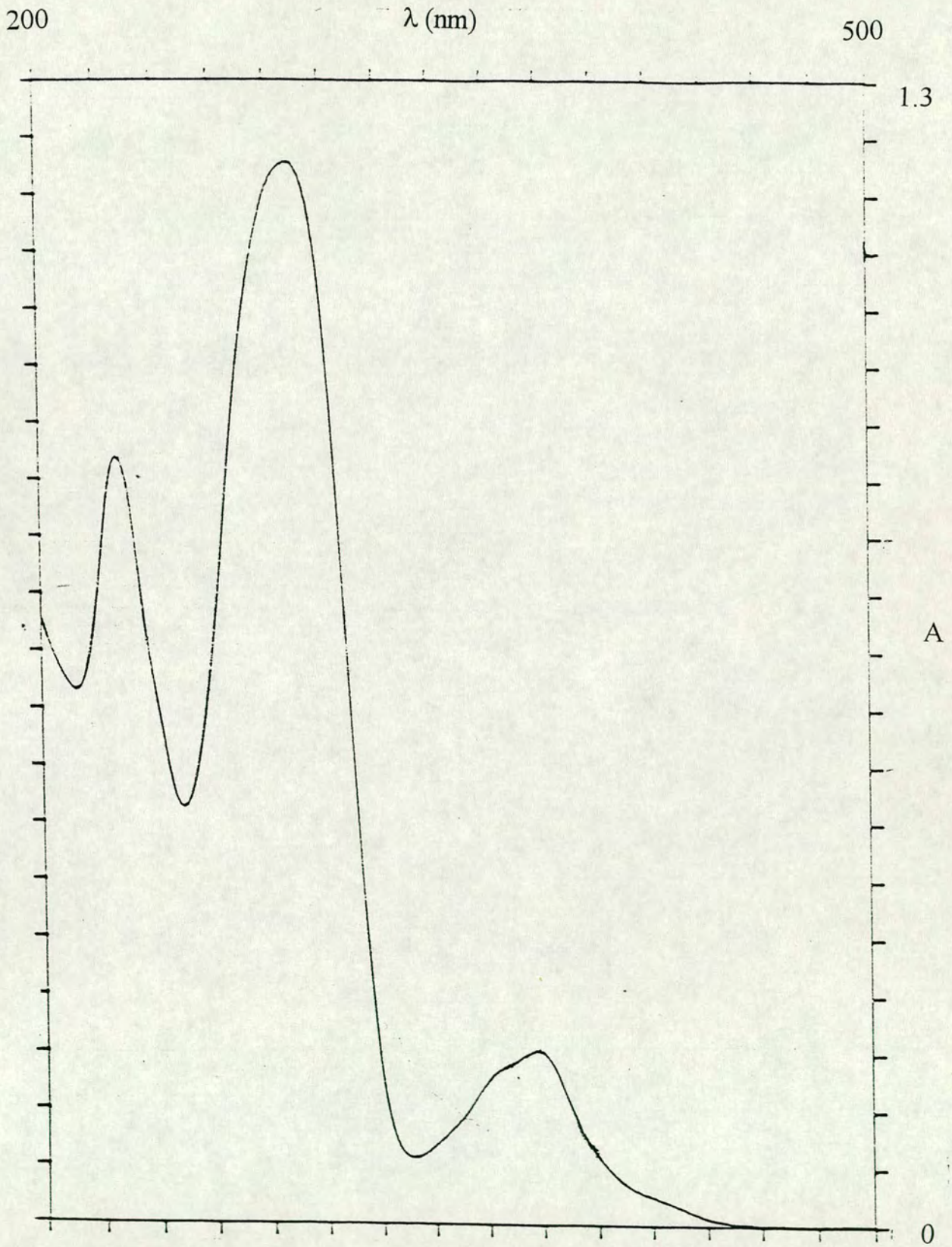

Figure 3.4 : Electrochemistry of dpb in DMF

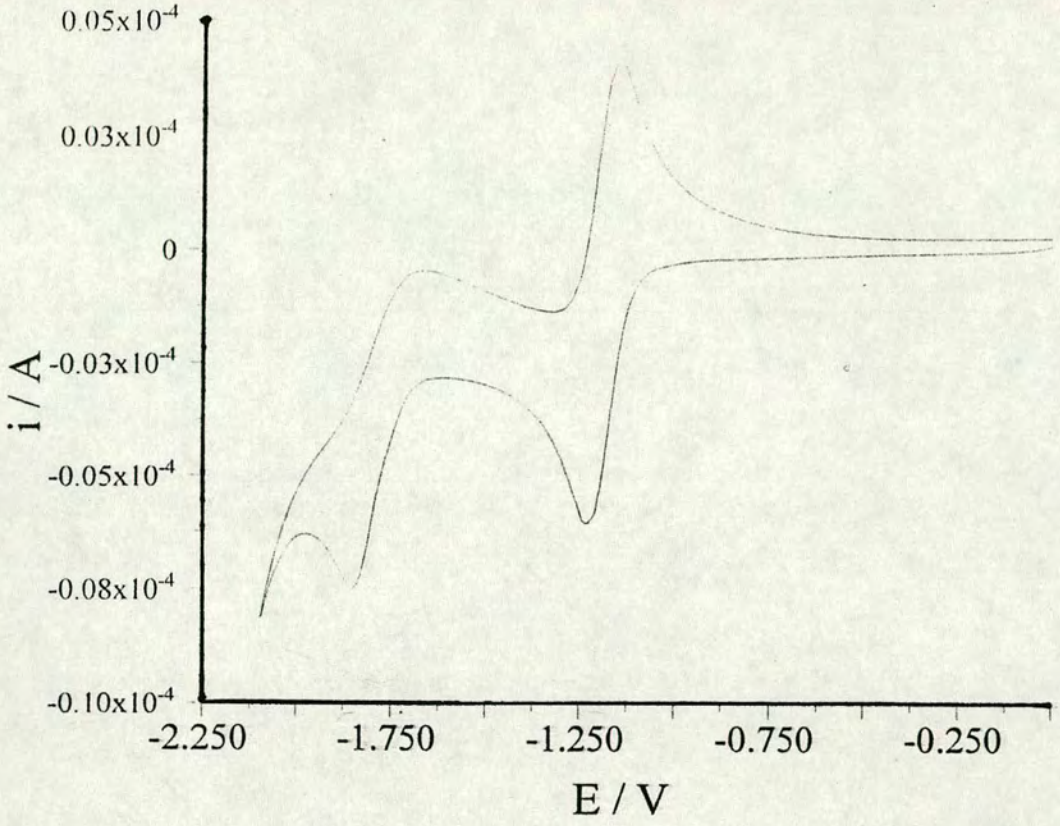

Table 3.1 : Electrochemical and UV/VIS data for ligands used

Ligand	$E_{½}$ L/L$^-$	UV/VIS absorbances (cm^{-1})
bpy	- 2.05 V	35000
dpp	-1.83 V	35336, 40650
dpb	-1.18	26385, 34722, 44053

3.3 : Monometallic complexes

Before considering complexes containing multiple transition metal centres, it is useful to consider monometallic complexes containing the various bridging ligands. A number of such complexes have been studied previously[4,6,8]. The electrochemistry and spectrochemistry of many of these complexes has been detailed. However, access to the OTE cell, and the availability of EPR facilities make it worthwhile to consider those complexes we have prepared in more detail, taking into account previous work where appropriate.

3.3.1 : $[Fe(bpy)_2(dpp)](BF_4)_2$

Previous work concerning complexes containing these polydentate bridging ligands has concentrated on complexes containing ruthenium and osmium, due to the more attractive photophysical properties of the Ru(bpy) and Os(bpy) moieties.

The electronic absorption spectrum of bis(bipyridyl)(dipyridylpyrazine)iron(II) tetrafluoroborate in DMF is shown in figure 3.5. This complex demonstrates the features commonly seen for transition metal polypyridyl complexes. At lowest energy there is a band that is commonly assigned as a MLCT process. In the case of this complex, there is a distinct shoulder on this band. This is due to the presence of a $d(\pi) \rightarrow$ bpy π^* transition and a $d(\pi) \rightarrow$ dpp π^* transition at very similar energies. At slightly higher energy, a second MLCT band is observed. This is the combination of the two $d(\pi) \rightarrow$ ligand $\pi^*(2)$ processes, although there is no obvious shoulder in this band.

In the UV area of the spectrum, one absorption is seen, although this too has a pronounced shoulder. This is assigned as a combination of the ligand internal

Figure 3.5 : Electronic Absorption spectrum of $[Fe(bpy)_2(dpp)](BF_4)_2$ in DMF

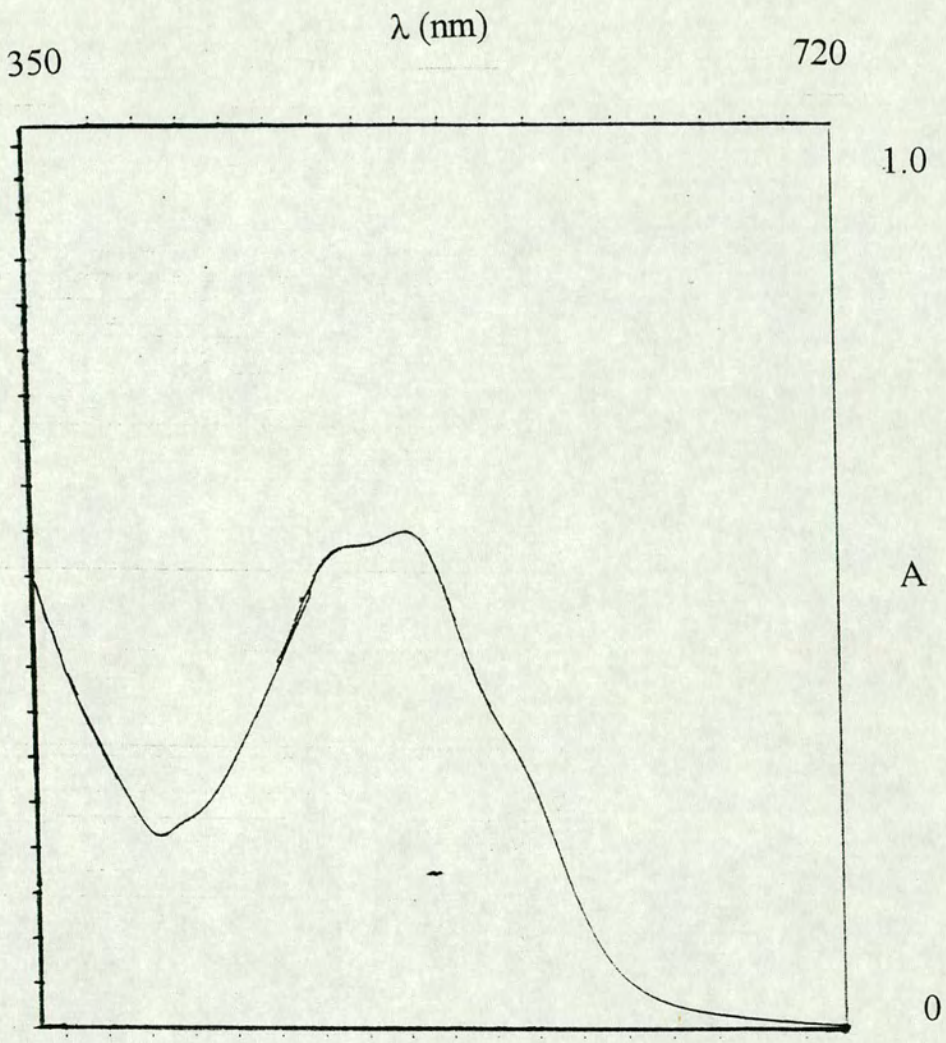

$\pi \rightarrow \pi^*(1)$ transitions. The expected $\pi \rightarrow \pi^*(2)$ transitions are obscured by the solvent.

The electrochemistry of the complex in DMF is shown in figure 3.6. The positive range shows one process, assigned as the iron(II)/iron(III) oxidation. This process has a half-wave potential of 1.15V when ferrocene/ferrocinium is used as a standard. This process is reversible at room temperature.

The negative range demonstrates three processes, at -1.16V, -1.35V and -1.60V respectively. All three are semi-reversible at room temperature, but can be made reversible on cooling to -35°C. Comparison with the electrochemistry of the free ligands and related complexes suggests that each ligand in turn is singly reduced, and that the dpp ligand will be easier to reduce than the bpy ligands. Thus the first reduction is assigned as the reduction of the dpp, and the second and third processes are assigned as sequential reduction of the two bipryridyl ligands.

We did not carry out any spectroelectrochemical studies on this complex. Monitoring the change in spectrum on carrying out the first reduction would allow us to determine which ligand was reduced by observation of the changes. Likewise, the oxidation of the complex may demonstrate the collapse of the MLCT processes, and perhaps the growth of LMCT bands.

3.3.2 : $[Ru(bpy)_2(dpp)](BF_4)_2$

The complex bis(bipyridyl)(di(pyridyl)pyrazine)ruthenium(II) tetrafluoroborate has been investigated previously by Roffia *et al*[9]. This work concentrated on the electrochemistry of this and related complexes in the reductive region, going to potentials as negative as -3V. The electronic absorption spectrum and oxidative

Figure 3.6 : Electrochemistry of $[Fe(bpy)_2(dpp)](BF_4)_2$ in DMF

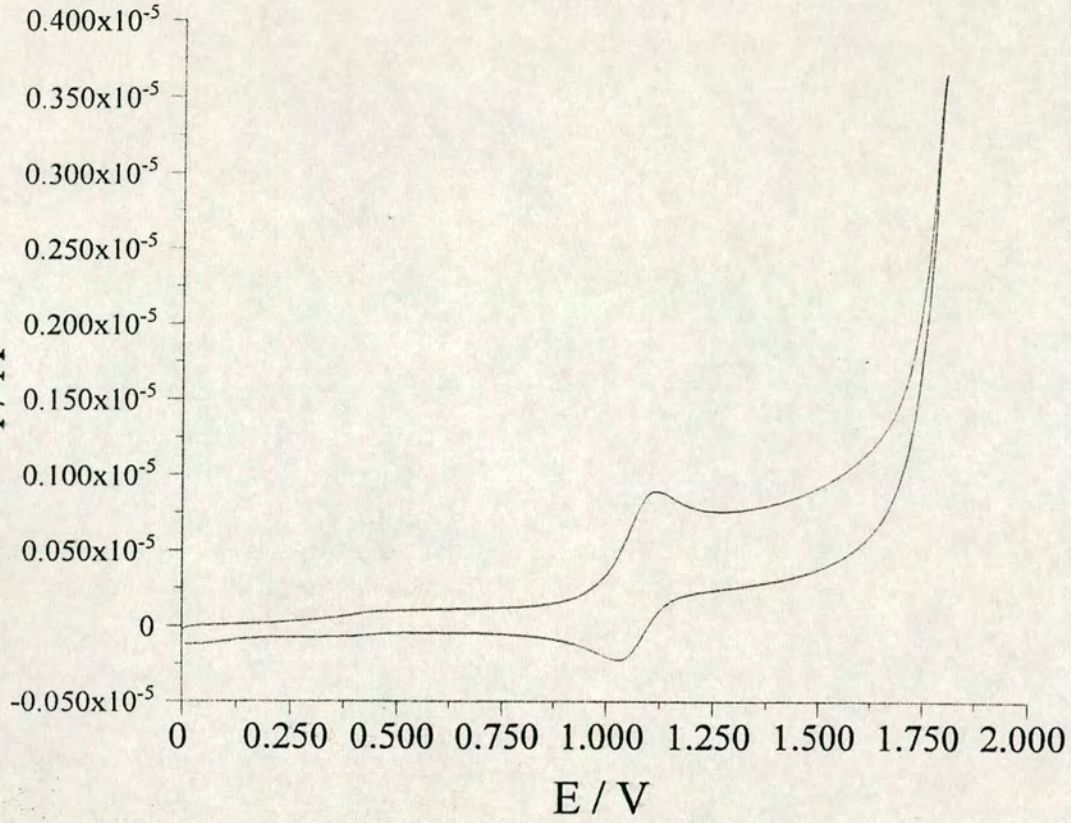

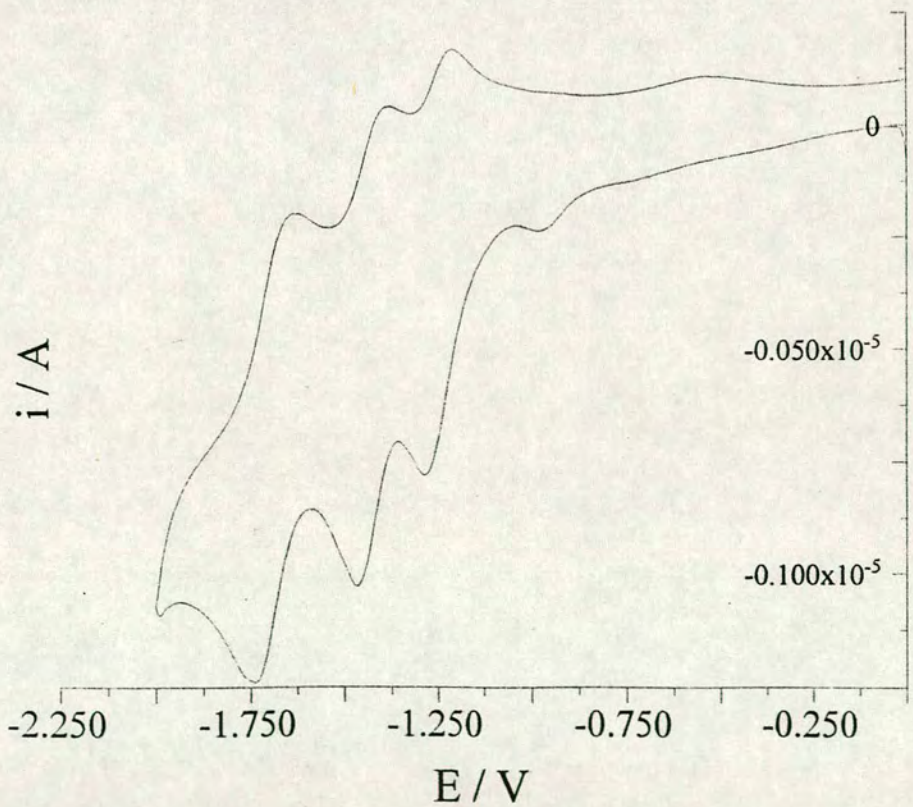

electrochemistry was not considered. The complex, and related bimetallic species, have also been investigated by Braunstein *et al*[5]. This work solely considered the oxidation of the complex and the MLCT portion of the electronic absorption spectrum. Combination of results from the two sources is difficult due to the lack of a common reference for the electrochemistry.

The electronic absorption spectra of the complex in acetonitrile is shown in figure 3.7. This spectrum exhibits features typical for a complex containing the Ru(bpy) unit. The low energy part of the spectrum consists of an MLCT band. In this case the band is not as well defined, due to the overlap of a Ru $\rightarrow$ bpy π^* transition and a Ru $\rightarrow$ dpp π^* transition. However, as the free dpp ligand is more easy reduced than free bpy, and we have demonstrated a relationship between MLCT band energy and electrochemical processes (see 2.3), we assign the lower energy portion of the absorbance as the Ru $\rightarrow$ dpp π^* transition, and the higher energy portion as the Ru $\rightarrow$ bpy π^* transition. At higher energy, the $\pi \rightarrow \pi^*$ transitions associated with the two ligands are observed. Again, the transitions associated with the bipyridine ligand overlap with those associated with the dipyridylpyrazine ligand. Indeed, the first $\pi \rightarrow \pi^*$ transition for each ligand cannot be distinguished.

The electrochemistry of the complex in DMF is shown in figure 3.8. The observed processes closely parallel those seen for tris(bipyridyl)ruthenium(II)[10]. At positive potentials a single process is observed at +1.40 V. This is assigned as the one electron oxidation of the ruthenium metal centre, and is reversible at room temperature. The negative range shows three processes, occurring at -0.97 V, -1.37 V and -1.61 V. The gap between the latter two reductions is typical for a complex with

Figure 3.7 : Electronic absorption spectrum of $[Ru(bpy)_2(dpp)](BF_4)_2$ in MeCN

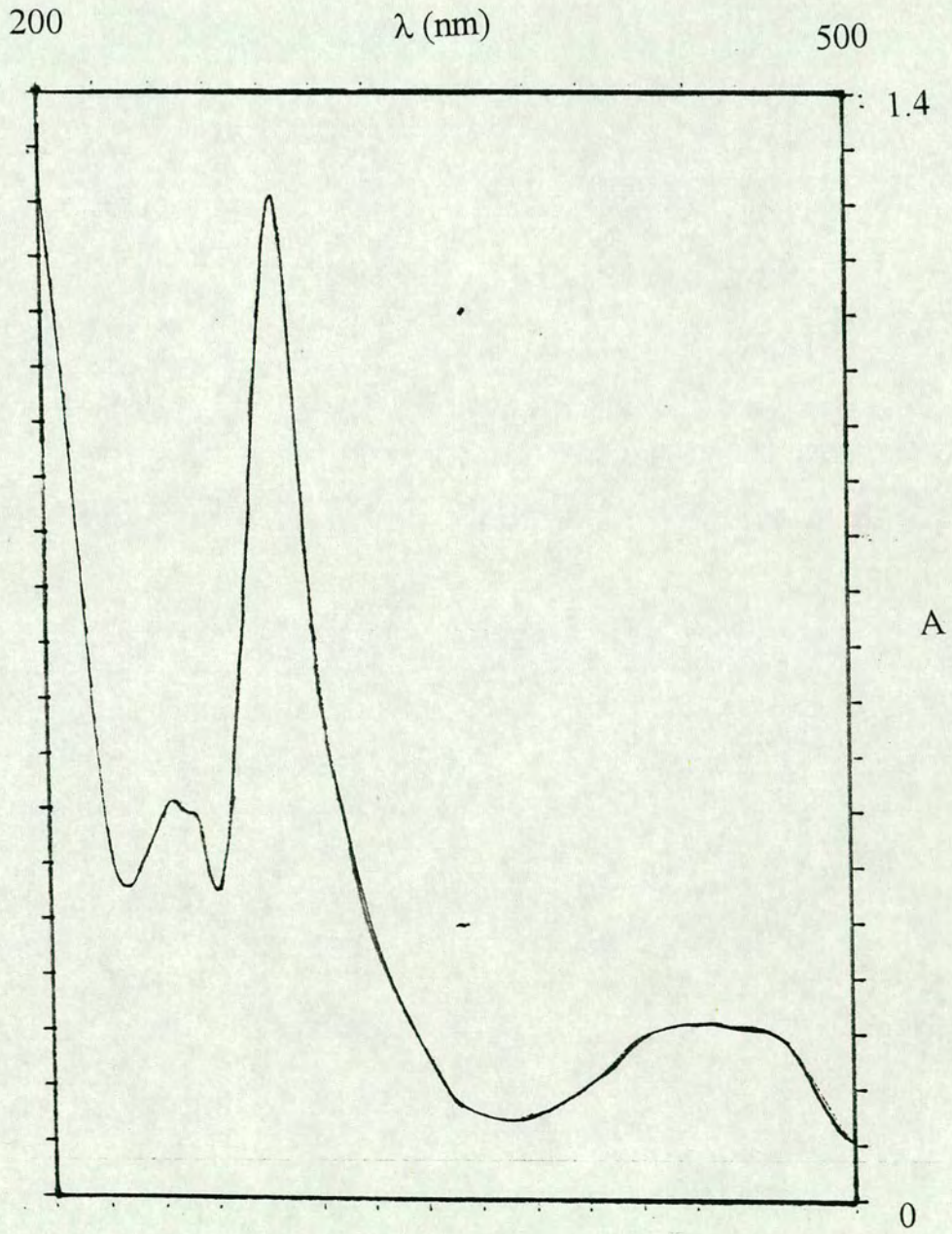

Figure 3.8 : Electrochemistry of $[Ru(bpy)_2(dpp)](BF_4)_2$ in DMF

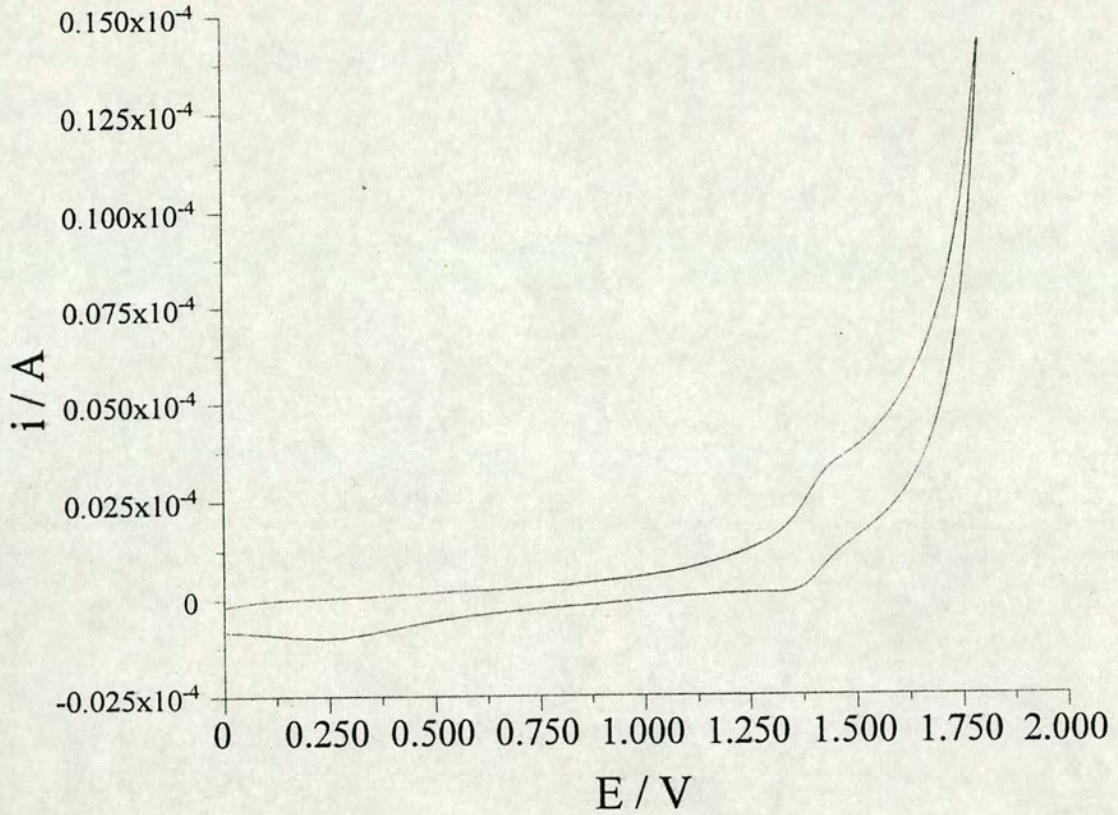

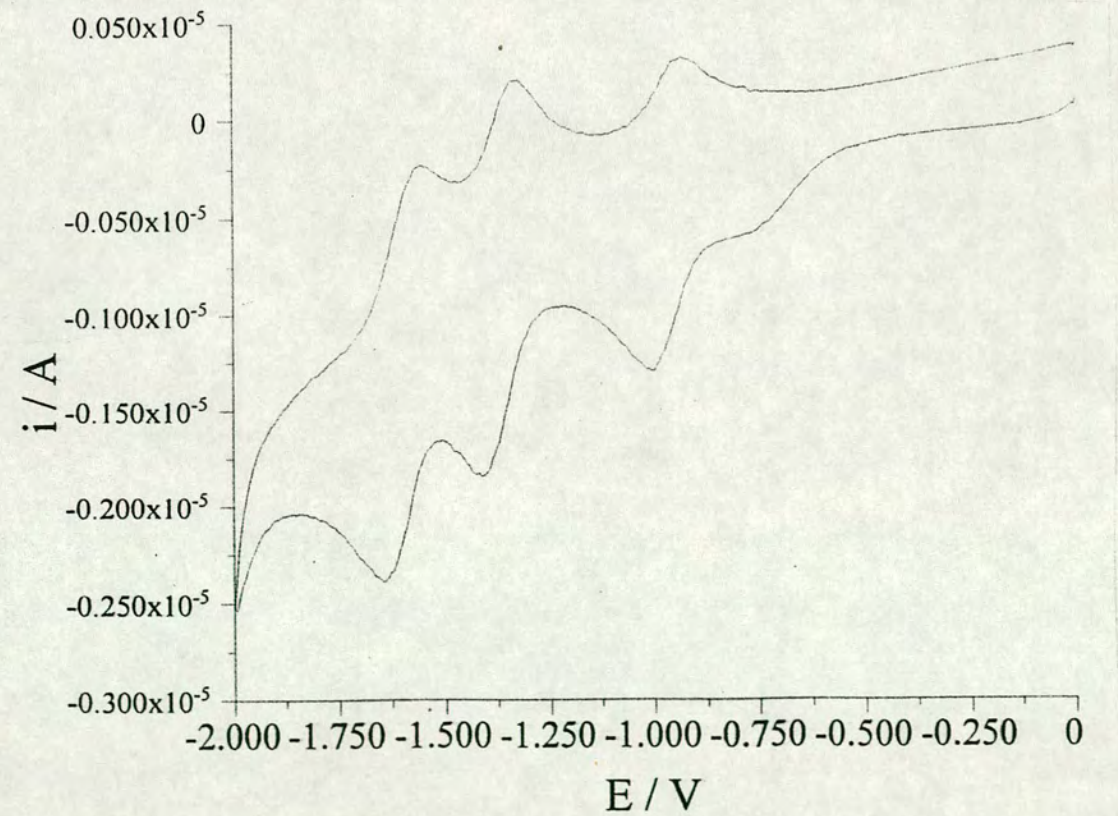

Figure 3.9 : Absorption spectrum monitoring of $[Ru(bpy)_2(dpp)](BF_4)_2$ in DMF

$T = 250$ K, $E_{appl} = + 1.6$ V

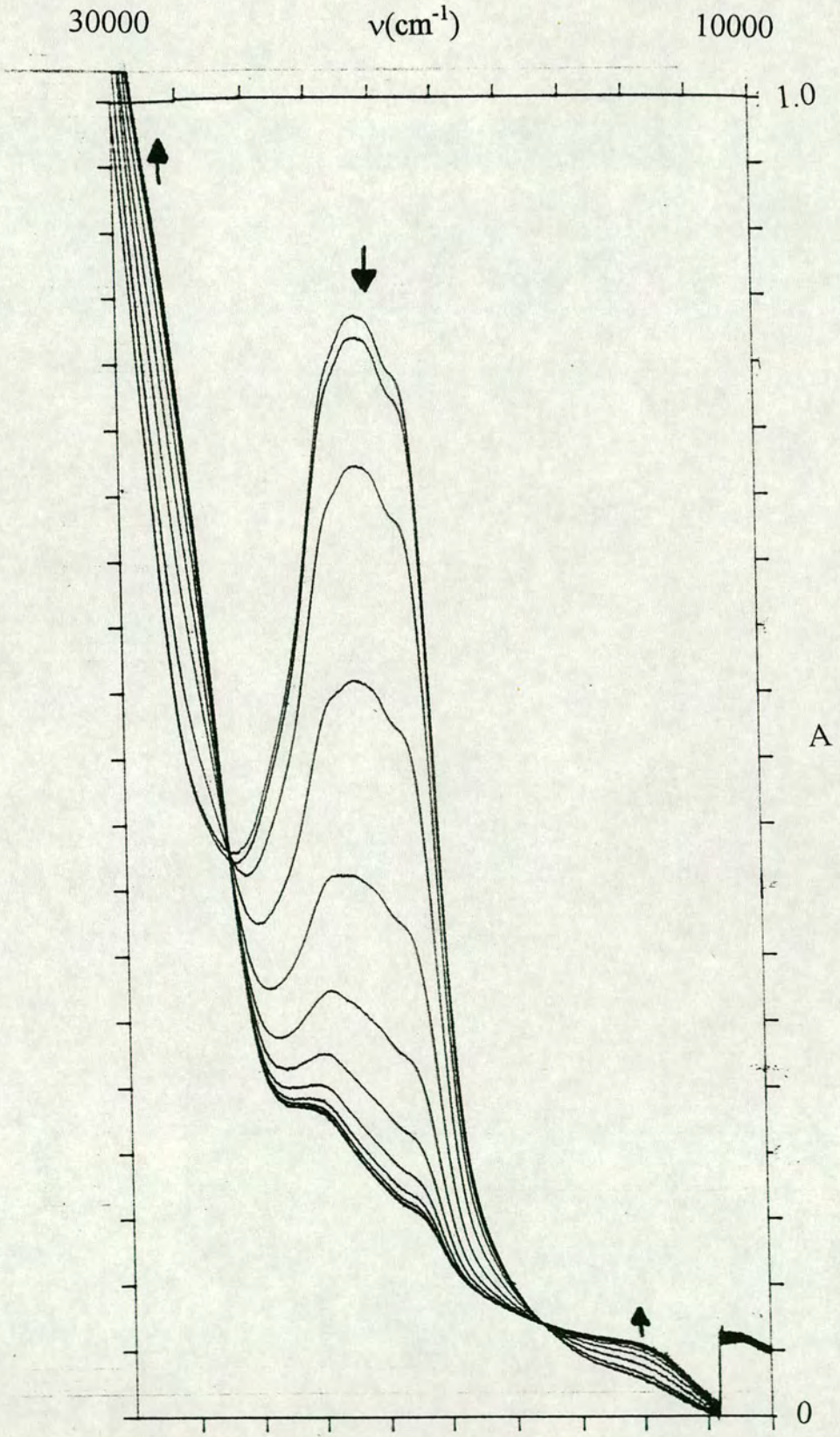

two bipyridine ligands, each being reduced in turn. We would also expect the dpp ligand to be easier to reduce, as is the case for the free ligands. We therefore assign the first process as reduction of the dpp ligand, and the other two as successive reductions of the two bpy ligands. All three processes are quasi-reversible at room temperature, but can be made reversible by cooling to around -30° C.

As with many complexes containing the Ru(bpy) unit, the spectroelectrochemistry of the complex is of interest. The results of such an experiment, showing the oxidation of the complex in DMF, are shown in figure 3.9. This clearly demonstrates the collapse of the MLCT process. The weak band growing in around 14000 cm^{-1} may be a LMCT process. Although it cannot be seen from these results, we would expect changes in the energies of the intraligand transitions upon removal of an electron from the complex. We therefore assume that the increase in absorption at energies higher than 27000 cm^{-1} is due to these changes. The presence of two isosbestic points, and the regeneration of the initial spectrum on return of the applied potential to zero, demonstrate that the process is fully reversible at 250 K.

3.3.3 : $[Ru(bpy)_2(dpq)](BF_4)_2$

The complex bis(2,2'-bipyridyl)(2,3-di-2-pyridylquinoxaline)ruthenium(II) hexafluorophosphate was described by Rillema and Mack[2]. They presented the electrochemistry of the complex in acetonitrile, observing one oxidative process and two reductive processes. They reported the UV/VIS/NIR spectrum of the complex in acetonitrile.

The electronic absorption spectrum of the complex in DMF is shown in figure 3.10. This is broadly similar to that seen in Rillema and Mack's work, demonstrating two overlapping MLCT processes between 19000 and 24000 cm^{-1}. The lower energy

Figure 3.10 : Electronic absorption spectrum of $[Ru(bpy)_2(dpq)](BF_4)_2$ in DMF

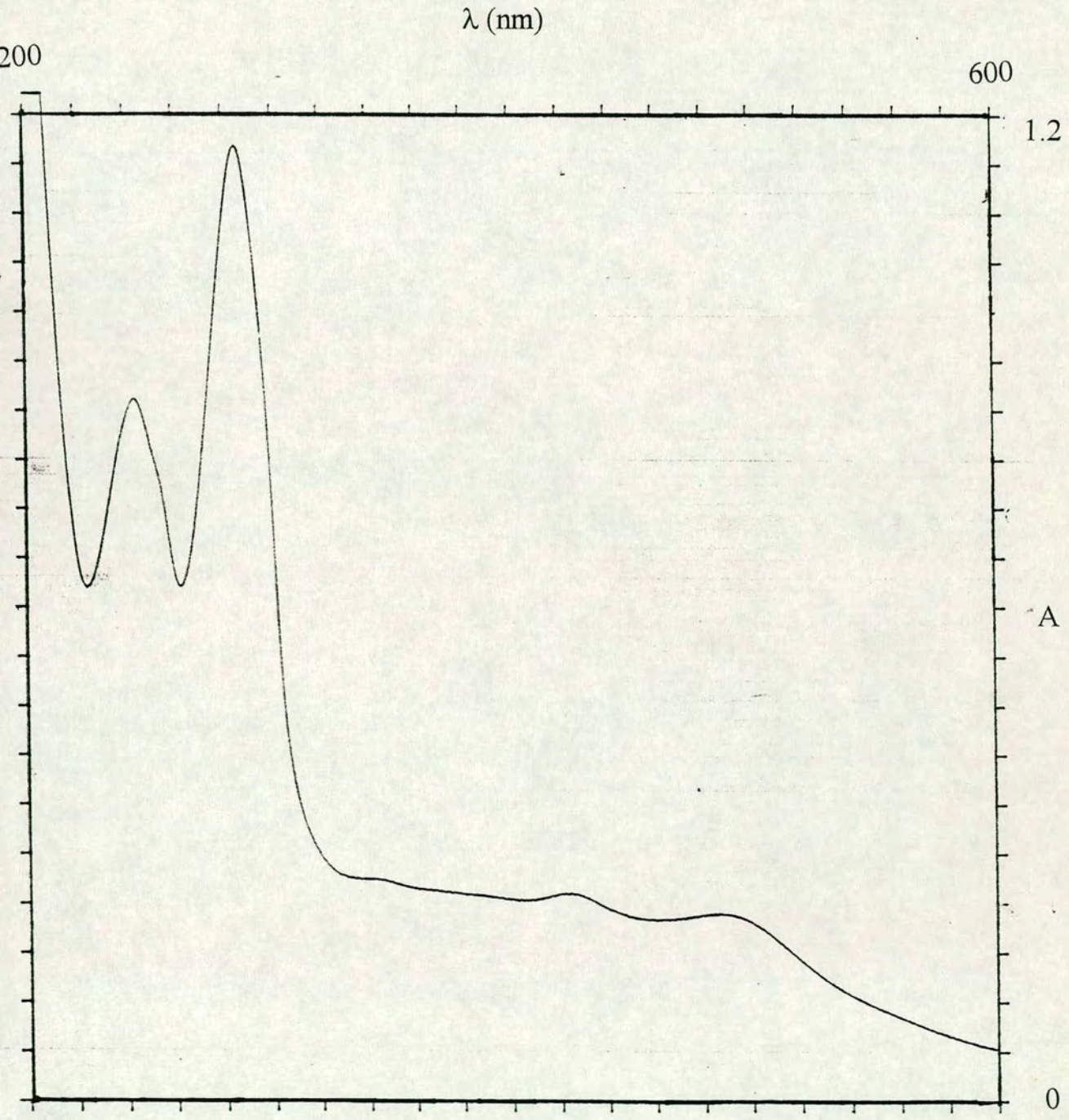

band is assigned as the ruthenium to dpq charge transfer process, due to the easier reduction of dpq compared to bpy. We also observe intraligand processes at 34500 cm^{-1}.

The electrochemistry of the complex in DMF is shown in figure 3.11. Again this is broadly similar to that observed by Rillema and Mack, although the potentials seen are all shifted by -500 mV. This is due to the change in solvent and electrodes between the two studies. We do, however, observe a third process in the reductive range, which was beyond the solvent window in the previous work. We assign the single oxidative process, at +0.9 V, to the Ru(II)/Ru(III) couple. This appears reversible at room temperature. The first reduction, at -0.67 V, is assigned as the reduction of the dpq ligand, and is semi-reversible at room temperature. It can be made reversible by cooling to 243 K. The other two reductions, at -1.4 V and -1.65 V, are assigned as sequential reduction of the two bpy ligands. These are both semi-reversible at room temperature, and the first one can be made reversible by cooling. The second, however, does not become fully reversible even at 243 K.

We also wished to study this complex by use of the OTE cell. The results of such an experiment, involving the oxidation of the complex, is shown in figure 3.12. This clearly demonstrates the collapse of the MLCT bands. We also observe a reduction of intensity in the main intraligand band, although we do observe a shoulder growing in at around 31000 cm^{-1}. This is the intraligand transition shifting to lower energy upon oxidation of the metal centre.

The presence of isosbestic points, and the regeneration of the starting spectrum on return of the applied potential to zero, suggests that the process is fully

Figure 3.11 : Electrochemistry of $[Ru(bpy)_2(dpq)](BF_4)_2$ in DMF

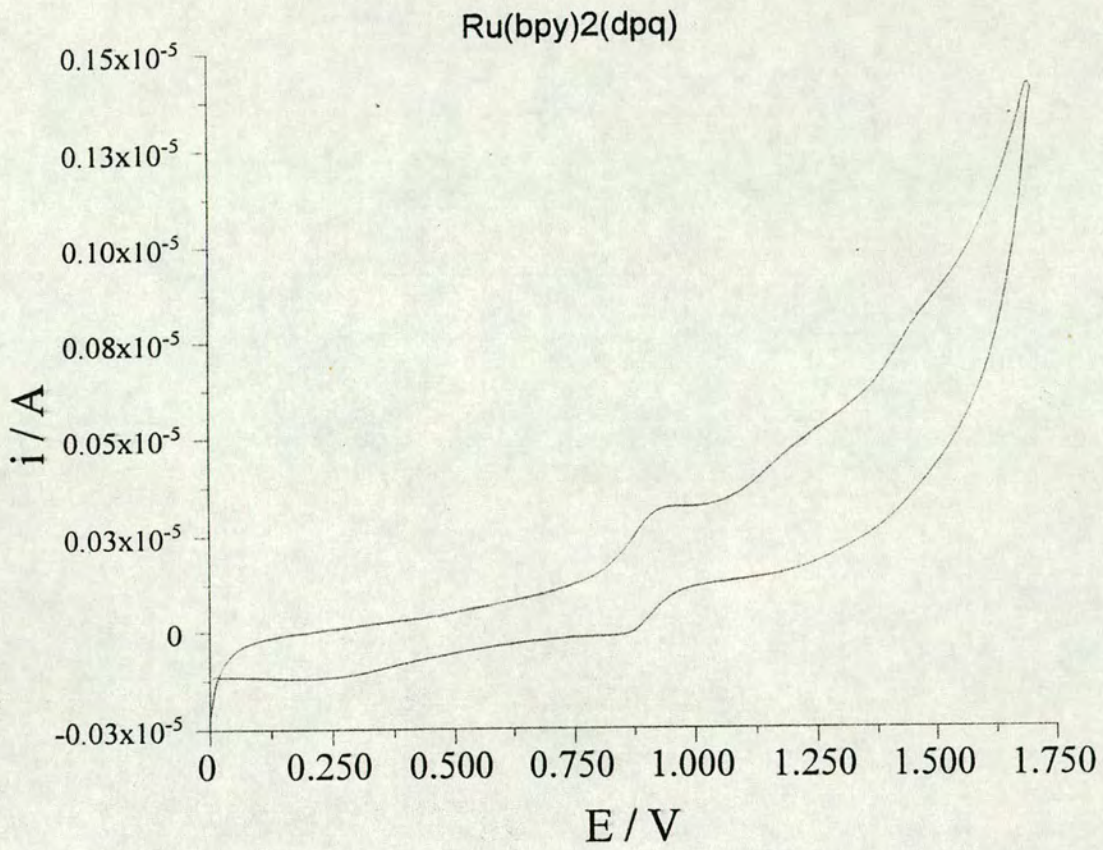

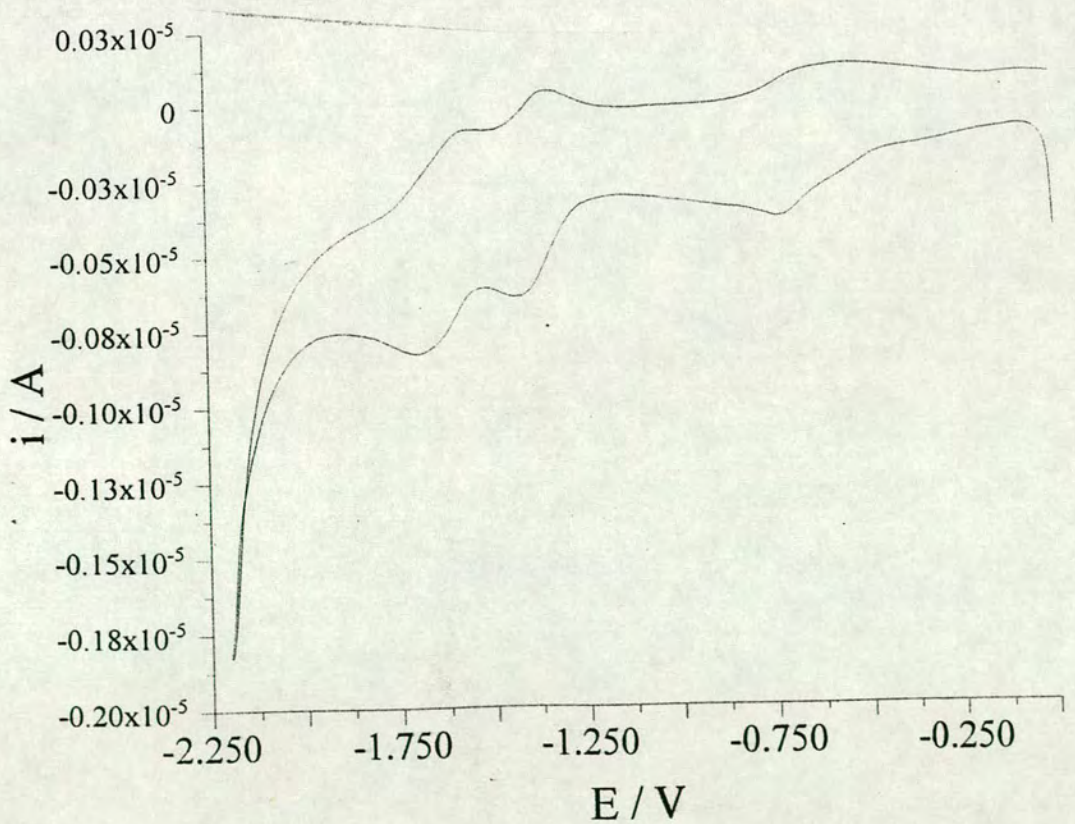

Figure 3.12 : Absorption spectrum monitoring of $[Ru(bpy)_2(dpq)](BF_4)_2$ in DMF

$T = 243$ K, $E_{appl} = + 1.6$ V

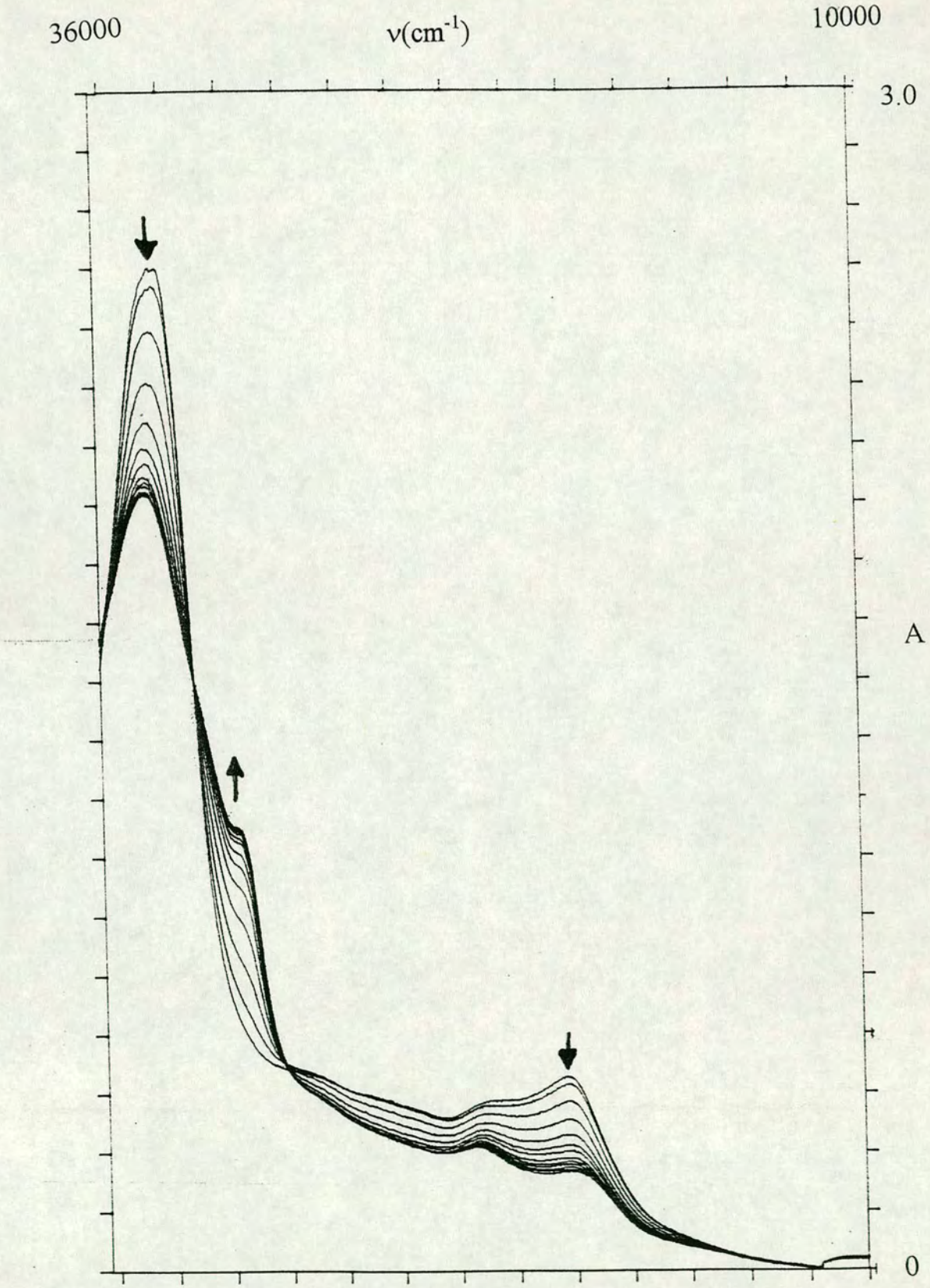

reversible at 243 K, and that the product formed is stable over the timescale of the experiment.

3.3.4 : $[Ru(bpy)_2(dpb)](BF_4)_2$

This complex has been previously reported in work by Carson and Murphy[6]. We present our own observations on the electronic absorption spectrum and electrochemistry of the complex for comparison with the other complexes synthesised.

The electronic absorption spectrum of the complex in acetonitrile is shown in figure 3.13. Again, this spectrum demonstrates all the typical features found in ruthenium (polypyridyl) complexes. At lowest energy, there is a MLCT band. This band is probably a combination of $d(\pi) \rightarrow$ bpy π^* and $d(\pi) \rightarrow$ dpb π^* transitions. The next lowest energy band is assigned as the lowest energy internal transition of dpb. The expected second MLCT band is visible as a shoulder at the base of the ligand $\pi \rightarrow \pi^*$ transitions, which occur in the UV. Both the ligand internal absorbances seen are a combination of bpy $\pi \rightarrow \pi^*$ and dpp $\pi \rightarrow \pi^*$ transitions. At lower energy, we observe the $\pi \rightarrow \pi^*(1)$ transitions, while at higher energy we observe the $\pi \rightarrow \pi^*(2)$ transitions.

The electrochemistry of the complex in acetonitrile is shown in figure 3.14. The oxidative range demonstrates one process, at +1.54 V. This process appears fully reversible at room temperature, and is assigned as the Ru(II)/Ru(III) couple.

The reductive range shows four processes at -0.45 V, -1.10 V, -1.38 V and -1.66 V. The first three are semi-reversible, but can be made reversible by cooling to around -40° C. The fourth process, only just discernible at very negative potentials, is irreversible even on cooling. We assign the first and fourth processes as dpb based,

Figure 3.13 : Electronic Absorption spectrum of $[Ru(bpy)_2(dpb)](BF_4)_2$ in MeCN

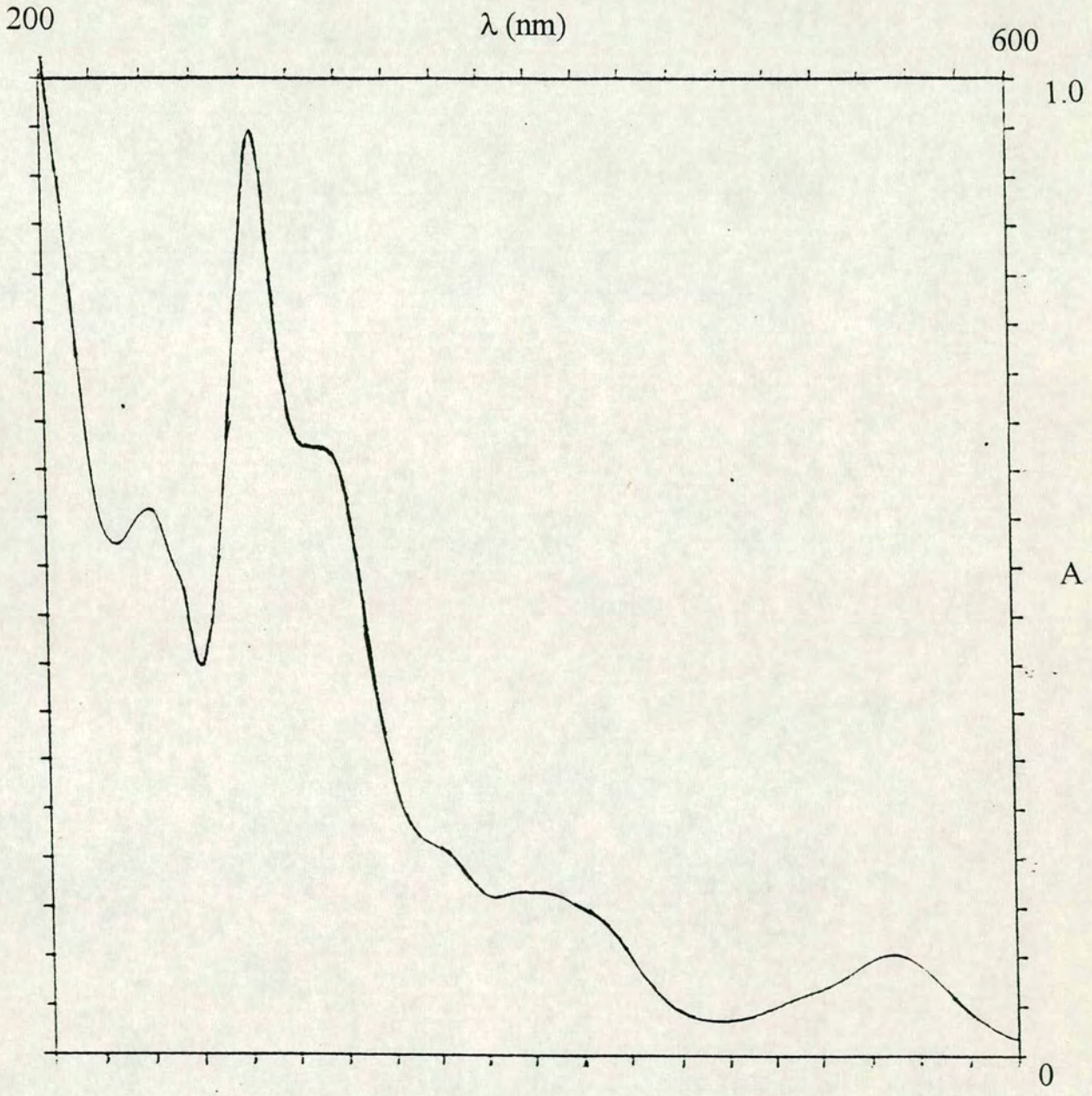

Figure 3.14 : Electrochemistry of $[Ru(bpy)_2(dpb)](BF_4)_2$ in MeCN

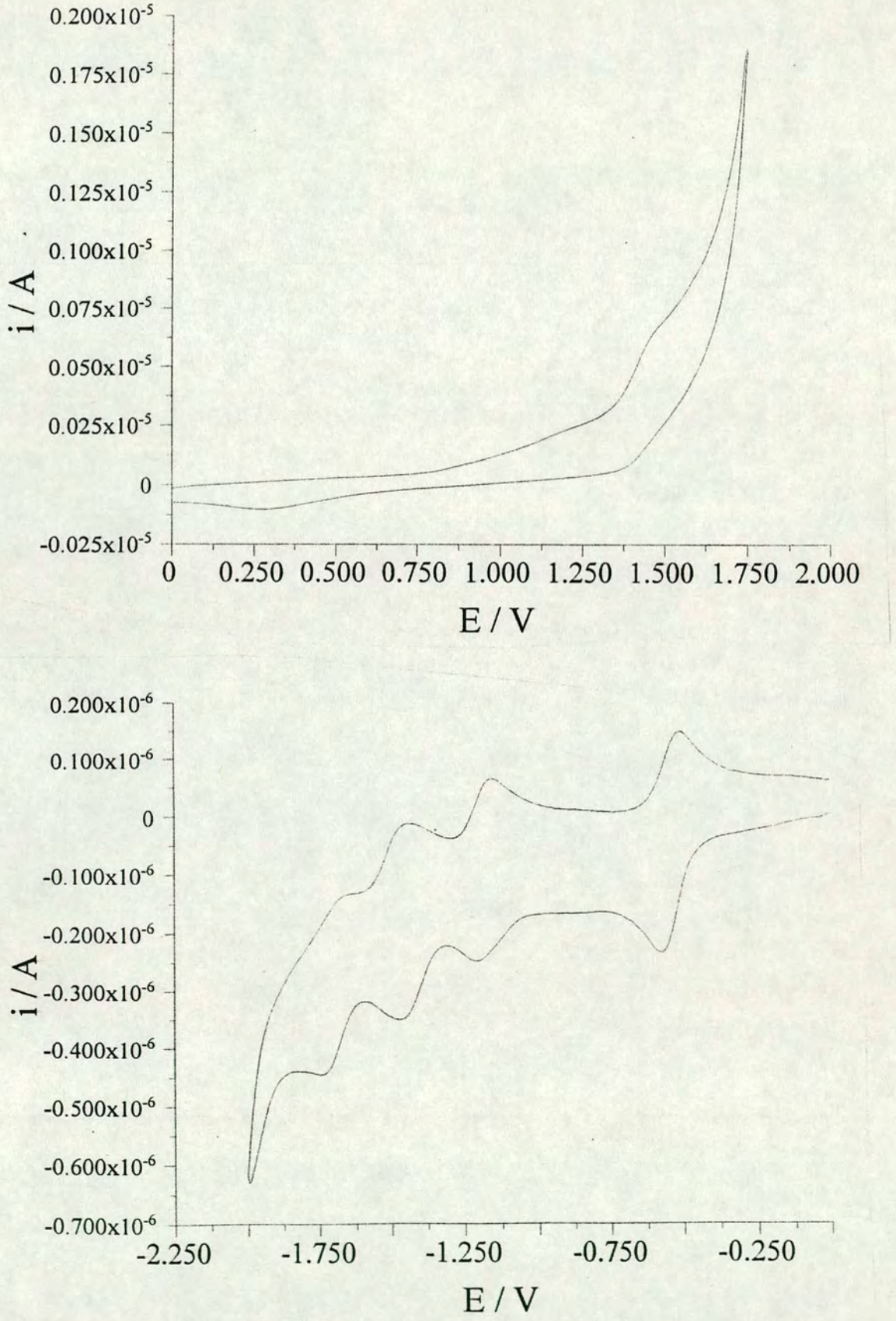

equivalent to those processes seen for the free ligand. As the first reduction of free dpb is less negative than that for free bpy, we assume the same is true in the complex. The other two processes are assigned as sequential reduction of the two bpy ligands.

We note that our assignment leaves first bpy-based reduction significantly easier than in the other complexes considered in this study. We suggest that this is because the dpb ligand is a considerably better π-accepting ligand than bpy itself. Therefore in $[Ru(bpy)_2(dpb)]^{2+}$ there will be reduced electron density on the bpy ligands. Thus it will be considerably easier to add an electron to the chelated bpy ligand, and hence the observed redox behaviour.

We have also studied the oxidation of this complex by use of the OTE cell. The results of such an experiment are shown in figure 3.15. As for the previously discussed complexes, we observe the collapse of the bands assigned as MLCT processes. In this case, this leaves a band at 23250 cm^{-1} which we can assign as the lowest energy intraligand transition associated with the dpb ligand. This band appears as a shoulder in the spectrum of the unoxidised material. We also observe the growth of a band at 20000 cm^{-1}. This band may be a LMCT process, or it may be a MLCT process involving the Ru(III) centre, which we would expect to be at higher energy than the original MLCT process. The presence of three isosbestic points suggests that the process is fully reversible. On return of the applied potential to zero, the starting spectrum is regenerated.

Figure 3.15 : Absorption spectrum monitoring of $[Ru(bpy)_2(dpb)](BF_4)_2$ in DMF

$T = 243$ K, $E_{appl} = + 1.6$ V

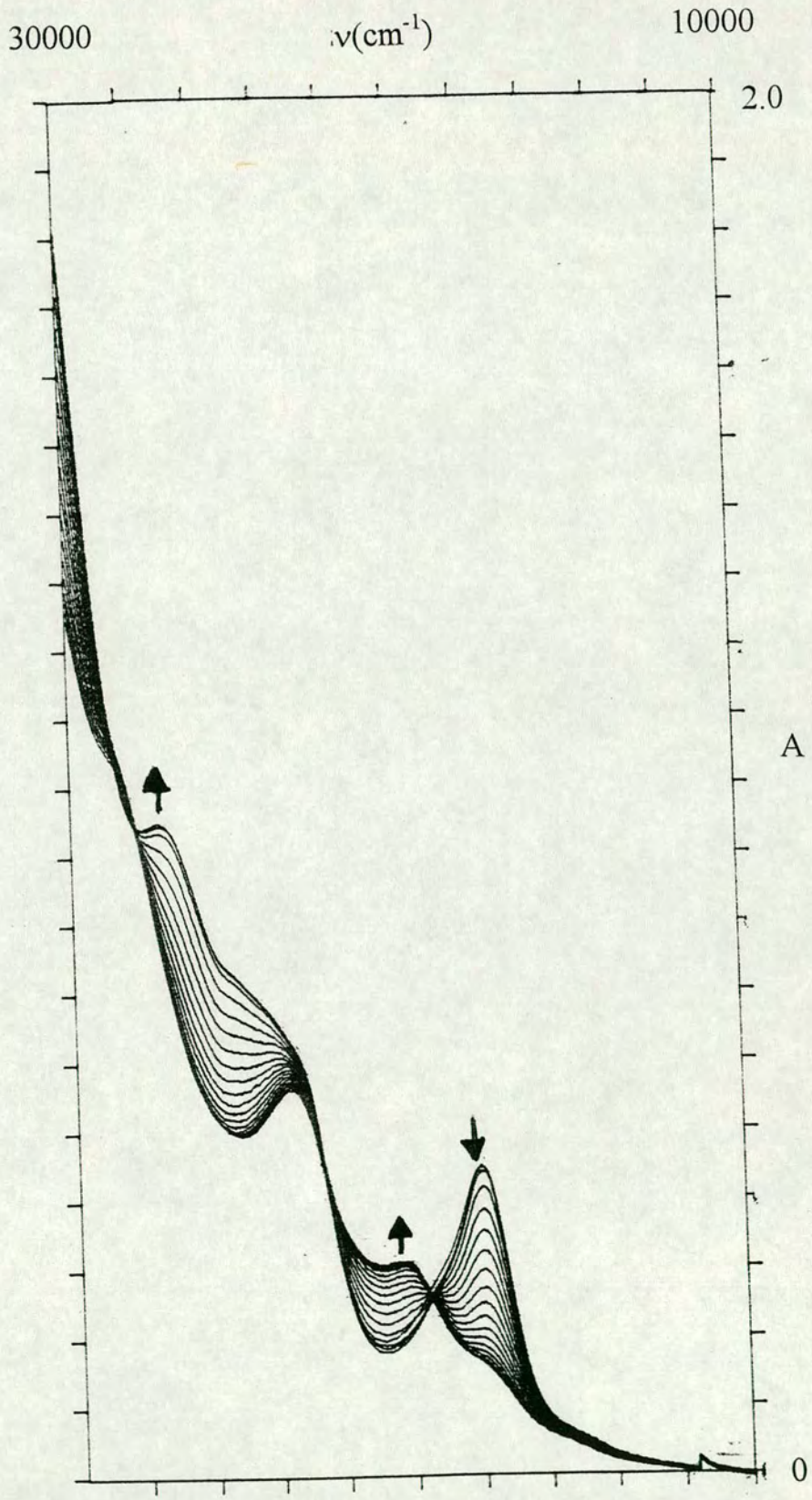

3.4 : Bimetallic Complexes

3.4.1 : $[Ru(bpy)_2(dpp)Fe(bpy)_2](BF_4)_4$

The electronic absorption spectrum of the heterometallic dpp bridged dimer complex in acetonitrile is given in figure 3.16. This spectrum has characteristics of both $[Fe(bpy)_2(dpp)](BF_4)_2$ and $[Ru(bpy)_2(dpp)](BF_4)_2$. The region normally containing those peaks assigned as MLCT processes shows three overlapping, but discernible, absorptions. The first two, at 19194 and 20833 cm^{-1}, are the Fe $d(\pi) \rightarrow$ ligand π^* and Ru $d(\pi) \rightarrow$ ligand π^* transitions. As for the monometallic species, these consist of overlapping M $d(\pi) \rightarrow$ bpy π^* and M $d(\pi) \rightarrow$ dpp π^* transitions. Comparison with the spectra of the monometallic parent complexes would indicate that the iron based band will likely be of lower energy. At slightly higher energy, 23529 cm^{-1}, is another MLCT band. This is probably a metal $d(\pi) \rightarrow$ ligand $\pi^*(2)$ transition. Again, comparison to the monometallic complexes suggests that this process is based on the Fe atom, and thus it is assigned as Fe $d(\pi) \rightarrow$ ligand $\pi^*(2)$ process. Again this is made up of overlapping processes involving bpy and dpp ligands.

In the UV region, the absorptions due to the aromatic ligands are observed. As for the monometallic complexes, the transitions due to the bpy and dpp ligands coincide, making their individual assignment impossible. The first band, at 34727 cm^{-1}, is assigned as the ligand $\pi \rightarrow \pi^*(1)$ processes, and the second, at 40816 cm^{-1}, as the ligand $\pi \rightarrow \pi^*(2)$ processes.

The electrochemistry of the complex is shown in figure 3.17. This demonstrates four observable processes in the reductive range and two processes in

Figure 3.16 : Electronic Absorption spectrum of $[Ru(bpy)_2(dpp)Fe(bpy)_2](BF_4)_4$ in MeCN

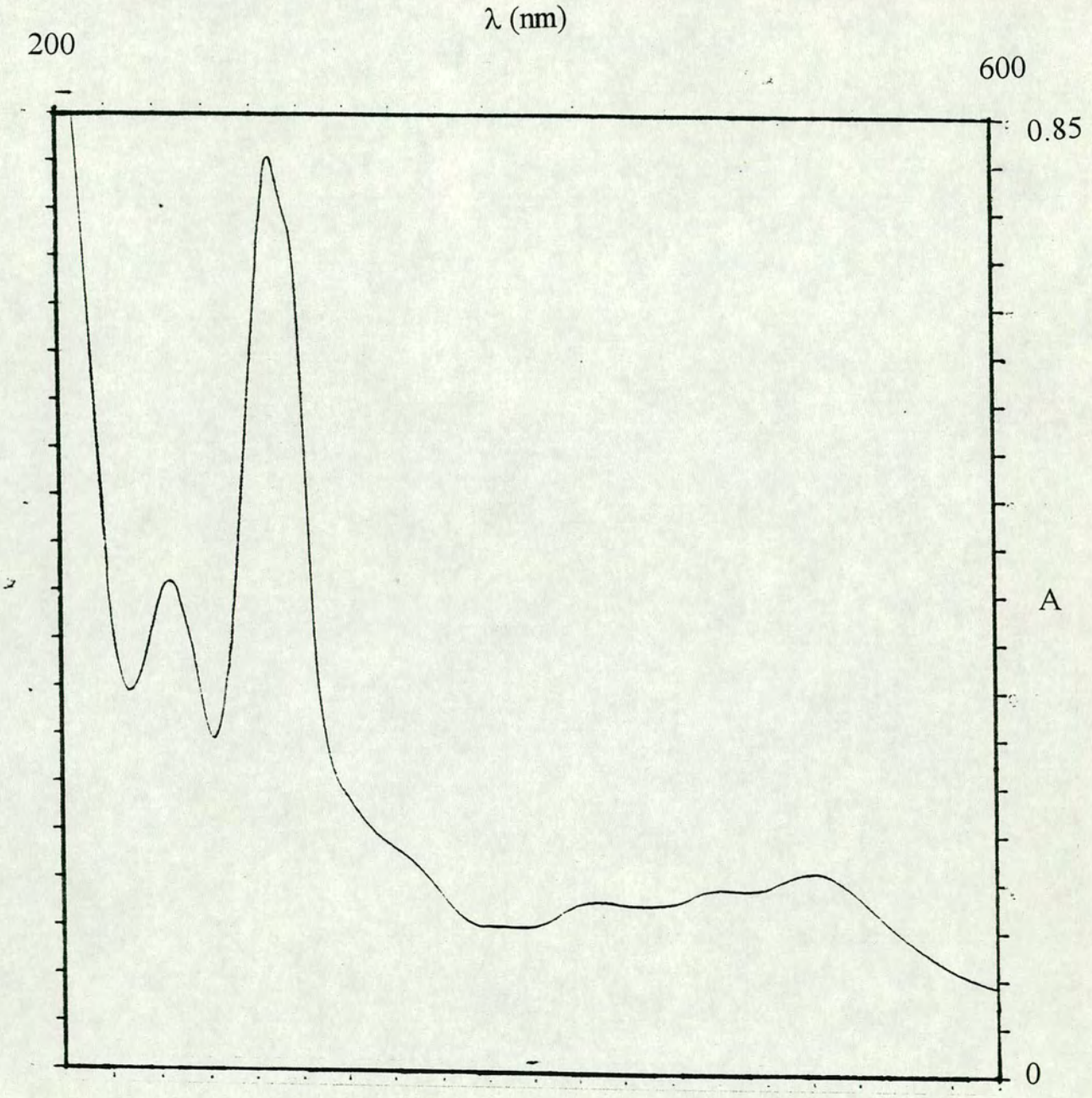

Figure 3.17 : Electrochemistry of $[Ru(bpy)_2(dpp)Fe(bpy)_2](BF_4)_4$ in DMF

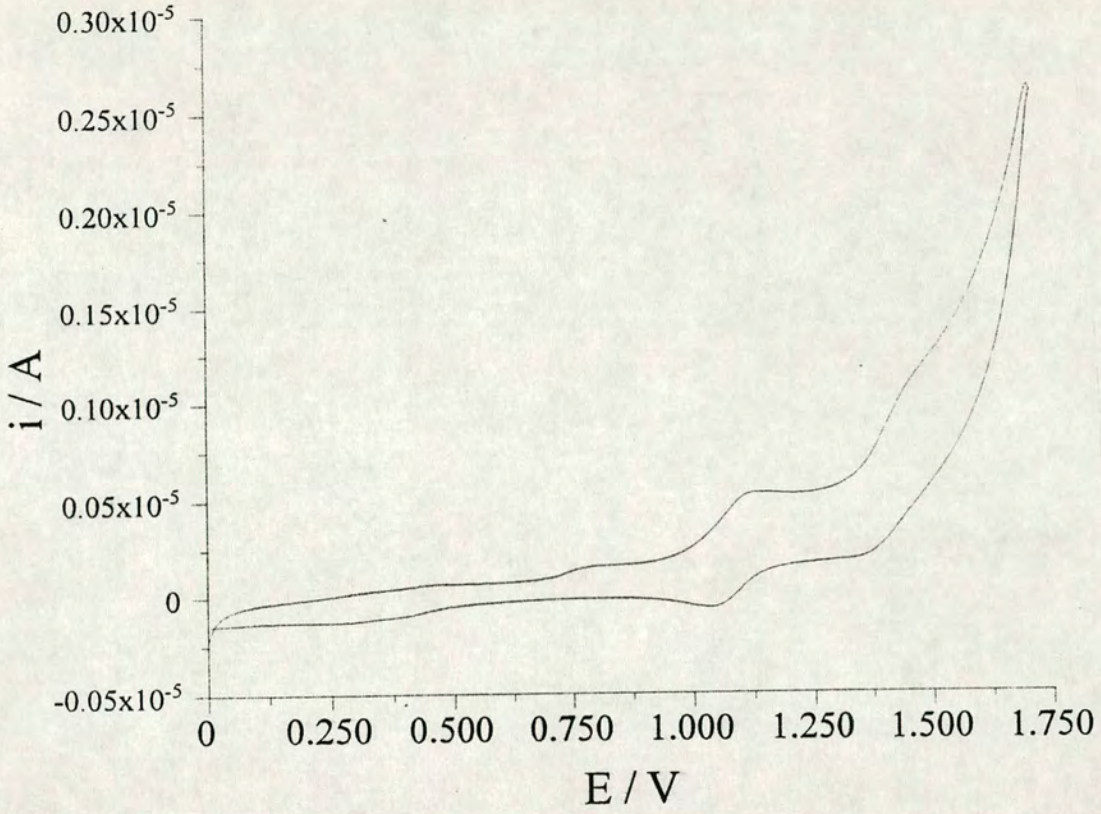

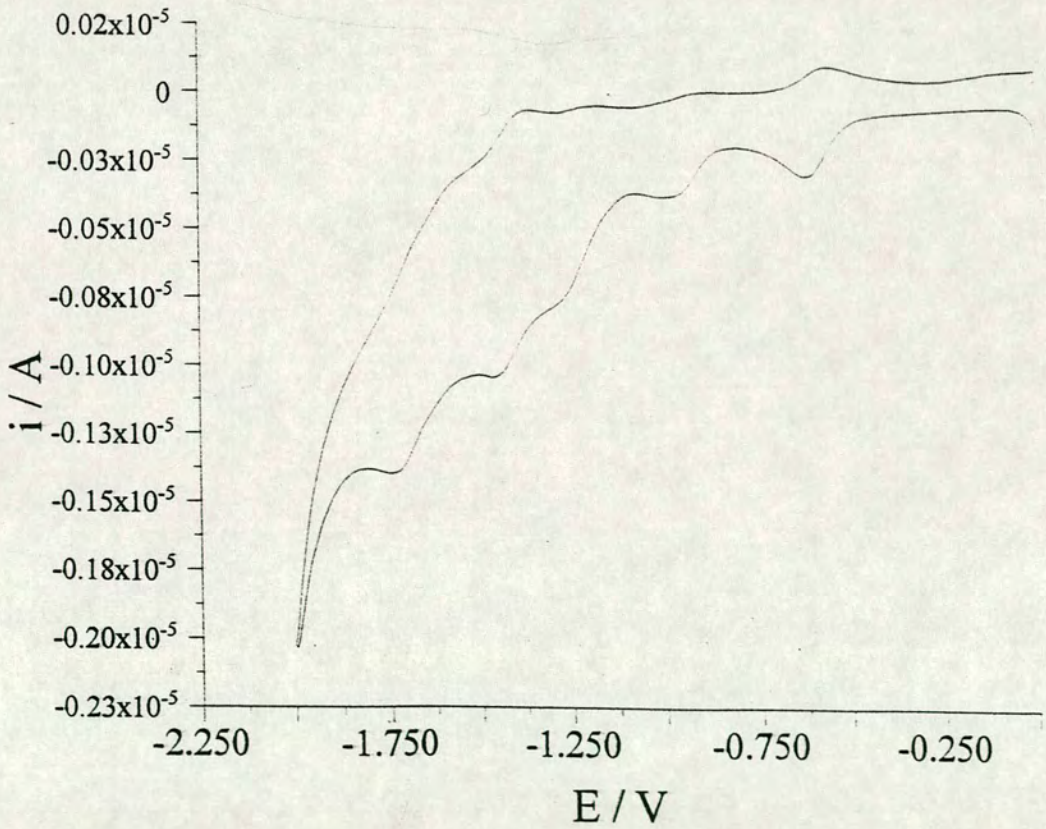

the oxidative range. The two processes in the oxidative range occur at +1.08 V and +1.45 V. The first of these appears fully reversible at room temperature, while the second appears semi-reversible at room temperature. Comparison with the appropriate mono-metallic species would suggest that the first process is the iron(II)/(III) couple, and that the second process is the ruthenium(II)/(III) couple.

The four processes in the negative range occur at -0.6 V, -1.21 V, -1.41 V and ~-1.74 V. The first is semi-reversible at room temperature, and we assign this as the reduction of the dpp ligand.

The next two processes are also semi reversible at room temperature, and the last process is irreversible. We would expect the first of these to be the second reduction of the dpp ligand, as this has been shown to be true in other systems[7]. The third process is therefore the reduction of one of the bpy ligands. We expect to see another three process, one for each bpy, but these may be obscured by the solvent window. It is not possible to assign these processes to the metal centres without further study, perhaps using the OTE cell and determining which MLCT process collapses upon reduction of the ligands.

We note that the first reduction of the dpp ligand is significantly easier for this complex than for either of the two parent complexes. This is because the dpp is acting as a bridging ligand, and therefore donating electron density to the metal centres in the form of four σ-bonds. Therefore the overall electron density on the ligand will be reduced compared to the monometallic species in which the lone pair of electrons on two of the nitrogen centres are not involved in σ-donation to a metal centre. Thus we observe the reduction of the dpp ligand at less negative potentials than in the related

Figure 3.18 : Absorption spectrum monitoring of $[Ru(bpy)_2(dpp)Fe(bpy)_2](BF_4)_4$ in DMF, T = 243 K, E_{appl} = + 1.3 V

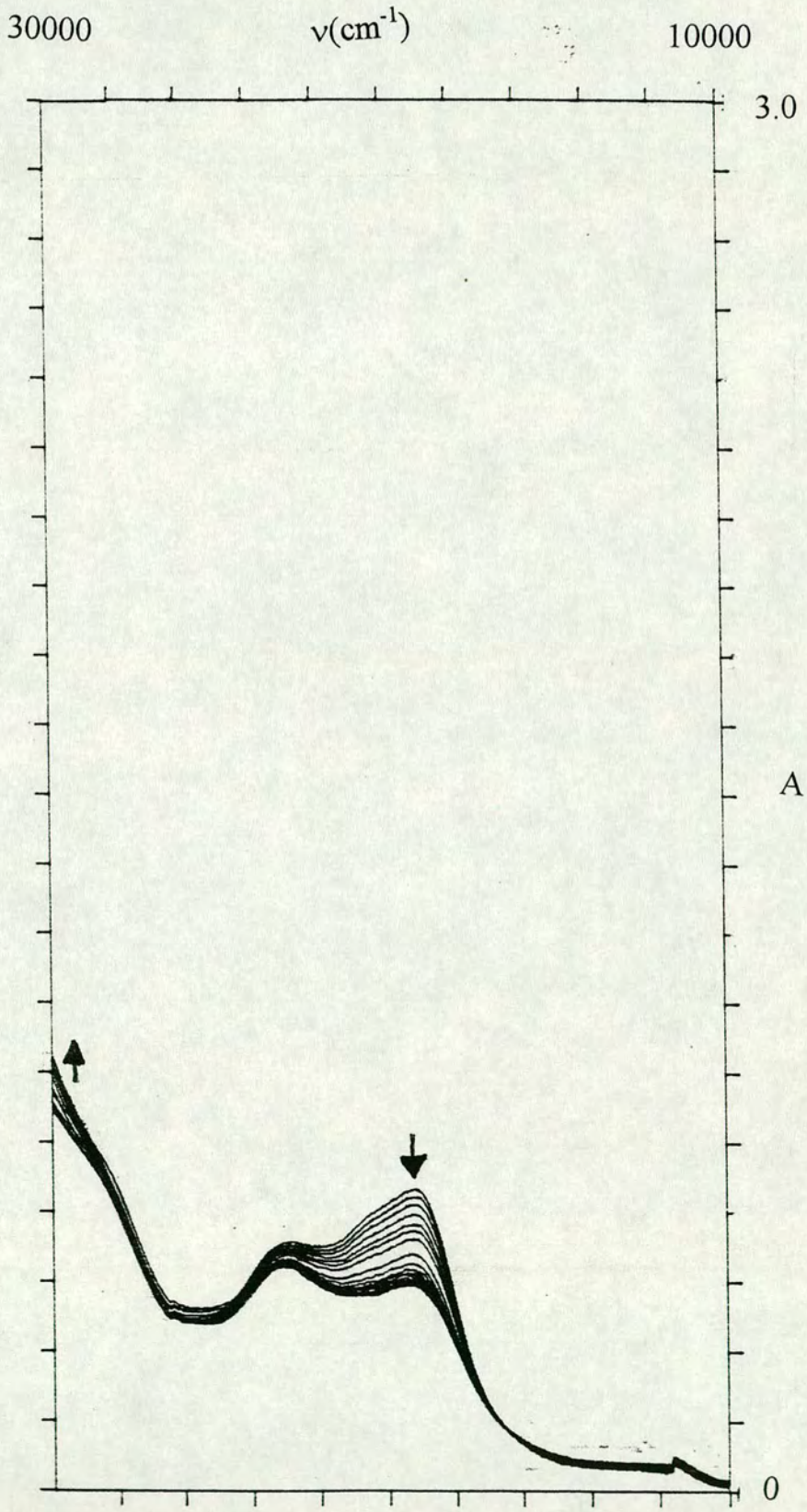

monometallic species. Note that the dpp ligand is reduced twice before the bpy ligands are reduced and therefore, on electrostatic arguments, the bpy based reductions are at more negative potentials.

With such a rich electrochemistry, this complex is a good candidate for spectroelectrochemical study. The results of such an experiment are shown in figure 3.18. This demonstrates the collapse of the lower energy MLCT process, on one electron oxidation of the complex, which we would expect, as we have assigned this as being based on the iron centre. The band we have assigned as the Ru based MLCT process undergoes no such reduction in intensity. No new bands are observed growing in, although we might expect to observe either a LMCT process or an inter-valence charge transfer (IVCT) process from the Ru(II) centre to the new Fe(III) centre. If either of these processes do occur then they are either outside the range studied in the experiment, or are obscured by the transitions already present. Upon return of the applied potential to zero, the original spectrum is regenerated, thus implying that the process is fully reversible.

3.5 : Conclusions

The series of complexes $[Ru(bpy)_2(LL)](BF_4)_2$ (LL = dpp, dpq, dpb) exhibit closely related behaviour. The electrochemistry of all three complexes, detailed in table 3.2, shows an increasingly easy first reduction, associated with the single non-bpy ligand, followed by sequential reduction of the bpy ligands. The complex with dpb then shows a second reduction of that ligand. All three complexes show a single oxidation, and this is in good agreement with the behaviour seen for other similar species.

Table 3.2 : Electrochemistry of $[Ru(bpy)_2(LL)](BF_4)_2$

LL	$E_{½}$ $Ru^{II/III}$	$E_{½}$ $LL^{0/-}$	$E_{½}$ $bpy^{0/-}$ (1)	$E_{½}$ $bpy^{0/-}$ (2)
dpp	+ 1.40 V	- 0.97 V	- 1.37 V	-1.61 V
dpq	+ 0.9 V	-0.67 V	-1.40 V	-1.65 V
dpb	+1.54 V	- 0.45 V	-1.10 V	-1.38 V

Upon oxidation all three show the collapse of the MLCT bands in the visible spectrum, and also the shift to lower energy of the ligand internal transitions. In the case of the dpp and dpb complexes there is some evidence for the growth of LMCT bands, but no such band is seen for the dpq complex. For all three complexes further investigation is merited, especially into the reductive spectroelectrochemistry.

The heterobimetallic species $[(bpy)_2Fe(dpp)Ru(bpy)_2](BF_4)_4$ also demonstrates interesting electrochemistry and spectroelectrochemistry. The electrochemistry of the complex is a combination of that seen for the parent monometallic species, although the order of reduction changes, to allow the second reduction of the dpp ligand to occur before any of the bpy ligands are reduced. The spectroelectrochemistry of the first oxidation shows, as expected, the collapse of MLCT processes associated with the Fe centre. Much further work is required to fully characterise all the electrochemical processes in this manner.

We would hope to expand on this work by investigating the spectroelectrochemistry of other related species, such as the previously synthesised ruthenium dimers containing all three bridging ligands[5,6], as well as synthesising other hetero- and homo-metallic systems.

3.6 : Preparation of compounds

3.6.1 : 2,3-di(pyridyl)quinoxaline (dpq)

This complex was prepared using the method outlined in the literature[11]. A solution of *o*-phenylenediamine in ethanol was added to a solution containing one equivalent of 2,2'-pyridil, also in ethanol. The mixture was refluxed for one hour, and then cooled. On cooling, light brown crystals of the product separated. These were filtered off and dried under suction.

3.6.2 : 2,3-di(pyridyl)benzoquinoxaline (dpb)

This compound was prepared using a modification of the method described in the literature[12]. A slurry of 2,3-diaminonapthalene (1.6g, 0.01 mol) and 2,2'-pyridyl in absolute ethanol was prepared. This mixture was refluxed for 5 hours. The resulting dark brown solution was aged overnight at 10° C. Activated charcoal was added and the mixture was refluxed for a further 7 hours. The solution was filtered hot, removing the charcoal, and leaving a bright yellow solution. Cooling overnight in a refrigerator yielded bright yellow crystals, which were filtered off and dried under suction.

Analysis: Calculated for $C_{22}H_{14}N_4$: C 79.0 % ; H 4.2 % ; N 16.8 %

Found : C 79.6 % ; H 4.4 % ; N 17.0 %

3.6.3 : $[Fe(bpy)_2(dpp)](BF_4)_2$

This complex was prepared by a very similar method to that for $[Fe(bpy)_2(CN)_2]$. Ferrous ammonium sulphate (338.4 mg, 8.54×10^{-4} mol) and 2,2'-bipyridine (267 mg, 1.71×10^{-3} mol) were dissolved in 200ml water. 2,3-di(pyridyl)pyrazine (200mg, 8.54×10^{-4} mol) was dissolved in 50ml water, and the

resulting solution was added to the stirring iron-bipyridine mixture. A dark red solution was obtained. Excess sodium tetrafluoroborate (Na BF_4) was added and the solution was reduced by evaporation. The crystals formed on cooling were filtered off, washed with ether and dried under suction. The product was further purified by column chromatography, using Sephadex LH-20 as the support and acetonitrile as the eluent. The band containing the product was evaporated to dryness, dissolved in the minimum of acetone and added dropwise to an excess of ether. The crystals so obtained were collected by filtration, washed with ether and dried.

Analysis : Calculated for $FeC_{32}H_{24}N_8B_2F_8$: C 52.6 % ; H 3.4 % ; N ;14.4 %

Found : C 46.2 % ; H 3.4 % ; N 12.4 %

corresponds to $[Fe(bpy)_2(dpp)](BF_4)_2.6H_2O$

3.6.4 : $[Ru(bpy)_2(dpp)](BF_4)_2$

This complex was prepared using the procedure outlined in the literature[5]. Bis(bipyridyl)dichlororuthenium(II) dihydrate ($Ru(bpy)_2Cl_2$, 250mg, 4.8×10^{-4} mol) was suspended in 50ml of a 1:1 water:ethanol mixture. An excess of 2,3-di(pyridyl)pyrazine (dpp, 222mg, 9.5×10^{-4} mol) was added. The solution was refluxed for 5 hours with stirring. The resulting red/purple solution was reduced to approximately one third of its original volume, and 35ml of water was added. This solution was filtered to remove unreacted ligand. An excess of sodium tetrafluoroborate was added, and the resulting precipitate was collected by filtration, washed with ether and dried under suction. The product was further purified by column chromatography using alumina as the support, and acetonitrile as eluent. The

product band was collected, the acetonitrile was removed, and the product was recrystallised from acetone/ether.

Analysis : Calculated for $RuC_{34}H_{26}N_8B_2F_8$: C 49.72 % H 3.19 % N 13.64 %

Found : C 45.03 % H 3.52 % N 11.97 %

3.6.5 : $[Ru(bpy)_2(dpq)](BF_4)_2$

This complex was prepared using the procedure outlined in the literature[2]. Bis(bipyridyl)dichlororuthenium(II) (200mg, 3.87×10^{-4} mol) was dissolved in 50ml acetone. Silver tetrafluoroborate ($AgBF_4$, 142mg, 7.74×10^{-4} mol) was added, and the resulting precipitate of silver chloride was removed by filtration. 2,3-Di(pyridyl)quinoxaline (dpq, 110 mg, 3.87×10^{-4} mol) was added and the solution was refluxed under nitrogen for 24 hours. The solvent was then removed and the product was purified by column chromatography using an alumina column and a 1:1 acetonitrile:dichloromethane mixture as eluent. The solvent was removed from the product, which was then recrystallised from acetone/ether.

Analysis : Calculated for $RuC_{38}H_{28}N_8B_2F_8$: C 52.38 % H 3.24 % N 12.86 %

Found : C : 40.99 % H 3.51 % N : 8.95 %

3.6.6 : $[Ru(bpy)_2(dpb)](BF_4)_2$

This complex was prepared using the procedure outlined in the literature[6]. Bis(bipyridyl)dichlororuthenium(II) (155mg, 3×10^{-4} mol) was dissolved in 50ml acetone. Silver tetrafluoroborate ($AgBF_4$, 110mg, 6×10^{-4} mol) was added, and the resulting precipitate of silver chloride was removed by filtration. 2,3-Di(pyridyl)benzoquinoxaline (dpb, 100mg, 3×10^{-4} mol) was added and the solution was refluxed under nitrogen for 24 hours. The solvent was then removed and the

product was purified by column chromatography using an alumina column and a 1:1 acetonitrile:dichloromethane mixture as eluent. The solvent was removed from the product, which was then recrystallised from acetone/ether.

Analysis : Calculated for $RuC_{42}H_{30}N_8B_2F_8$: C 54.75 % H 3.28 % N 12.16 %

Found : C 51.34 % H 3.80 % N 11.23 %

3.6.7 : $[Fe(bpy)_2(dpp)Ru(bpy)_2](BF_4)_4$

Bis(bipyridyl)dichlororuthenium(II) (100mg, 1.9×10^{-4} mol) was dissolved in 60ml acetone and silver tetrafluoroborate (75mg, 3.9×10^{-4} mol) was added with stirring. the resulting brown precipitate of silver chloride was removed by filtration. Bis(bipyridyl)(di(pyridyl)pyrazine)iron(II) tetrafluoroborate (150mg, 1.9×10^{-4} mol) was added and the solution was heated at reflux for 48 hours. The solvent was removed by use of a rotary evaporator, and the product was recrystallised from acetone/ether. The resulting crystals were washed with ether and dried under suction.

Analysis : Calculated for $FeRuC_{54}H_{34}N_{12}B_4F_{16}$: C 47.86 % H 2.53 % N 12.40 %

Found : C 43.19 % H 3.25 % N 10.85 %

3.7 : References

1. M.K. Nazeeruddin, P. Liska, J. Moser, N. Vlachopoulas, M. Grätzel, *Helv. Chim. Acta*, **1990**, 73, 1788
2. D.P. Rillema, K.B. Mack, *Inorg. Chem.*, **1982**, 21, 3849
3. M.M. Richter, K.J. Brewer, *Inorg. Chem.*, **1993**, 32, 5762
4. A. Juris, V. Balzani, S. Campagna, G. Denti, S. Seroni, G. Frei, H. Grudel, *Inorg. Chem.*, **1994**, 33, 1491
5. C.H. Braunstein, A.D. Baker, T.C. Strekas, H.D. Gafney, *Inorg. Chem.*, **1984**, 23, 857
6. D.L. Carson, W.R. Murphy, *Inorg. Chim. Acta*, **1991**, 181, 61
7. M.M. Richter, K.J. Brewer, *Inorg. Chem.*, **1993**, 32, 2827
8. R.R. Ruminski, D. Serveiss, M. Jacquez, *Inorg. Chem.*, **1995**, 34, 3358
9. S. Roffia, M. Marcaccio, C. Paradisi, F. Paulocci, V. Balzani, G. Denti, S. Serroni, S. Campagna, *Inorg. Chem.*, **1993**, 32(14), 3003
10. N.E. Tokel-Takvoryan, R.E. Hemmingway, A.J. Bard, *J. Am. Chem. Soc.*, **1973**, 95, 6582
11. H.A. Goodwin, F. Lions, *J. Am. Chem. Soc.*, **1959**, 81, 6415
12. A.J. Baiano, D.L. Carson, G.M. Wolosh, D.E. DeJesus, C.F. Knowles, E.G. Szabo, w.R. Murphy, *Inorg. Chem.*, **1990**, 29, 2327

Chapter 4 : Cyano-bridged Polymetallic Complexes

4.1 : Introduction

One of the main areas of interest in studies involving the Ru(bpy) chromophore has been in attempting to change the photochemical properties of the species, whilst maintaining the useful redox and excited state properties associated with the chromophore. One obvious way of achieving this is to introduce another metal centre into the complex, allowing for the possibility of separation of the charges associated with the excited state, via intramolecular charge transfer.

As *cis*-dicyanobis(2,2'-bipyridyl)ruthenium(II) maintains some of the desirable properties associated with tris(2,2'-bipyridyl)ruthenium(II), and cyanide is known to be capable of acting as a bridge between metal centres (e.g. in Prussian Blue), this complex has often been used as a starting point for species containing more than one metal centre.

The first example of $Ru(bpy)_2(CN)_2$ forming bridges in this manner was in work by Demas *et al*[1], where they considered the quenching of the complexes' excited state by a range of inorganic species, including Cu^{2+}, Ni^{2+} and Co^{3+}. To explain their observations, they proposed that the cyanide ligands complexed with the metal ions, to form short lived bi- and tri- metallic species. Later work by Kinnaird and Whitlen[2] investigated the reaction of the complex with silver(I) ions in acetonitrile, and they studied three adducts with different stoichiometry. The 1:1 adduct was isolated and showed a longer excited state lifetime and enhanced luminosity when compared with the starting ruthenium complex.

The first isolated example of cyanide bridging between the $Ru(bpy)_2(CN)_2$ centre and another complexed transition metal centre was described by Bignozzi and Scandola[3], when they detailed the addition of one or two $Pt(dien)^{2+}$ units to the ruthenium centre via the cyanide ligands (dien = diethylenetriamine). The addition of the platinum centres blue-shifted both the absorption and emission maxima associated with the ruthenium centre. The excited state lifetime for the complexes varied with the solvent, with the mono-metallated species having a lifetime of 630 ns in DMF compared with the ruthenium monomers' lifetime of 205 ns in DMF. In water, however, both bridged complexes had a shorter excited state lifetime than $Ru(bpy)_2(CN)_2$.

Since that work, a wide range of metal centres have been attached to the $Ru(bpy)_2(CN)_2$ unit, including $[Ru(NH_3)_5]^{3+}$ [4], $[Ru(NH_3)_4(py)]^{3+}$ [5], $[Ru(phen)_2(CN)]^{2+}$ [6], $[Ru(bpy(COO)_2)_2]^{2-}$ [7], $[Rh(NH_3)_5]^{3+}$ and $[Cr(NH_3)_5]^{3+}$ [8]. Many of these species show considerable variation in properties associated with the $Ru(bpy)_2(CN)_2$ chromophore (electrochemistry, absorption properties, excited state lifetimes etc.), as well as the properties associated with the additional metal centre.

This chapter is concerned with the synthesis and characterisation of some new species containing the $Ru(bpy)_2$ unit, utilising cyano bridges as a means of achieving poly-metallic complexes. As other work in this department was concerned with the behaviour of species containing the Pt(bpy) unit[9], we decided to make use of this readily available data and attempt to attach Pt(bpy) and Pt(terpy) units to the ruthenium core. The pt(bpy) unit is also photoactive.

The method of choice in the preparation of cyanide bridged species is to prepare a halide substituted species (frequently chloride, but occasionally bromide), e.g. ML_5Cl, remove the halide by use of Ag^+, and then add an excess of the cyanide containing unit (e.g. $Ru(bpy)_2(CN)_2$). The resulting mixture is then heated for a short period of time (typically 2-4 hours), before the bimetallic product is isolated. We typically followed this general scheme when attempting to prepare these complexes. The synthetic procedures are detailed in section 4.5.

4.2 : Attempted synthesis of $[Ru(bpy)_2((NC)Pt(bpy)(CN))_2](BF_4)_2$ **[RuPt$_2$]**

In this case we removed the chlorides from $[Ru(bpy)_2Cl_2]$ by use of $AgBF_4$, and then added an excess of $[Pt(bpy)(CN)_2]$ in order to prevent polymerisation.

The UV/VIS/NIR spectrum of the product from this reaction in DMF is shown in figure 4.1. This demonstrates three clearly discernible bands. At highest energy, we observe a band at 34107 cm^{-1} with a well defined secondary peak at around 31000 cm^{-1}. Comparison with the spectra of $[Pt(bpy)(CN)_2]$[9] and other species containing the $Ru(bpy)_2$ unit[3-8] suggest that both absorbances are due to bpy internal $\pi \rightarrow \pi^*$ transitions, with the main peak associated with bpy ligands attached to the Ru centre, and the smaller peak associated with bpy chelated to the Pt centre.

The lower energy process has its maximum at 21542 cm^{-1}. This is significantly higher than the energy of the first MLCT band for $[Ru(bpy)_2(CN)_2]$ (19904 cm^{-1} in DMF). Complexes containing cyano bridged $Ru(bpy)_2$ units typically show a blue shift in the MLCT process associated with this chromophore[3,4]. Indeed, the oligomeric systems prepared by Bignozzi *et al*[6], which contain $Ru(bpy)_2$ units both C-bound and N-bound to the cyanide ligand, show considerable sharpening of the MLCT band as

Figure 4.1 : Electronic absorption spectrum of [**$RuPt_2$**] in DMF

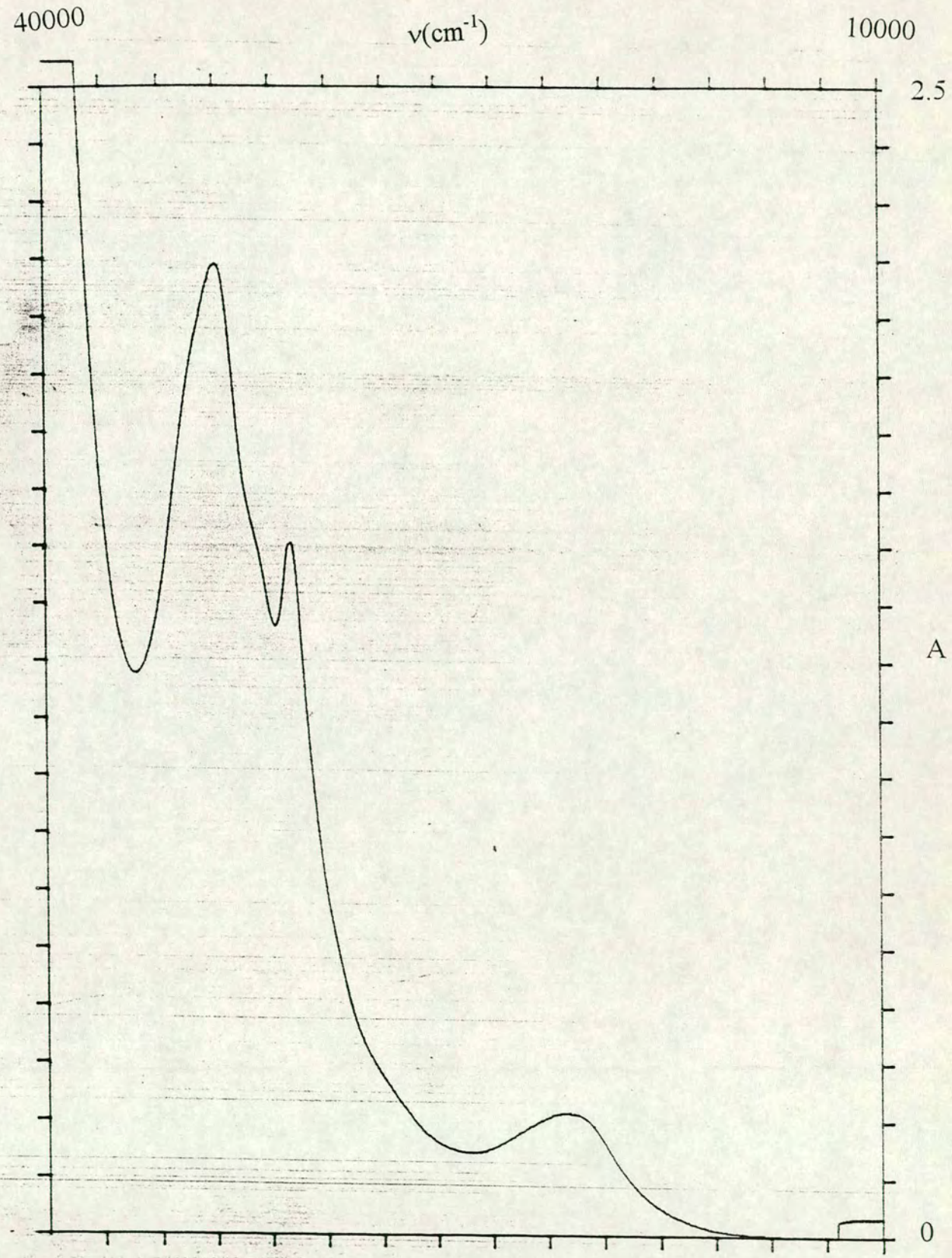

well as the blue shift, suggesting that the difference between the different ends of the cyanide bridge, in electronic terms, appears to be minimal. We therefore propose that this absorbance is due to a $d(\pi) \rightarrow$ bpy π^* MLCT process involving the Ru(bpy) chromaphore. Taking $[Ru(bpy)_2(CN)_2]$ as a baseline, and applying a similar blue shift to the second observed MLCT process (at 28441 cm^{-1}), we obtain an estimated energy for the second MLCT process of 29989 cm^{-1} in the new material. If this estimate is correct, we would expect this to be masked by the more intense intraligand transitions at higher energy. Consideration of the electronic absorption spectrum of $[Pt(bpy)(CN)_2]$[9] shows that the MLCT process, Pt $d\pi \rightarrow$ bpy π^*, associated with the platinum centre is of sufficiently high energy to be apparent only as a shoulder on the bpy intraligand transition. It is therefore reasonable to assume that the transition associated with the Pt centre in the product is also masked by the intraligand transitions. Thus the absorption spectrum of the product is not simply the superposition of the two isolated monometallic species.

The electrochemistry of the product in DMF is shown in figure 4.2. This demonstrates four processes in the negative range (0 to -2 V) and 1 process in the positive range (0 to +1.7 V). The four processes in the negative range occur at -0.90 V, -1.38 V, -1.61 V and ~-1.83V. The first process is semi-reversible at room temperature, but appears to become fully reversible on cooling to 243 K. The second process is semi-reversible at room temperature, and remains so on cooling. The third process is irreversible at room temperature, and becomes semi-reversible on cooling. The fourth and final process is irreversible at both 293 K and 243 K.

Figure 4.2 : Electrochemistry of **[$RuPt_2$]** in DMF

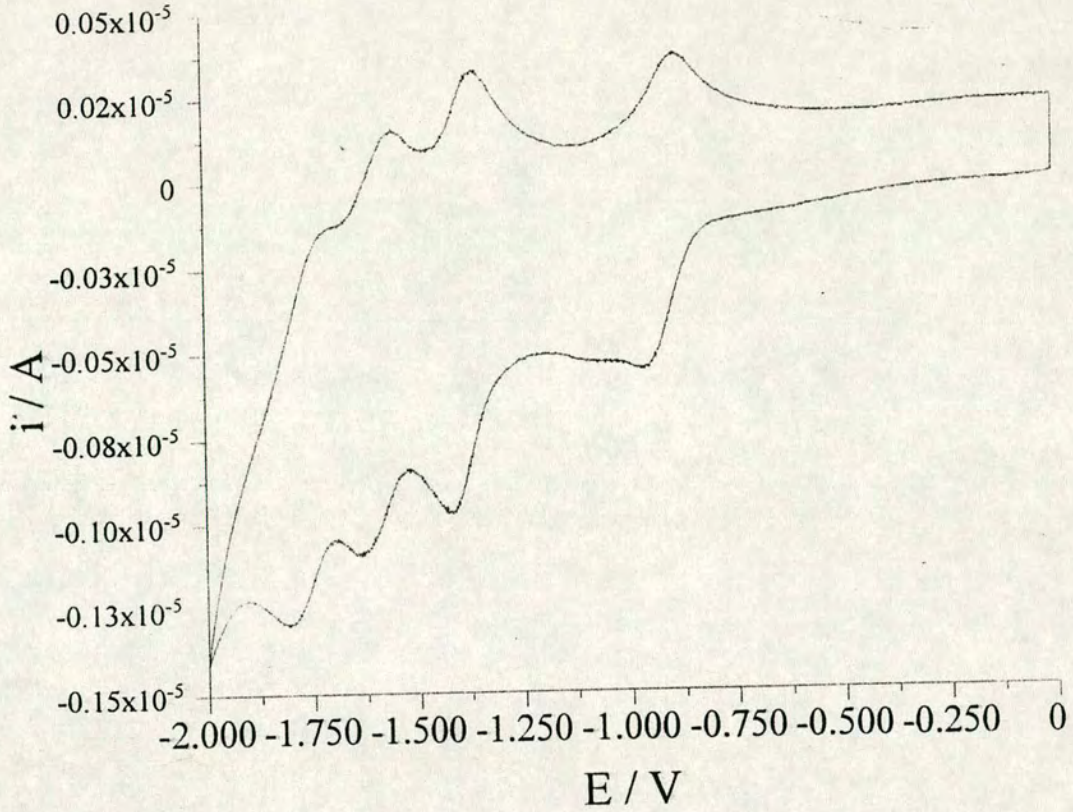

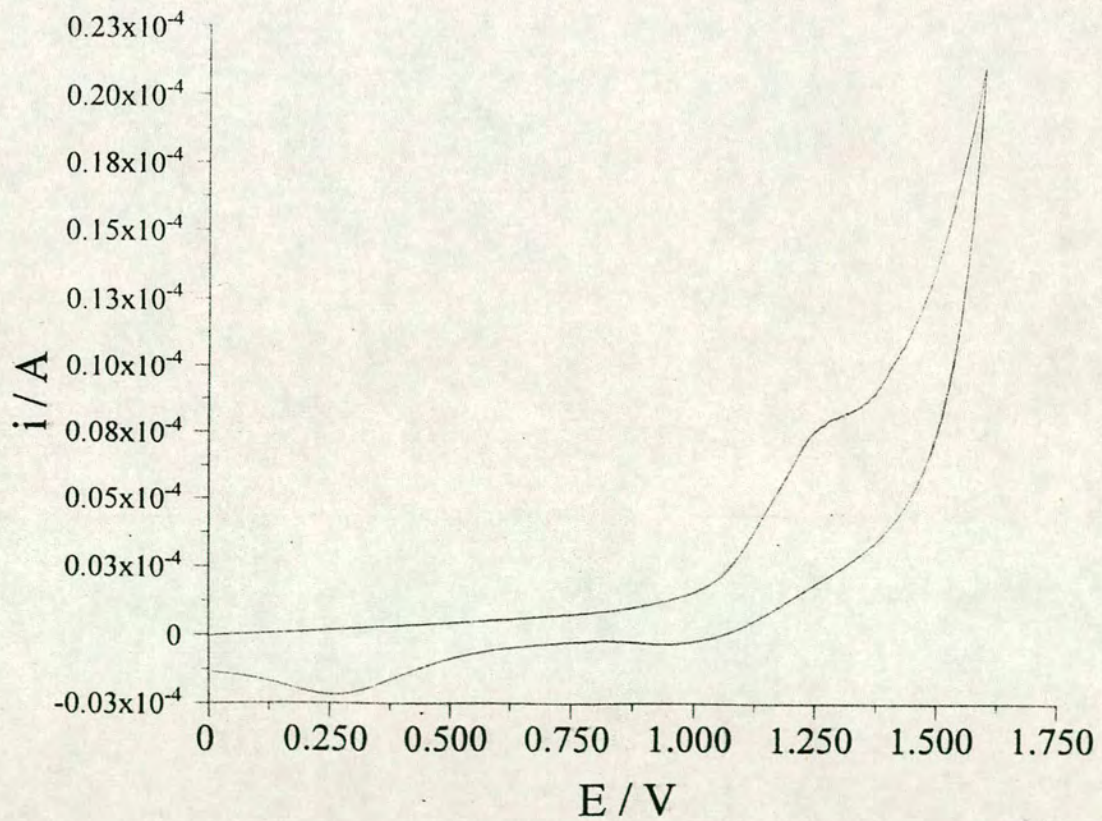

Comparison with the starting mono-metallic complexes allows us to make tentative assignments of these processes. The electrochemistry of $[Pt(bpy)(CN)_2]$ demonstrates two reductive processes, at -0.94 V and -1.61 V[9]. The first of these is reversible on cooling, while the second remains semi-reversible. Complexes containing the $Ru(bpy)_2$ unit typically show two reductions separated by around 280 mV (i.e. $[Ru(bpy)_2(CN)_2]$ $E_{½}$ = -1.495 V and -1.78 V). We therefore assign the first process as a one electron reduction of the bpy ligand chelated to the Pt centre.

If we then consider the other three processes, this is consistent with a second Pt based reduction (as seen for $[Pt(bpy)X_2]$[9]) and sequential reduction of the two bpy ligands chelated to the Ru centre. However, precise assignment of the nature of these processes is difficult. If the desired product was synthesised, we would expect the processes based on the Pt centre to result in twice the number of electrons as those based on the Ru centre. Comparison with $[Pt(bpy)(CN)_2]$ suggests that the third process, at -1.61 V, is likely to be the second Pt based reduction. This, however, gives a separation of around 450 mV between the other two processes, which would then be assigned as sequential reduction of the Ru bound bpy ligands. This is a much larger separation than that normally seen. As such, without further work, accurate assignment of these processes is not possible.

The process in the positive range is at around +1.3 V, and appears to be irreversible, even on cooling. If we have synthesised the desired product, we would expect to see a process due to the Ru(II)/Ru(III) couple. However, we would also expect this to be a reversible process, as is seen for other cyanide bridged complexes[x,y]. We explain this behaviour by consideration of the environment around

the Ru centre. If we have synthesised the product then the cyanide ligands attached to the ruthenium are in a bridging mode. Because of this, the cyanides have no electron density with which to stabilise the Ru(III) centre generated upon oxidation, as this is used in forming the bridge. Therefore the oxidation becomes harder when compared with $[Ru(bpy)_2(CN)_2]$, and the oxidation product may decompose.

The wealth of electrochemical processes observed for the product make it an ideal candidate for further investigation using the OTE cell. The results of such an experiment are shown in figure 4.3. This shows the result of an electrogeneration performed in DMF, at 243 K, and with an applied potential of -1.2 V. This clearly demonstrates the collapse of the absorbance we previously defined as the Pt bpy based $\pi \rightarrow \pi^*$ transition at 30000 cm^{-1}. We also observe the growth of a number of bands which are associated with the presence of a bpy^- ligand in the complex. There is no collapse of the process previously assigned as a Ru $d(\pi) \rightarrow$ bpy π^* MLCT transition, but rather a superimposition of this band and the bpy^- bands. There is also a slight shift in energy of the other bpy internal transition. Comparison with the UV/VIS/NIR spectrum of $[Pt(bpy^-)(CN)_2]^-$ [9] (see figure 4.4) shows many similarities with the spectrum obtained for the reduced product. Since the visible part of the absorption spectrum of the starting material is dominated by transitions involving the Ru(bpy) chromaphore and the reductive electron is thought to be primarily located on the Pt(bpy) chromaphore, we might expect the low energy spectrum of reduced $[RuPt_2]$ to be a superposition of the spectrum of $[RuPt_2]$ and $[Pt(bpy^-)(CN)_2]^-$. This is indeed what is observed.

Figure 4.3 : Absorption spectrum monitoring of {**$RuPt_2$**] in DMF

T = 243 K, E_{appl} = - 1.2 V

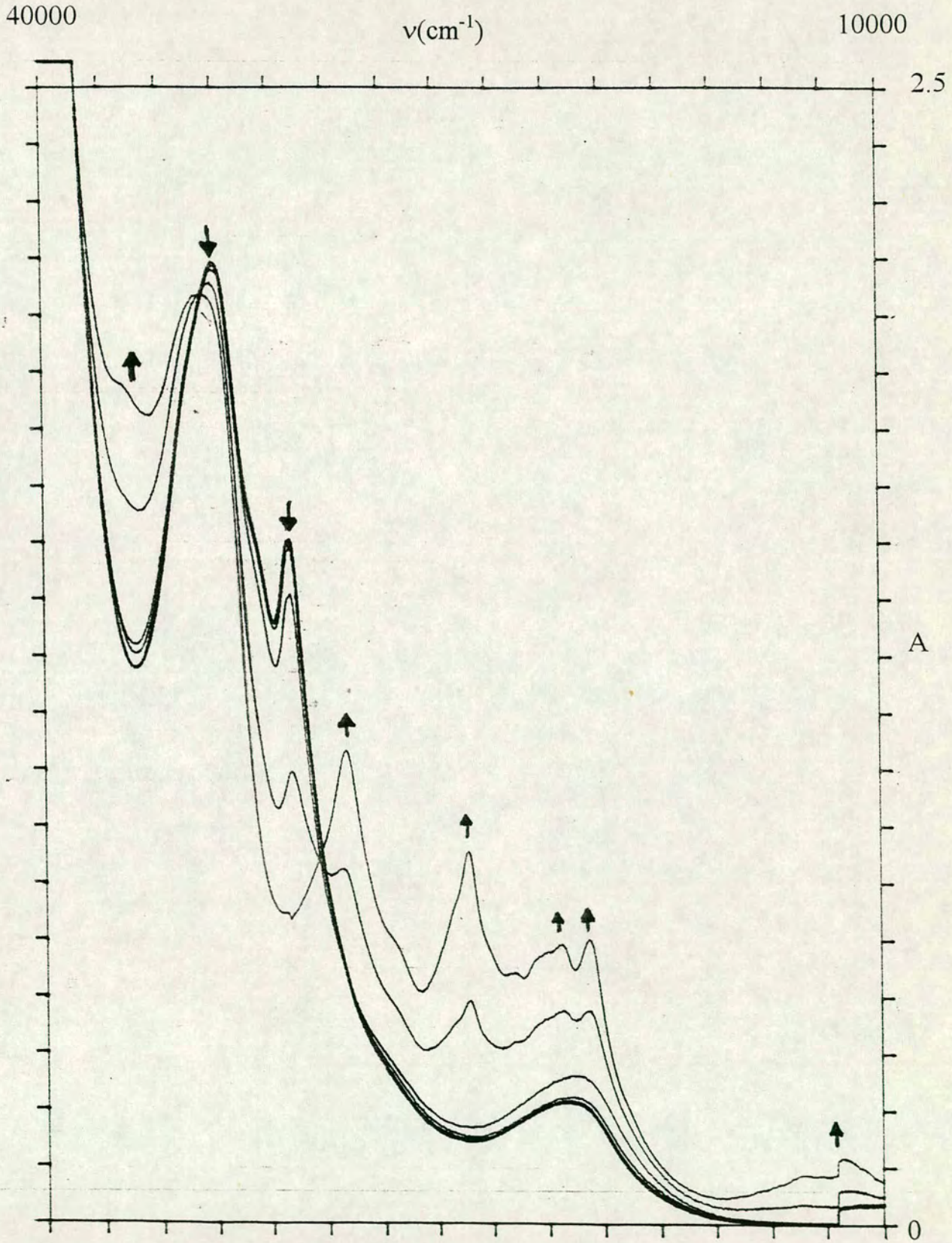

Figure 4.4 : Electronic absorption spectrum of $[Pt(bpy^{-})(CN)_2]^{-}$

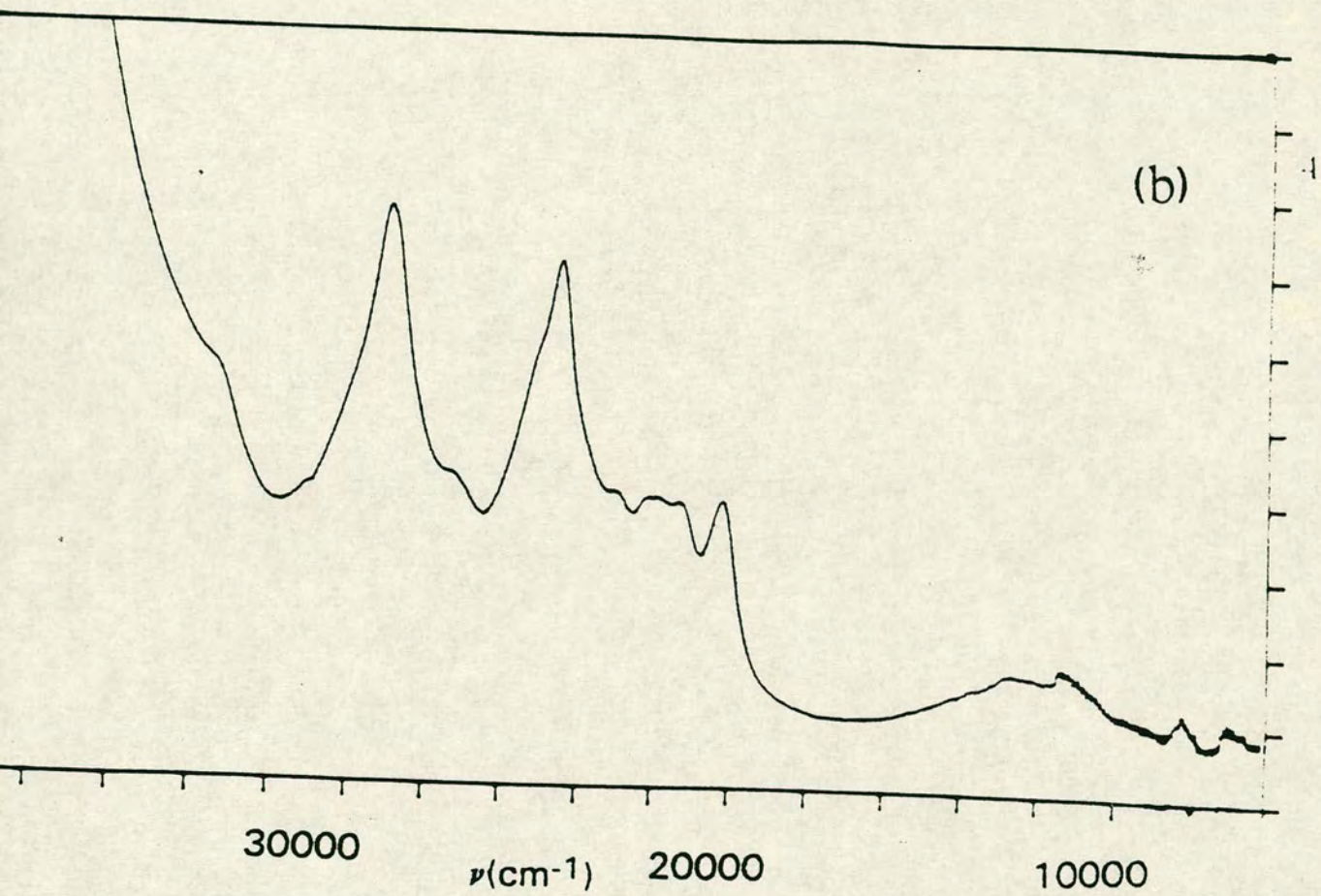

The presence of isosbestic points, and the regeneration of the starting spectrum on return of the potential to 0 V, suggest that the process is fully reversible at 243 K. Thus we can further assign the first reduction of the complex as the reduction of a Pt(bpy) unit to Pt(bpy^{-}). This is in accordance with the expected product.

Unfortunately, no other positive evidence for the formation of the expected product was gathered. The very poor CHN data obtained is detailed in the synthetic section at the end of this chapter, and mass spectrometry was similarly inconclusive, despite numerous attempts using both different techniques (both electron impact (EI) and fast atom bombardment (FAB)) and a range of matrices. A number of attempts to grow crystals suitable for X-ray diffraction studies were made, but no single crystals of suitable quality could be grown, despite the use of a range of solvents. Thus, although the electrochemical, spectroelectrochemical and spectroscopic data discussed previously is on the whole encouraging, it is not possible to confirm the identity of the product as that desired. It may be a related complex that has formed, or even a mixture of two or more products. Further work is needed to fully characterise the product.

4.3 : Attempted synthesis of [((NC)Ru(bpy)$_2$(CN))$_2$Pt(bpy)](BF$_4$)$_2$ [Ru$_2$Pt]

In our attempt to synthesise this complex, we started with [Pt(bpy)Cl$_2$] and added AgBF$_4$ to remove the chlorides. We then added an excess of [Ru(bpy)$_2$(CN)$_2$] in an attempt to make the desired complex, and to prevent a polymeric product from forming.

Figure 4.5 : Electronic absorption spectrum of **[Ru_2Pt]** in DMF

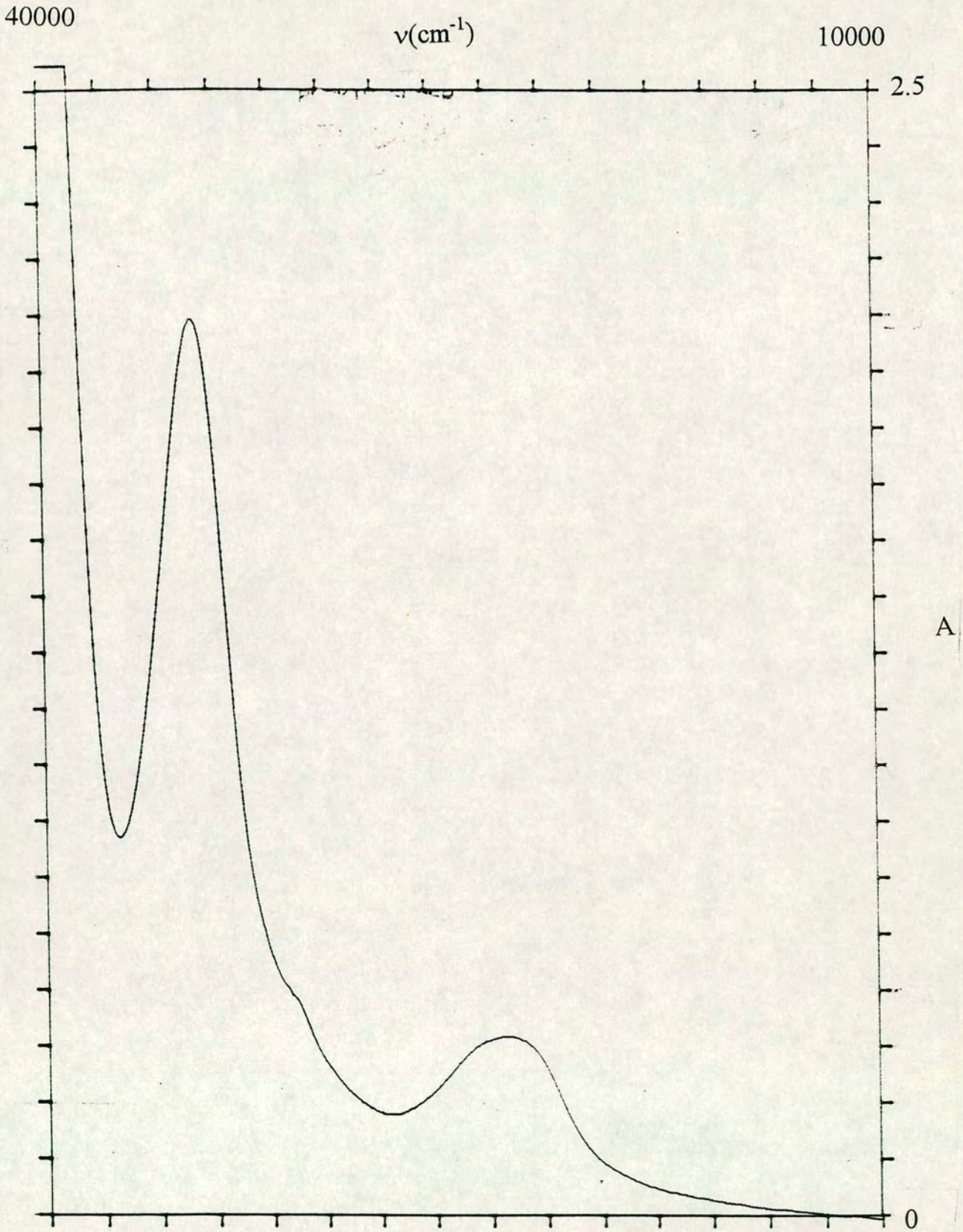

The electronic absorption spectrum of the product of this reaction in DMF is shown in figure 4.5. This has two clearly defined peaks. The first of these has a maximum at 35361 cm^{-1}, and exhibits a shoulder at around 31000 cm^{-1}. Comparison with the electronic absorption spectra of $[Ru(bpy)_2(CN)_2]$ and $[Pt(bpy)Cl_2]$[9] suggest that this band is a combination of bpy internal $\pi \rightarrow \pi^*$ transitions. We thus assign the main peak as arising from such transitions on bpy ligands chelated to the ruthenium centre, and the shoulder as arising from these transitions on the ligand associated with the platinum centre.

The second absorption has a maximum at 25317 cm^{-1}. This is at significantly higher energy than the lowest energy MLCT transition for the parent $[Ru(bpy)_2(CN)_2]$ complex (19904 cm^{-1} in DMF). As for the previous complex, this blue shift is consistent with the formation of a cyanide bridged complex. This is a particularly large shift when compared with the first complex, but similarly large shifts have been observed for bi- and tri-metallic species based on a $[Ru(bpy)_2(CN)_2]$ core[3-8]. We therefore assign this transition as a ruthenium $d(\pi) \rightarrow$ bpy π^* (MLCT) process.

Applying a similar blue shift to the second MLCT band of $[Ru(bpy)_2(CN)_2]$ places it around 34000 cm^{-1}, which is underneath the more intense higher energy transition, and we therefore do not expect to observe a second MLCT process. Similarly, in Pt(bpy) containing complexes, the Pt $\rightarrow$ bpy MLCT usually is seen as a shoulder on the bpy internal transition, and thus we expect any such transition to be masked by the intraligand transitions seen.

The electrochemistry of the product in DMF is shown in figure 4.6. This shows four processes between 0 V and -2 V, but no discernible processes occur

Figure 4.6 : Electrochemistry of **[Ru_2Pt]** in DMF

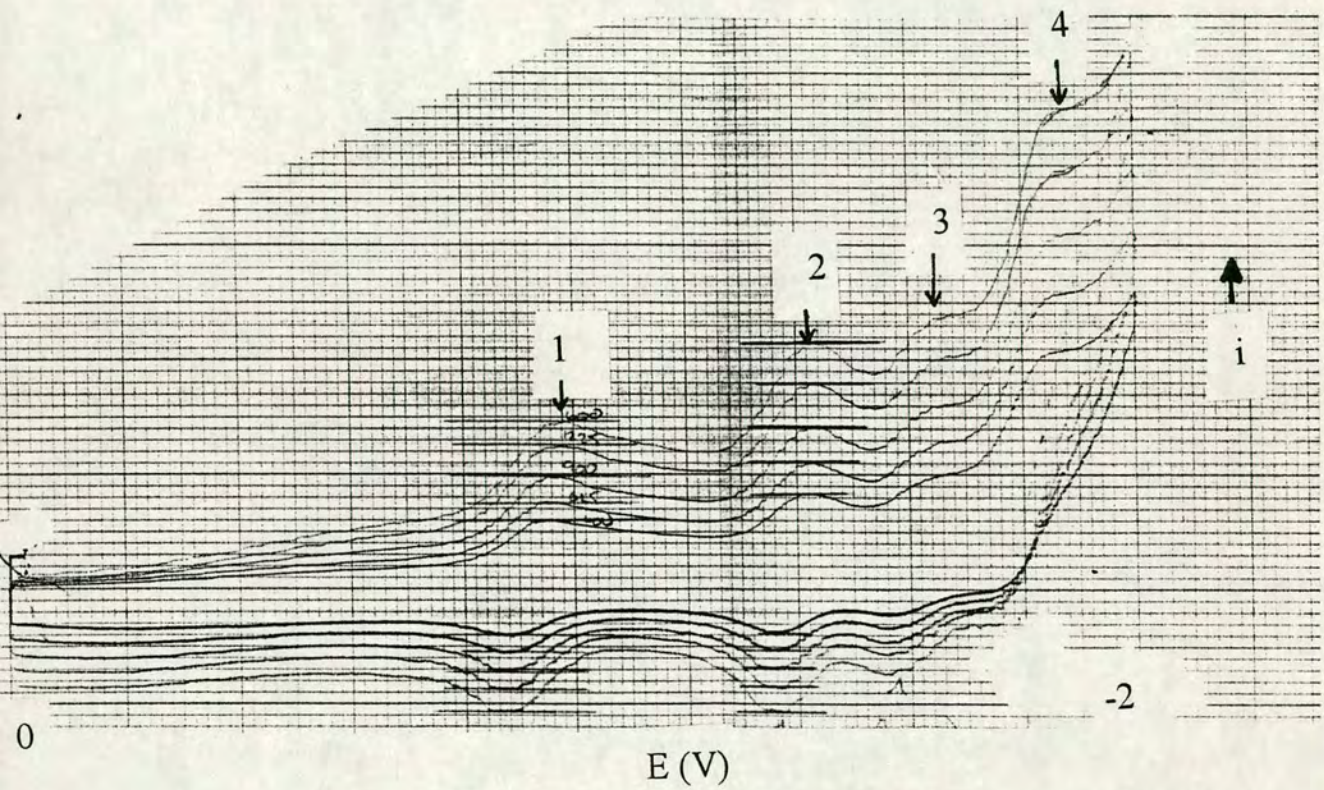

between 0 V and +2 V. The four processes have half wave potentials of -0.93 V, -1.40 V, -1.61 V and ~-1.83 V. The first process is semi-reversible at room temperature, and fully reversible on cooling to 243 K. The second process remains semi-reversible, even upon cooling. The third process is irreversible at room temperature, but becomes semi-reversible at 243 K. The fourth and final process is irreversible at all temperatures at which the experiment was performed.

A stirred voltammagram was also obtained for the solution. This showed that all four processes were reductions, and that the number of electrons involved was in the ratio 1:2:1:2 (from least negative to most negative potential).

Combining this data with the previously observed electrochemical behaviour of $[Ru(bpy)_2(CN)_2]$ and $[Pt(bpy)Cl_2]$[9], we can attempt to assign these electrochemical processes. We therefore assign the second and fourth processes (- 1.40 V and ~-1.83 V) as sequential reductions of the bpy ligands on the two ruthenium centres (i.e. both ruthenium centres have one bpy ligand reduced at each potential). We assign the first and third processes as being associated with the Pt(bpy) unit, and expect each to be a one electron reduction.

As for the previously described product, if we have indeed synthesised the target molecule then we would expect to see electrochemical behaviour due to the Ru(II)/Ru(III) couple in the oxidative range. The seemingly absent response may be due to absorption of the species on the electrode or the oxidation occurring at very positive potentials. The latter suggestion would agree with the very large high energy shift of the band maximum in the UV/VIS spectrum. If this shift was also observed in

the electrochemistry of the product, this would leave the Ru(II)/Ru(III) couple at greater than +2 V, hence the lack of a positive response.

The well defined reductive electrochemistry makes this species an ideal subject for spectroelectrochemical examination. This will provide more data to help determine the nature of the product. The results of such an experiment are shown in figure 4.7, where a potential of -1.2 V has been applied. This demonstrates the collapse of the shoulder on the high energy band that we previously ascribed to the Pt(bpy) ligand internal absorption. We also observe the growth of bands associated with the presence of bpy^- superimposed on the band we have assigned as the Ru $d(\pi) \rightarrow$ bpy π^* transition. There is also a slight shift in the maximum of the main bpy intraligand absorbance. This behaviour is entirely consistent with the first reduction being the reduction of the Pt(bpy) unit to $Pt(bpy^-)$.

The presence of three isosbestic points and the fact that the initial spectrum is regenerated on return of the applied potential to 0 V indicate that this first reduction is fully reversible at 243 K.

The infra-red spectrum of the product dissolved in DMF is also of interest. This shows two bands in the area associated with CN stretches. These occur at 2079.7 cm^{-1} and 2109.2 cm^{-1}. The band at 2079.7 cm^{-1} is indicative of a terminal cyanide ligand, while the band at 2109.2 cm^{-1} is indicative of a bridging cyanide[(x,y,z)]. Thus the product contains both bridging and terminal cyanide ligands, which is consistent with the expected product.

Unfortunately, no other positive evidence for the formation of the expected product was gathered. The very poor CHN data obtained is detailed in the

Figure 4.7 : Absorption spectrum monitoring of **[Ru_2Pt]** in DMF

T = 243 K, E_{appl} = - 1.2 V

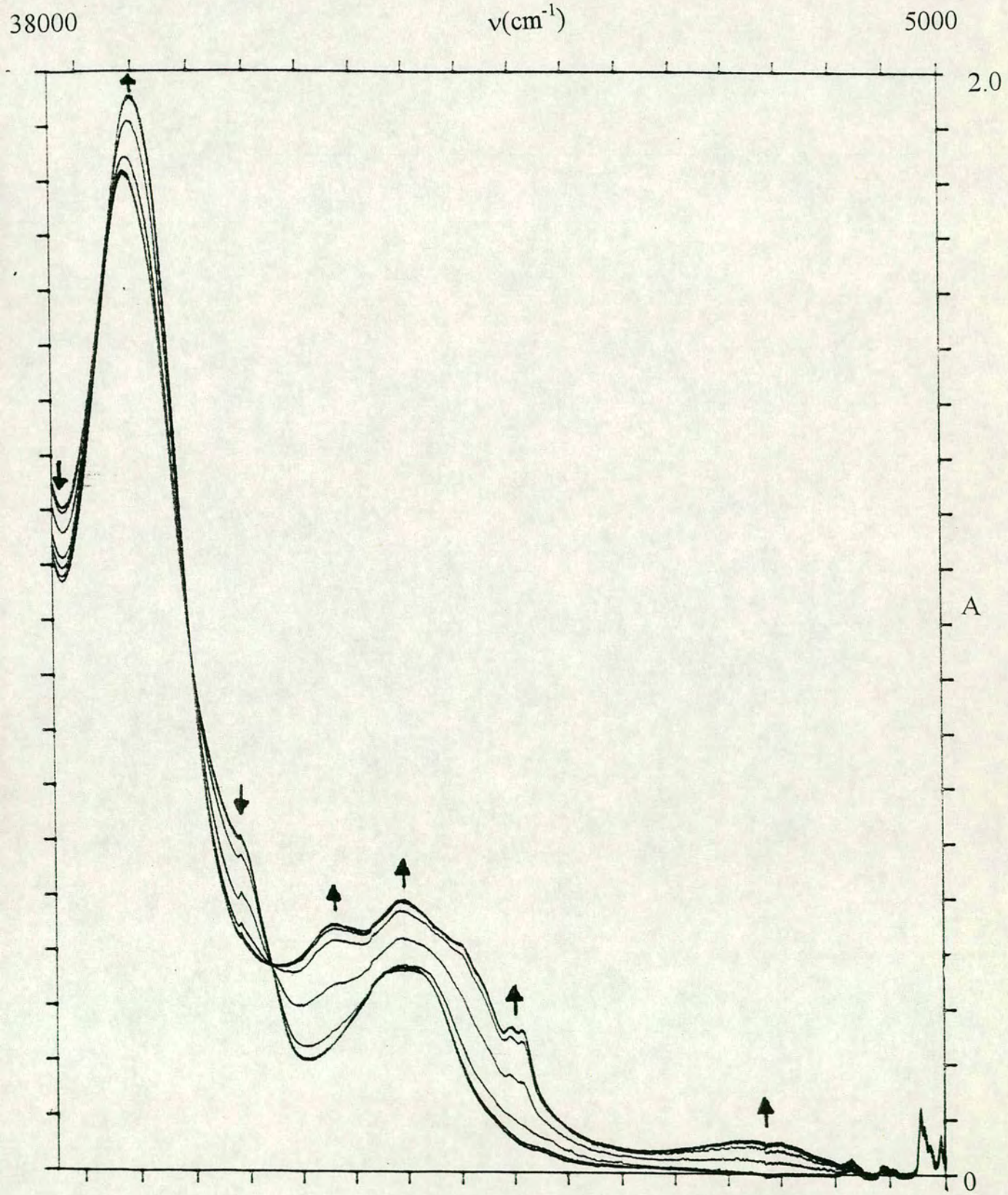

synthetic section at the end of this chapter. Mass spectrometry was also inconclusive, despite numerous attempts using both different techniques (both electron impact (EI) and fast atom bombardment (FAB)) and a range of matrices, although a number of possible peaks corresponding to possible fragments of the expected product were observed. However, these were all of small fragments (m/z ~500), and so no conclusions could be drawn. A number of attempts to grow crystals suitable for X-ray diffraction studies were made, but no single crystals of suitable quality could be grown, despite the use of a range of solvents. Thus, although the electrochemical, spectroelectrochemical and spectroscopic data discussed previously is on the whole encouraging, it is not possible to confirm the identity of the product as that desired.

4.4 : Attempted synthesis of $[Ru(bpy)_2((CN)Pt(terpy))_2](BF_4)_2$ [RuPt'$_2$]

To try and synthesise this complex, we started with $[Pt(terpy)Cl](BF_4)$, and then removed the chloride using $AgBF_4$. One half equivalent of $[Ru(bpy)_2(CN)_2]$ was then added. No excess was required as the Pt(terpy) unit has only one free co-ordination site, thus no polymeric product is possible.

The electronic absorption spectrum of the product of this reaction in methanol is shown in figure 4.8. There are five well defined absorptions between 20000 and 50000 cm^{-1}. For purposes of comparison the electronic absorption spectrum of $[Pt(terpy)Cl](BF_4)$ in DMF is given in figure 4.9.

At 41169 cm^{-1} and 35486 cm^{-1} there are two peaks which look very similar to the intraligand transitions normally seen for complexes containing the bpy ligand, and are assigned as such. The next two bands, at ~30500 cm^{-1} and 29499 cm^{-1}, are very similar to absorptions seen for $[Pt(terpy)Cl](BF_4)$, which we assign as terpy $\pi \rightarrow \pi^*$

Figure 4.8 : Electronic absorption spectrum of **[RuPt'$_2$]** in MeOH

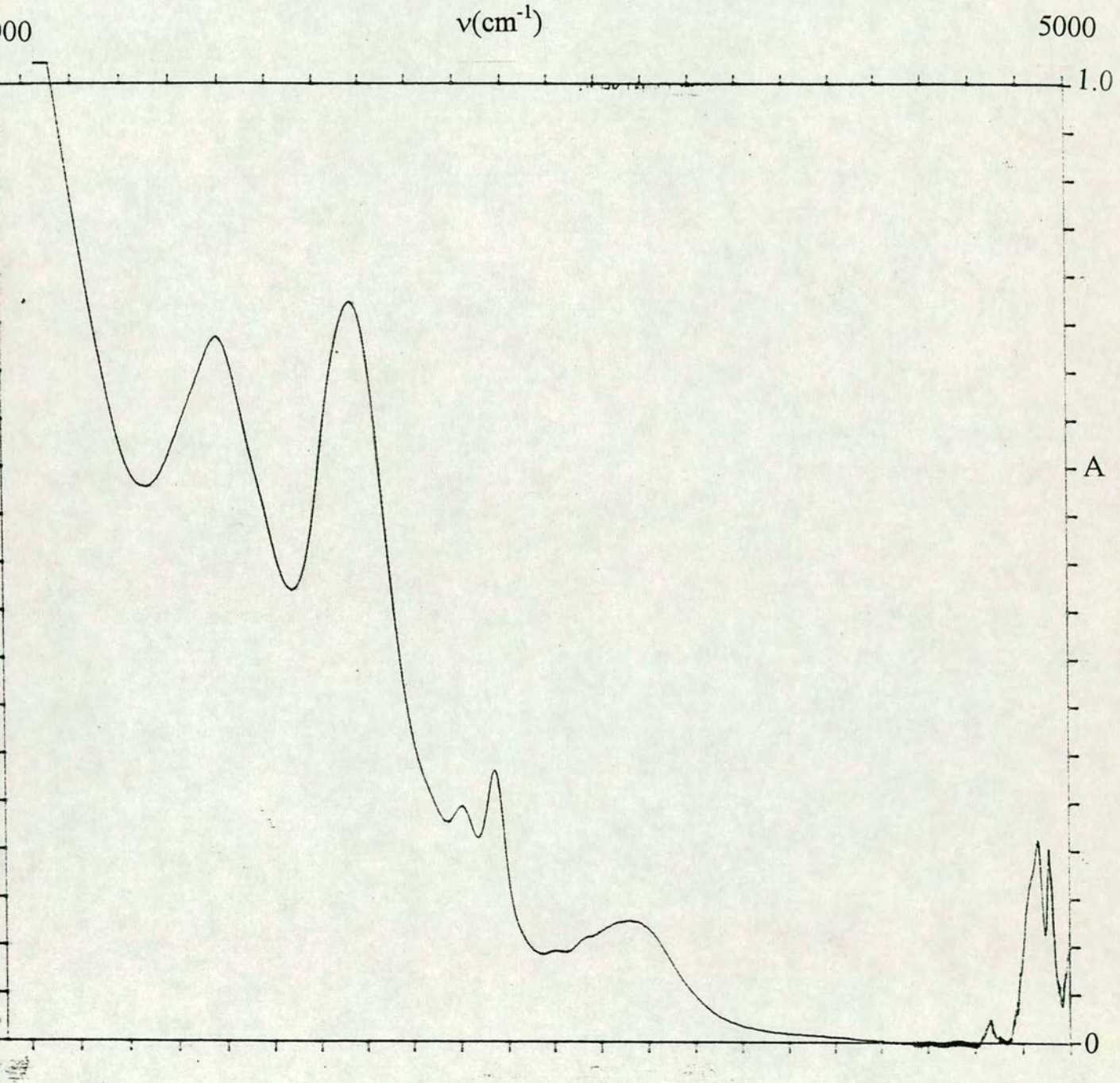

Figure 4.9 : Electronic absorption spectrum of [Pt(terpy)Cl](BF_4) in DMF

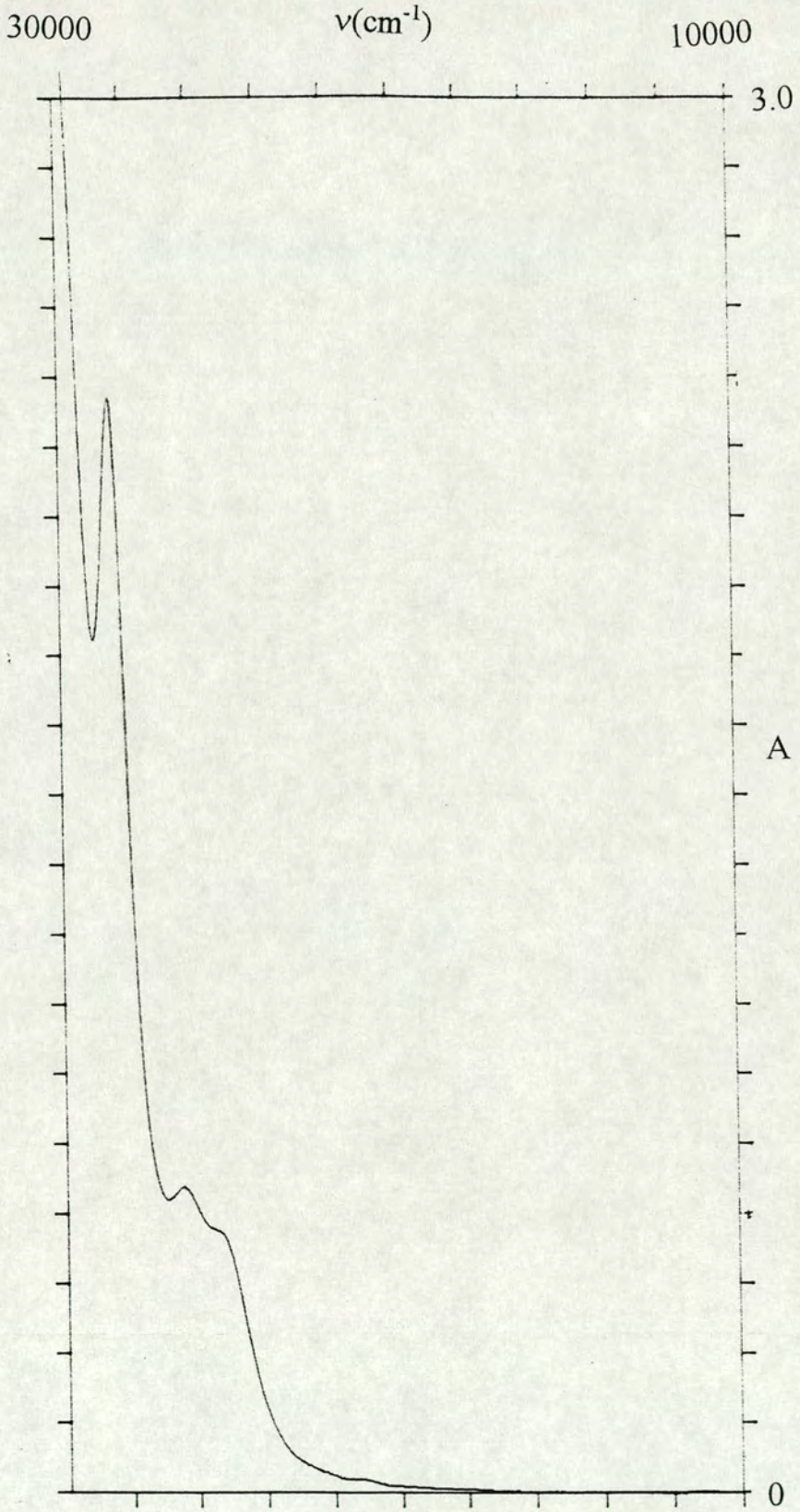

transitions in that complex. Thus we assign these bands similarly in the product. The final absorption occurs at 23849 cm^{-1}. Comparison with the two products previously studied suggests that this is a Ru $d\pi \rightarrow$ bpy π^* MLCT process, demonstrating the characteristic blue shift associated with using the cyanide ligand as a bridge. The lowest energy MLCT for $[Ru(bpy)_2(CN)_2]$ in methanol occurs at 21978 cm^{-1}.

The spectrum of $[Pt(terpy)Cl](BF_4)$ also shows a band at 26413 cm^{-1}. By analogy with Pt(bpy) complexes, this band is a Pt(II) $\rightarrow$ bpy π^* MLCT process. Careful examination of the spectrum of the product reveals two shoulders on the lowest energy band which may well be the Pt $\rightarrow$ terpy charge transfer processes, eclipsed by the other, more intense transitions.

The electrochemistry of the product is shown in figure 4.10. This demonstrates four processes in the negative range, and one in the positive range. The four reductive processes occur at -0.68 V, -1.24 V, -1.50 V and ~-1.7 V. The first process appears semi-reversible at room temperature, and appears to become fully reversible upon cooling to 243 K. The second and third processes are semi-reversible both at room temperature and on cooling. The fourth and final process is irreversible at room temperature, and shows a small degree of semi-reversibility on cooling. For purposes of comparison, figure 4.11 shows the reductive electrochemistry of $[Pt(terpy)Cl](BF_4)$ in DMF, corrected against Fc/Fc^+. This has two reversible processes at -0.67 V and -1.22 V. Consideration of this and the previously described electrochemistry of $[Ru(bpy)_2(CN)_2]$ would suggest that, if we have synthesised the desired product, the first two processes would be based around the terpy ligand bound to the Pt centre, and the second two would be based around the two bpy

Figure 4.10 : Electrochemistry of **[RuPt'$_2$]** in DMF

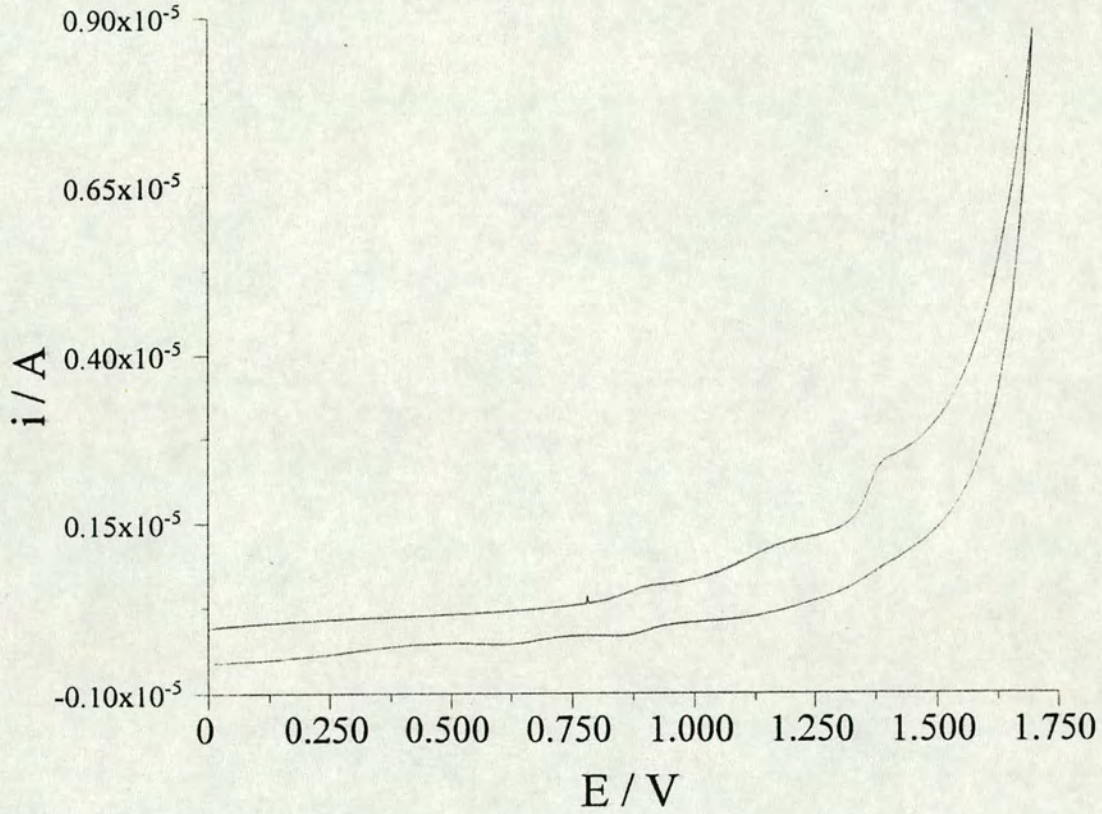

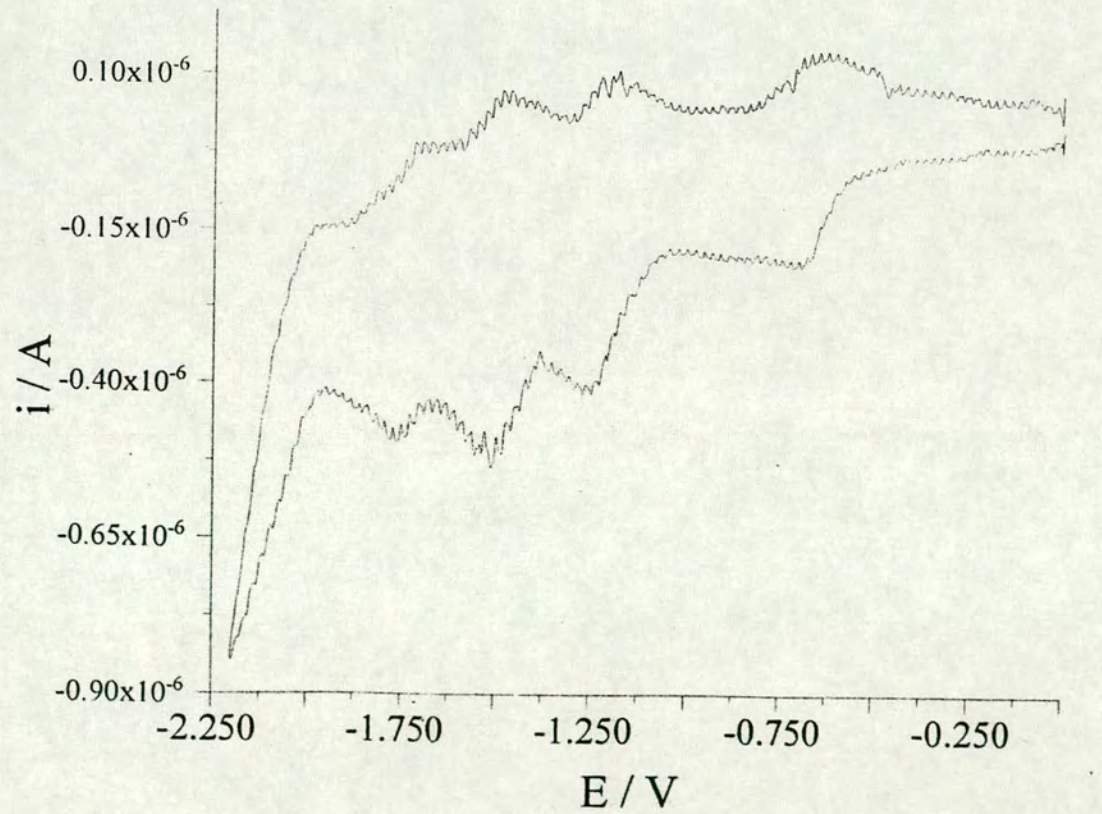

Figure 4.11 : Electrochemistry of $[Pt(terpy)Cl](BF_4)$ in DMF

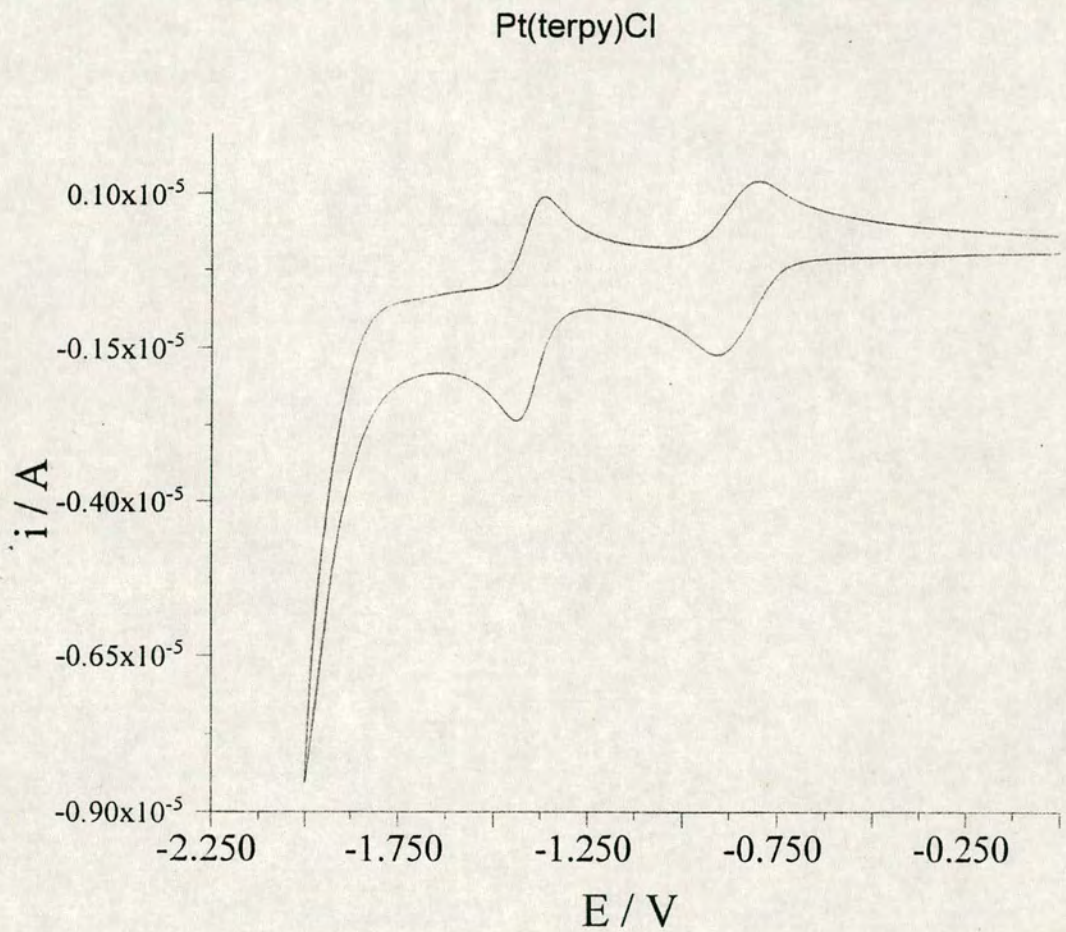

ligands chelated to the Ru centre. We would also be expect the number of electrons involved in Pt(bpy) based processes to be double that for $Ru(bpy)_2$ based processes. Thus proper assignment of these processes would be aided by performing a stirred voltammagram. However, lack of time prevented this experiment from being carried out.

The single process in the oxidative range, at around +1.4 V appears to be completely irreversible, even on cooling to 243 K. As for the previous products, we would expect to see behaviour associated with the Ru(II)/Ru(III) couple.

Unfortunately, no other positive evidence for the formation of the desired product has been obtained. Lack of time precluded the use of spectroelectrochemical techniques to investigate the rich reductive electrochemistry of the product. The poor CHN analysis obtained is detailed in the section devoted to the synthetic methods. As before, mass spectrometry yielded no definite information, although some peaks corresponding to possible fragments of the desired product were noted. Attempts to grow a single crystal suitable for X-ray analysis were unsuccessful, despite the use of a range of solvents. Further work is needed to fully characterise the product.

4.5 : Conclusions

Although there is some electrochemical and spectroscopic evidence that we have formed all three desired products ($[Ru_2Pt]$, $[RuPt_2]$ and $[RuPt'_2]$), this evidence is not conclusive.

Regardless of the nature of the difficulty, it is clear that further work is required to fully identify the products of these reactions which show interesting electronic characteristics. The large blue shifts of the absorption spectrum of the

Ru(II) → bpy CT are not mirrored in the reductive electrochemistry. In fact, the potentials of the reduction processes are very close to those observed in the related isolated monometallic species. However, the metal based Ru(II) oxidations are significantly affected - always to more positive potentials. Therefore the bpy and terpy π^* orbitals are relatively unaffected by the multimetallic assembly but the Ru $d\pi$ orbitals are grossly changed. In view of the work presented in Chapter 2 this is unsurprising. We noted there that the energy of the Ru metal based d orbitals is dependent on the cyanide ligand and its interaction with solvent molecules. In the multinuclear systems discussed in this chapter we have simply increased this effect on the cyanide orbitals by bonding other metal centres to them. Thus we see large shifts in the Ru(II)/Ru(III) potential.

4.6 : Preparation of compounds

As noted earlier, a common method of preparing cyanide bridged species is to prepare a halide derivative of one of the metal centres, and then use Ag^+ to remove the halide and free a co-ordination site for the cyanide bridge to form. This general method was employed in all three cases.

4.6.1 : Attempted synthesis of $[Ru(bpy)_2((NC)Pt(bpy)(CN))_2](BF_4)_2$ [**$RuPt_2$**]

Preparation of this compound was attempted using methods similar to those in the literature. In a typical preparation, $[Pt(bpy)Cl_2]$ (0.02088 g, 4.948×10^{-5} mol) was dissolved in DMF (50ml). Two equivalents of silver tetrafluoroborate ($AgBF_4$, 0.01920 g, 9.896×10^{-5} mol) were added, and the solution was stirred overnight in the dark. The resulting precipitate of AgCl was removed by centrifuging the solution. An approximately tenfold excess of $[Ru(bpy)_2(CN)_2]$ was added, and the solution was heated with stirring for around 8 hours. This resulted in an orange/red solution. The solution was evaporated to dryness, and the solid was redissolved in a minimum volume of DMF. This was then loaded onto a column of Sephadex LH-20, and eluted with acetonitrile. The unreacted $[Ru(bpy)_2(CN)_2]$ passed rapidly down the column, leaving the final product as an orange band on the column. This was collected, and diethyl ether was added to precipitate out the final product.

Analysis : Calculated for $C_{54}H_{40}N_{14}Ru_2PtB_2F_8$: C 44.53 %, H 2.75 %, N 13.47 %

Found : C 38.09 %, H 2.75 %, N 10.95 %

4.6.2 : Attempted synthesis of $[((NC)Ru(bpy)_2(CN))_2Pt(bpy)](BF_4)_2$ [Ru_2Pt]

In a typical preparation, dichlorobis(2,2'-bipyridyl)ruthenium(II) ($Ru(bpy)_2Cl_2$, 0.03607 g, 7.4525×10^{-5} mol) was dissolved in DMF (50 ml). Two equivalents of silver tetrafluoroborate ($AgBF_4$, 0.02892 g, 1.4905×10^{-4} mol) was added, and the solution was stirred overnight in darkness. The solution was then centrifuged to remove the precipitated AgCl. A three fold excess of $[Pt(bpy)(CN)_2]$ (0.14882 g, 3.6928×10^{-4} mol) was dissolved in DMF, and added to the solution. The resulting solution was then refluxed for four hours, and cooled. The solution was reduced to dryness and the resultant solid redissolved in acetonitrile, leaving the unreacted $[Pt(bpy)(CN)_2]$ as a solid which was filtered off. The product was then purified by passing it down a Sephadex LH-20 column, using acetonitrile as an eluant. The product was then precipitated by addition of diethyl ether to the resultant solution.

Analysis : Calculated for $C_{44}H_{32}N_{12}Pt_2RuB_2F_8$: C 37.92 %, H 2.31 %, N 12.06 %

Found : C 31.59 %, H 2.74 %, N 8.30 %

4.6.3 : Attempted synthesis of $[Ru(bpy)_2((CN)Pt(terpy))_2](BF_4)_2$ [$RuPt'_2$]

In a typical preparation chloro(terpyridyl)platinum(II) tetrafluoroborate ($[Pt(terpy)Cl](BF_4)$, 0.34292 g, 6.2292×10^{-4} mol) was dissolved in DMF. Silver tetrafluoroborate ($AgCl_4$, 0.12147g, 6.229×10^{-4} mol) was added, and the solution was left to stir overnight. The solution was centrifuged to remove the precipitated AgCl. *Cis*-dicyanobis(bipyridyl)ruthenium(II) ($[Ru(bpy)_2(CN)_2]$, 0.15428 g, 3.3178×10^{-4} mol) was added, and the solution was refluxed for three hours, undergoing a colour change from orange to a deep red/brown. The solution was reduced in volume, and purified using a Sephadex LH-20 column, with acetonitrile as eluant. The product

appeared as a slow moving red/brown band, which was collected, and reduced in volume. The product was then precipitated by addition of diethyl ether.

Analysis : Calculated for $C_{52}H_{38}N_{12}RuPt_2B_2F_8$: C 41.76 %, H 2.56 % N 11.24 %

Found : C 39.02 % H 2.56 % N 10.59 %

4.7 : References

1. J.N. Demas, J.W. Addington, S.H. Peterson, E. Harris, *J. Phys. Chem.*, **1977**, 81, 1039
2. M.G. Kinnaird, D.G. Whitlen, *Chem. Phys. Lett.*, **1982**, 88, 275
3. C.A. Bignozzi, F. Scandola, *Inorg. Chem.*, **1984**, 23, 1540
4. S. Roffia, C. Paradisi, C.A. Bignozzi, *J. Electroanal. Chem.*, **1986**, 200, 105
5. C.A. Bignozzi, C. Paradisi, S. Roffia, F. Scandola, *Inorg. Chem.*, **1988**, 27, 408
6. C.A. Bignozzi, S. Roffia, C. Chiorboli, J. Davila, M.T. Indelli, F. Scandola, *Inorg. Chem.*, **1989**, 28, 4350
7. R. Amadelli, R. Argazzi, C.A. Bignozzi, F. Scandola, *J. Am. Chem. Soc.*, **1990**, 112, 7099
8. Y. Lei, T. Buranda, J.F. Endicott, *J. Am. Chem. Soc.*, **1990**, 112, 8820
9. E.J.L. McInnes, Ph.D. thesis, University of Edinburgh, **1995**

Lecture Courses and Conferences Attended

Electron Paramagnetic Resonance Spectroscopy - Dr. R.E.P. Winpenny

d- and f- Block Elements - Dr. R.E.P Winpenny

Nuclear Magnetic Resonance Spectroscopy - Dr. I. Sadler

An introduction to X-ray crystallography - Dr. A.J. Blake & Dr. R.O. Gould

Electron Paramagnetic Spectroscopy - Prof. P. Reiger

Departmental research seminars and colloquia

University of Strathclyde Inorganic Club conferences 1992 and 1993

Butler postgraduate electrochemistry meetings 1992, 1993 and 1994

RSC Scottish Dalton meetings 1992, 1993 and 1994

Irvine Memorial Lectures, St. Andrews, 1993

RSC (Dalton Division) international conference on the chemistry of the platinum group metals, St. Andrews, 1993

RSC (Dalton Division) international conference on the chemistry of the copper/zinc group of metals, Edinburgh, 1992

Electrochem '94, Edinburgh, 1994